NOVEL MULTILAYERED MAGNETOPLASMONIC NANOPARTICLES FOR THERANOSTIC APPLICATIONS

By

Charleson Sherard Bell

Dissertation

Submitted to the Faculty of the

Graduate School of Vanderbilt University

in partial fulfillment of the requirements

for the degree of

DOCTOR OF PHILOSOPHY

in

Biomedical Engineering

December, 2015

Nashville, Tennessee

Approved:

Todd D. Giorgio, Ph.D.

Frederick R. Haselton, Ph.D.

Melissa C. Skala, Ph.D.

Richard F. Haglund, Ph.D.

Eric P. Skaar, Ph.D., M.P.H.

To my Mom and Dad… this is for you.

ACKNOWLEDGEMENTS

First, I give all thanks and glory to GOD, my father in heaven, his Son, Jesus Christ my Lord and Savior, the Holy Spirit, a gift from God himself – without Him I am nothing and would have never made it this far…

I would like to gratefully acknowledge the Department of Defense Concept CDMRP Award (#W81XWH-08–1-0502), Department of Defense PRMRP Award(#W81XWH-13-1-0397) and the Vanderbilt University intramural Discovery Grant Award (#4–48-999–9132) for funding of my dissertation work.

My research was successfully completed thanks to the help of many individuals who assisted me along the way. I gratefully acknowledge my Preceptor, first nanotechnology professor and friend, Dr. Todd D. Giorgio, for the patience and guidance he gave me towards the completion my degree. The road was long and obstacle-ridden and I am grateful for his persistence in guiding me through my early struggles and later triumphs.

I am extremely grateful to my Dissertation Committee as they thoughtfully guided me through the completion of my aims and my development as a researcher and problem solver.

I would like to *deeply* acknowledge Dr. Raquel Mejias, Sinead Miller and Jasmine Greer for their hands-on contributions to the completion of this work. Without them, their contributions and their support, it would have been an arduous struggle to complete this breadth of work in the time that was allotted. Furthermore, I would like to thank Andre

Stevenson, Dr. Ryan Ortega, Dr. Shann Yu, Mary Dockery, Dr. Ian McFadden, Zoe Johnson, Andrew Cook, Sue Hyun Lee, Cheryl Lau and Kristin Engerer for their support during our long days and nights in the laboratory and office.

I would also like to thank, Dr. Sarah Sewell Pierce, Dr. Amanda Lowery, and Dr. Chinmay Soman for their guidance and assistance in my early graduate school endeavors. Without their hands-on approach to training, I would not have quickly obtained the laboratory experience and dexterity that I have today. I would like to thank Dr. James McBride, Dr. Don Stec, Dr. Daniel Colvin, Dr. Anthony Hmelo, and Rosanne Delapp for the contribution of their expertise, time and kind patience.

I would like to thank my immediate and extended family for their undying support and encouragement through this process. Mom, Dad, Charreau, Maceo, Grandpa, my late Grandma, aunts, uncles, cousins and the like – I thank you and love you all!

To my Brothers of the Nu Rho Chapter of Kappa Alpha Psi, your passionate support and our deep Bond as a family-away-from-family helped me *Achieve* this goal. *φνπ*

Finally, thank you to all who I have not specifically named in this acknowledgement. You *know who you are* and I sincerely and graciously thank you for your encouragement and support throughout my experiences here at Vanderbilt University.

Thank you.

TABLE OF CONTENTS

ACKNOWLEDGEMENTS iii
TABLE OF CONTENTS v
LIST OF TABLES vii
LIST OF FIGURES viii
LIST OF ABBREVIATIONS ix

CHAPTER 1 1
INTRODUCTION 1
Objectives 3
Specific Aims 4
Background and Significance 4

CHAPTER II 18
THE MULTISTRATA NANOPARTICLE: 18
Introduction 21
Materials and Methods 23
Results and Discussion 28
Conclusions 39
Summary 39

CHAPTER III 42
SONOCHEMICAL SYNTHESIS AND TOMOGRAPHIC CHARACTERIZATION 42
Introduction 44
Methods and Materials 48
Results and Discussion 53
Conclusion 63
Summary 64

CHAPTER IV 65
NANOTECHNOLOGY-MEDIATED MAGNETIC SEPARATION 65
Introduction 66
Materials and Methods 70
Results and Discussion 80
Conclusion 97
Summary 98

CHAPTER V 100
SYNOPSIS AND CONCLUSIONS 100
BIBLIOGRAPHY 103

LIST OF TABLES

Table

TABLE 1. SUMMARY OF NANOPARTICLE CHARACTERIZATION RESULTS 58

TABLE 2. CONJUGATED NANOPARTICLES DO NOT CAUSE HEMOLYSIS. 88

TABLE 3. CONJUGATED AND UNCONJUGATED NANOPARTICLE CHARACTERIZATION. 94

LIST OF FIGURES

FIGURE

FIGURE 1. THE INTERIOR STRUCTURE OF CORE-SHELL NANOPARTICLES 19

FIGURE 2. SCHEMATIC OF THE MULTISTRATA NANOPARTICLE 29

FIGURE 3. THE MULTISTEP FABRICATION OF THE MULTISTRATA NANOPARTICLE 32

FIGURE 4. CHARACTERIZATION OF MULTISTRATA NANOPARTICLES. 34

FIGURE 5. COMPARISON OF GOLD AND SILVER MULTISTRATA FABRICATION PROTOCOLS 35

FIGURE 6. COMPARATIVE EXTINCTION PROPERTIES OF GOLD AND SILVER MULTISTRATA NANOPARTICLES. 37

FIGURE 7. CANDIDATE'S RESEARCH FEATURED ON THE FRONTISPIECE OF THE JOURNAL *SMALL*. 40

FIGURE 8. SCHEMATIC OF SONOCHEMICALLY SYNTHESIZED NANOPARTICLES. 52

FIGURE 9. CHARACTERIZATION OF FEOX/AU CORE/SHELL NANOPARTICLES.. 54

FIGURE 10. CHARACTERIZATION OF FEOX-AU COMPOSITE NANOCLUSTERS. 56

FIGURE 11. DETAILED CHARACTERIZATION OF FEOX-AU COMPOSITE NANOCLUSTERS. 60

FIGURE 12. MORPHOLOGICAL ANALYSIS OF FEOX-AU COMPOSITE NANOCLUSTERS 62

FIGURE 13. INTRODUCTORY SCHEMATICS FOR NANOTECHNOLOGY-MEDIATED, MAGNETIC EXTRACTION 71

FIGURE 14. QUANTIFICATION OF MACROSCALE *A. BAUMANNII* SEPARATION BY FEOX-AU NANOCLUSTERS. 81

FIGURE 15. COMPARATIVE QUANTITATIVE ANALYSIS OF SEPARATION BY FEOX-AU NANOCLUSTERS. 82

FIGURE 16. COLISTINATED NANOCLUSTERS BIND TO THE SURFACE OF *A. BAUMANNII*. 85

FIGURE 17. BACTERIAL TOXICITY OF PEGYLATED AND COLISTINATED NANOCLUSTERS WITH *A. BAUMANNII IN VITRO* 87

FIGURE 18. CYTOCOMPATIBILITY RESULTS 90

FIGURE 19. FEOX-AU CHARACTERIZATION CONFIRMING NANOMATERIAL SYNTHESIS.. 93

FIGURE 20. CONFIRMATION OF COLISTIN CONJUGATION 96

LIST OF ABBREVIATIONS

3D	Three dimensional
APTES	[(3-aminopropyl)triethoxysilane]
AuNPs	Gold Nanoparticles
CA	Community-acquired
CFU	Colony Forming Units
CPMG	Carr-Purcell-Meiboom-Gill Sequence
CT	Computed Tomography Imaging
CR	Combat-related
EDS	Energy Dispersive X-ray Spectroscopy
EDX	Energy Dispersive X-ray Spectroscopy
EtOH	Anhydrous Ethanol
FeOx	Superparamagnetic Iron-oxide Nanoparticle
FeOx/Au	Iron-oxide/Gold Core/Shell Nanoparticle (also AuFeOx)
FeOx-NH_2	Aminated Iron-oxide Nanoparticle
HA	Hospital-acquired
HAADF	High Angle Annular Dark Field
HAADF-STEM	High Angle Annular Dark Field Scanning Transmisison Electron Microscopy
LB	Lysogeny broth (a.k.a. Luria broth, Lennox broth, or Luria-Bertani medium)
LPS	Lipopolysaccharide

MDR	Multi-Drug Resistant
MF	Magnetic Field
MRI	Magnetic Resonance Imaging
MS**NP**	Multistrata Nanoparticle
NP	Nanoparticle
NS	Nanosphere (Dielectric/Metal Nanoparticles)
PAT	Photoacoustic Tomography
PBS	Phosphate Buffered Saline
PT-OCT	Photothermal Optical Coherence Tomography
PTT	Photothermal Therapy
RT	Room Temperature
SN	Supernatant
SPION	Superparamagnetic Iron-oxide Nanoparticle
STEM	Scanning Transmission Electron Microscopy (Microscope)
TCCC	United States Tactical Casualty Combat Care
TE	Echo Time
TEM	Transmission Electron Microscopy (Microscope)
TEM-EDS	Transmission Electron Microscopy - Energy Dispersive X-ray Spectroscopy
TEOS	Tetraethyl orthosilicate
THPC	Tetrakis (hydroxymethyl) phosphonium chloride
TR	Relaxation Time
UV-Vis-NIR	Ultraviolet Visible-Near Infrared (electromagnetic spectrum)

CHAPTER 1

INTRODUCTION

For over half a century, nanotechnology has been the focal point of cutting edge technology in a multitude of disciplines and fields (Feynman 1960; Editorial 2009). With the ability to specifically synthesize structures less than 100 nm, investigators are able to control, manipulate and explicitly interact with matter and substances on an atomic or molecular scale. The ramifications of the implementation of nanotechnology are of great importance in the medical field as biological processes occur mechanistically and molecularly at the microscale and nanoscale, respectively (Roco 2003). With the advent of bionanotechnology, bioengineers and medical scientists utilize these tools to better characterize and modify biological process in an effort to enhance medical applications (Ernest & Shetty 2005). Described as the convergence of materials-centric nanotechnology and biology-focused biotechnology, bionanotechnology platforms normally include a fabrication step where the nanomaterial is biofunctionalized with a specific molecule for specific targeting or protection from unwanted interactions with biological materials. Over the past two decades, the rise of bionanotechnology has accelerated innovations in pathogen biodetection (Driskell & Tripp 2009; Kaittanis et al. 2010; Cheng et al. 2009), disease diagnostics (Johnson et al. 2008; Wei et al. 2010), tissue engineering (Bose & Wui Wong 2015; Pham et al. 2006), drug development and discovery (Chung et al. 2007), drug delivery (de Villiers et al. 2009; Farokhzad & Langer 2009), protein detection and extraction (Soman & Giorgio 2008; Soman & Giorgio 2009; Bordelon et al. 2013),

biomedical imaging (Tucker-Schwartz et al. 2012; Skala et al. 2008), tumor ablation (Huang et al. 2008; Rozanova & Zhang 2009) and cell extraction (Radisic et al. 2006).

Most bionanotechnological applications are single-purpose and utilize only a single property of the biofunctionalized nanomaterial. For example, nanotechnology-mediated innovations in MRI imaging routinely use superparamagnetic iron oxide nanoparticles for their image contrast characteristics alone (F. H. Wang et al. 2011; Ma et al. 2015). Furthermore, nanotechnology applications in pathogen detection commonly utilize the nanomaterials for only their magnetic properties (Chen et al. 2015) or optical properties (Ali et al. 2012). These limitations are not only due to the focus of the investigators; but, are also due to the narrow properties and characteristics of the nanomaterial. Whether the material has been discovered to, or specifically designed to, exhibit a particular characteristic, I propose that improvements in nanomaterial design through variation in fabrication technique will allow multiple characteristics and properties to be combined into a single, nanoscale entity.

From a chemical perspective, the combination of multiple nanoscale properties into a single nanoparticle is achieved through the addition of *functional* layers. This assertion forms the basis of core/shell nanotechnology. The combination of multiple characteristics into a single nanoscale unit unleashes a host of potential combinatorial applications; many of which are biomedical in nature. Most importantly, nanomaterials used solely for diagnostics or therapeutics, individually, can be combined into a single *theranostic* nanoconstruct.

Herein, we have developed multilayered, core/shell nanoparticles that possess optical, magnetic-constrast and dual-plasmonic properties. From there, we modified the fabrication techniques utilized in the development of this material to synthesize magnetoplasmonic core/shell nanoparticles with the capacity for magnetomotion in the presence of a magnetic field. Thereafter, we evaluated the core/shell nanomaterial *in vitro* in a biomedical application.

Objectives

The central hypothesis of my dissertation is that inorganic, multilayered, magnetoplasmonic core/shell nanomaterials can be specifically designed and synthesized for biological applications which require both diagnostic detection and therapeutic elimination of a disease causing agent. Furthermore, I hypothesize that these materials can be fabricated in such a way that biomedical functionalization of the material can proceed without detriment to the function of the biological component. Therefore, the objectives of this work are to (1) develop multilayered nanomaterials that combine at least two nanoscale characteristics into a single entity, (2) modify the synthesis strategy to enhance the properties of the composite material while decreasing the synthesis duration such that freshly synthesized materials can be rapidly utilized in biological applications, (3) ensure the conservation of the activity of the biological component while binding and eliminating a disease causing agent *in vitro*.

Specific Aims

Specific Aim 1: Novel multilayered, magneto-metallodielectric, core/shell nanoparticles will be fabricated using a unique synthesis protocol. Characterization of the multimodal nanoscale characteristics of the nanomaterial will be performed. Assessment of the theranostic potential of the nanoparticulate will also be performed here.

Specific Aim 2: Multilayered, magnetoplasmonic core/shell nanoparticles will be fabricated by adapting the synthesis protocol used in *Aim 1*. The magnetic properties of the material will be enhanced to provide magnetomotive functionality to the nanostructure. Further, the synthesis duration will be decreased enabling the rapid fabrication and use of fresh materials for biological applications.

Specific Aim 3: The magnetoplasmonic core/shell nanoparticles fabricated in *Aim 2* will be biofunctionalized with an antibiotic which targets and binds gram negative bacteria. These biofunctionalized nanostructures will then be characterized and utilized to magnetically extract *Acinetobacter baumannii* from saline solution *in vitro*.

Background and Significance

For my dissertation, I proposed to develop magnetoplasmonic core/shell nanoparticles that could be used for theranostic biomedical applications. These magnetoplasmonic core/shell nanostructures, in particular, possess combinatorial concentric configurations whose properties stem from the combination of two or more nanoscale materials. Because of the unique, multimodal properties of nanostructure, the

nanomaterials were assessed as a potential theranostic for *Acinetobacter baumannii* bacteremia – a disease where a strategy is urgently needed to improve patient outcomes. In this section, I will discuss the clinical ramifications and therapeutic state-of-the-art for *Acinetobacter baumannii* bacteremia to establish the biomedical impact of this work. Thereafter, I will review previous nanotechnology-based strategies for both disease detection and eradication which govern the design of both the novel and functional magnetoplasmonic core/shell nanostructures described herein.

Bacterial Infection: The Impact on Humanity and the Rise of Resistance

Throughout history, human health has been influenced by a multitude of external factors, invaders, and pathogens; but none more notable than the impact of bacterial infection. As early as 3000 BCE, bacterial infections caused some of the most memorable pandemics which lead to the decline of major cities, nations and diverted human history (Rasmussen et al. 2015). The existence of multi-drug resistant organisms in healthcare facilities predates the modern scientific era. Upon the advent of penicillin, its effectiveness pushed the demand to such heights that scientists and clinicians had concerns regarding its indiscriminate distribution (Falk 1945). Fears were realized when clinicians reported 'profound changes in the number and character of infections that were occurring' – particularly those within hospitals (Finland et al. 1959). In fact, the first penicillin-resistant *Staphylococcus aureus* emerged less than a year after the first administration of penicillin in 1945 (Prabaker & Weinstein 2011). From that point, nearly every antibacterial agent developed has faced significant resistance problems. Within the last decade, there has been a substantial rise in nosocomial and community-acquired multi-drug resistant infection

worldwide (Mumtaz et al. 2011). Multi-drug resistant (MDR) bacterial infection is of critical concern to both foreign and domestic medical authorities due to its recent rise and environmental persistence in mainstream, pediatric, elderly-care and urgent-care military medical facilities (Rybak and R.L. Akins 2001; Lindsay and M.T. Holden 2004).

Acinetobacter baumannii: Impact and Resistance

The recent emergence of *Acinetobacter baumannii* as a resistant pathogen acquired by wounded personnel in military field hospitals is of particular concern due to its recent transition to domestic healthcare facilities (Scott et al. 2007). Known as the quintessential gram-negative nosocomial pathogen for the past few decades (Prabaker & Weinstein 2011), *A. baumannii* is a significant MDR pathogen that causes a range of infections, including respiratory and urinary tract infections, meningitis, endocarditis, wound infections, and bacteremia (Jacobs et al. 2010).

A. baumannii is now responsible for up to 20% of all intensive care unit infections in some regions of the world. Further, more than 6% of all Gram-negative infections in the intensive care units of the United States can be attributed to *A. baumannii*. In the United States, this incidence of the resistant strain of this organism is has risen from 6.7% in 1993 to 29.9% in 2004 – more than twice that for any other Gram-negative bacterium causing infections in ICUs (Lockhart et al. 2007). Comparable to the rise of resistant *S. aureus*, the clinical significance of *A. baumannii* has been exacerbated by its rapid acquisition of resistance to virtually all antibiotics.

The uncanny ability of *Acinetobacter baumannii* to persist on dry surfaces for extended periods of time prepares this resistant strain for survival in desert field hospital conditions (Jawad et al. 1998). Even further, these microbes can be transferred from foreign, military medical institutions and colonize domestic communities. Also, this organism has the ability to form biofilms on abiotic surfaces which could create a favorable environment for persistence (Getchell-White et al. 1989). These bacteria selectively persist in host infections and also have the ability to biosynthesize lipopolysaccharide (LPS) partially via the glycosyltransferase, LpsB (Luke et al. 2010). Further, these strains increase their tolerance to antibiotics in response to the existence of monovalent cations (as released by compounds such as NaCl) in their culture environment (Hood et al. 2010). Monoclonal antibodies or antibiotics such as colistin (Levin et al. 1999) specifically target these biochemical, surface moieties, however they remain generally inefficient against resistant strains. The latter is of significant importance as it is informative of a conserved targeting motif well suited for nanotechnology-mediated bactericidal theranostics. Existence of such a motif is paramount when surface labelling any organism with a particular nanostructure. Such a label will allow for the design of a number of nanostructures that can possess many detection or therapeutic characteristics for specific targeting to the bacterium.

Acinetobacter species can cause a number of disease states including pneumonia, meningitis, urinary tract infections, peritonitis, skin and soft tissues infections and bacteremia (Bergogne-Bérézin & Towner 1996). These primary ailments contribute to the incidence of *Acinetobacter* species bloodstream infections (BSIs) which account for over

3% of all nosocomial acquired BSIs (Hidron et al. 2008). Disturbingly, the mortality rate associated with *A. baumannii* infection is high: bacteremia-associated mortality is 52% and pneumonia-associated mortality ranges from 23% to 73% (Rodriguez-Guardado et al. 2013).

Current Battlefield Treatment Strategies in Combat Related Infection

In both community-acquired (CA) and hospital-acquired (HA) infection types, multi-drug resistant (MDR) pathogens gain access to host tissues when patients are either injured or are in immuno-compromised states. Although CA and HA infections comprise the majority of MDR infections in the world, over the last three decades, the incidence of combat-related (CR) MDR infection is rising due to the increase in war-time activity in the Middle East in concert with the intercontinental transport of infected military personnel to combat installations worldwide. Due to an impending rise of CA and HA infections caused by the return of military personnel to domestic homes and healthcare institutions, I will briefly discuss the current state-of-the-field treatment of CR MDR infections as they are a point of origin for the newest global MDR infections.

Historically, the extremities have been the most common sites of combat injury; remaining true as current combat in the Middle East and Afghanistan continues (Murray, Hospenthal, et al. 2011). CR extremity injuries – usually violent in occurrence - result in gross contamination of the wound; along with anatomic and physiologic devastation of the local tissue. Further, such a traumatic physiological event is likely to detrimentally alter the patient's immune response thus complicating their ability to resist infection (Stoecklein et al. 2012). Thus, antimicrobial treatment, systemic or at the site of injury, must be

administered to prevent infection following combat injury. Currently, there are a number of preventative, clinical treatments for post-injury control of infection. Infection through the gross contamination of wounds can be impeded through the utilization of continuous irrigation with debridement at the site of injury to prevent ongoing bacterial replication. Further, surgical wound closure following irrigation, debridement, and a 5 day delay period - to ensure no evidence of infection is apparent – has yielded positive outcomes as far as inhibiting infection (Dufour et al. 1998). Failure to prevent infection progression at the site of injury leads to the onset of bacteremia and septicemia.

Pharmaceutical Treatments for Point-of-Injury Infection and Bacteremia

Aside from physical treatment of the wound area, chemical treatments including antimicrobials and antibiotics are administered to patients to impede the onset of infection. The current recommendation by the United States Tactical Casualty Combat Care (TCCC) committee is rapid delivery of intravenous or oral antimicrobial therapy at the point-of-injury. The antimicrobial agents of choice to deliver at the site-of-injury vary depending on the nation. Currently, the recommended antibacterial of choice is cephalosporin cefazolin utilized due to its antibacterial coverage of possible infectious pathogens and its appointment as the standard of care in the United States for extremity injuries (Murray et al. 2011). The International Committee of the Red Cross (ICRC) recommends intravenous penicillin for amputations, compound fractures, and major soft tissues wounds (Dufour et al. 1998). For *A. baumannii* treatment in particular, Colistin (polymyxin E), a polymyxin antibiotic produced by certain strains of *Bacillus polymyxa* var. colistinus, is the antibiotic of choice and is thus delivered intrathecally and intraventricularly if infections have

reached the point of meningitis/ventriculitis. Nevertheless, some colistin resistance has been described (Qureshi et al. 2014; Cai et al. 2012).

For treatment of *A. baumannii* bacteremia, aside from colistin, treatment options are increasingly limited due to the rapid acquisition of multi-drug resistance to the few antibiotics readily available (Fournier et al. 2006). Normally, upon presentation, empiric therapy is implemented based on local susceptibility patterns. Broad-spectrum cephalosporin with sulbactam is utilized until susceptibility tests from blood cultures are available. Carbapenems are highly bactericidal against susceptible *Acinetobacter* strains (Fishbain & Peleg 2010). However, multidrug resistant, extensively drug-resistant and pandrug-resistant strains do not effectively respond to these therapeutics. Furthermore, increasing dosage is correlated with decreased cytocompatibility and is a common problem upon administration of toxic therapeutics. Because of this, many have investigated a number of therapies which function as adjuvants to conventional antibiotic regimens in order to effectively curtail bacteremia. Furthermore, combinatorial delivery of colistin with sulbactam, rifampin and tigecycline proved suboptimal as it has been shown to lead to the development of resistance (Vila & Pachón 2008).

Motivation for New Innovative Approaches

There are an inadequate number of antimicrobial pharmaceuticals which are active against MDR (especially Gram-negative) pathogens in the pharmaceutical pipelines. This requires renewed emphasis in the search for viable means of treating MDR pathogens (Murray et al. 2011). Further, it has been determined that the incidence of MDR infection increases as the

length of combat durations increases. Even further, when comparing the susceptibility patterns of MDR organisms over time, that antimicrobial resistance increases with hospitalization time (Matsumoto et al. 1969) leading to further hospitalization and opportunities for the MDR organism to spread to other compromised patients. Even more disturbing, the presence of MDR pathogens persisted during intercontinental travel and remained in wounds upon arrival in the United States (Heggers et al. 1969). Due to these facts, I assert that more novel means of bacterial treatment that do not rely on the antimicrobial traits of antibiotics need to be developed.

Novel Treatments of Multi-drug Resistant Bacteria

Although the majority of traditional antibiotics can treat and somewhat manage drug-resistant bacteria, many commonly used antibiotics are ineffective (Levy 1998; Wright 2010). In the past year, a number of novel compounds and strategies have been devised to treat MDR bacterial infections (Kurek et al. 2011). Some of the more recent studies have been utilizing bacteriophages as antibacterial agents able to naturally defeat MDR resistance (Chibani-Chennoufi et al. 2004; Górski et al. 2009). This research is ongoing and is limited by bacteriophage specificity. Recently, some investigators have turned to plant-derived compounds – antibacterial phytochemicals. More specifically, certain terpenes and phenolics/polyphenols interfere with bacterial peptidoglycan metabolism (Kurek et al. 2010) and cause cell wall/envelope disruption (Tsuchiya et al. 1996), respectively. The difficulty with this natural approach is that drug delivery to the intended target is challenging.

Nanotechnology-mediated Bactericidal Treatments

Another direct approach to antibacterial treatment is the use of nanotechnology. Silver ions have shown antibacterial affects against various bacterial species since antiquity (Rai et al. 2009). Silver nanoparticles (AgNPs) have an even greater advantage due to their increased surface area to volume ratio and 1.4-1.9 times higher antibacterial potential (Ingle et al. 2008). The mechanism of action of the AgNPs, like the some of the aforementioned antibacterial phytochemicals, includes the disruption of bacterial envelope due to the production of reactive oxygen species. Silver toxicity is one major problem with utilizing silver nanoparticles in patients. Other novel 'nanoantibiotics' utilized for MDR infection include zinc oxide NPs, titanium dioxide NPs, aluminum NPs, copper NPs, antimicrobial peptides, chitosan, fullerenes (C60), carbon nanotubes (CNTs), nitric oxide (NO) releasing NPs, surfactant based nanoemulsions, drug delivery based liposomes, polymeric NPs, and dendrimers (Huh & Kwon 2011).

Alternatively, gold nanoparticles (AuNPs) have also been used as antimicrobial agents. Unlike the use of AgNPs the mechanism of action of AuNPs does not involve the delivery of antimicrobial ions to the surface of the cells. Instead, AuNPs have been leveraged as either pharmaceutical agent delivery vehicles or photodynamic enhancement mediators (Pissuwan et al. 2010). For instance, AuNP-vancomycin conjugates proved to be 50-fold more active than free antibiotics against bacterial populations (Gu et al. 2003). In other examples, AuNP-ciprofloxacin (Tom et al. 2004) and AuNP-aminoglycosidic antibiotics (Nirmala Grace & Pandian 2007) have also been described. In these examples, the role of the AuNPs was to facilitate the attachment of the conjugated antibiotics to the

bacterium. Following attachment, the antibiotic constructs penetrate the cell wall. AuNPs have also been utilized as stabilizers and enhancers of dye-mediated photodynamic therapy. A four-fold increase in *S. aureus* eradication was observed when photodynamic dyes (toluidine blue O and methylene blue dyes) were conjugated to AuNPs as compared to lone administration (Gil-Tomás et al. 2007; Perni et al. 2009). The mechanism for this enhancement lies in the ability of the AuNPs to enhance the absorption of light due to their surface plasmon resonance (Pitsillides et al. 2003). The downfall of dye-mediated photodynamic therapy is twofold where there exists host toxicity to the dye and widespread cell death due to non-specific targeting after photoexposure.

Core/Shell Nanotechnology-mediated Antimicrobial Photothermal Therapy

Antibiotics are utilized in bacterial infections because they specifically target and effectively treat bacterial strains without significant detriment to host tissue. Nanotechnology-mediated photothermal (PT) therapy was designed for a similar purpose where treatment only occurs at the site of nanoparticulate localization (Zharov et al. 2006). Per protocol, specifically-targeted near-infrared (NIR; 700-1200 nm) sensitive nanoparticles are delivered to the site of treatment. Following deposition and specific binding to targeted moieties, the treatment area is washed to remove unbound nanoparticles. Thereafter, coherent NIR laser light is administered to the treatment area (Huang et al. 2008). NIR light is not significantly absorbed by albumin, hemoglobin, water or other constituents making it biologically benign; however, the NIR sensitive nanoparticles will strongly absorb this coherent light which safely penetrates up to one cm into tissue (Hirsch et al. 2003). Due to the absorption of the laser energy, the nanoparticles

will convert the incident laser light energy to heat; thus depositing heavy doses of thermal energy to the biological target.

A number of NIR sensitive nanoparticles have been utilized to successfully administer PT therapy. The particles absorb light strongly in the visible region due to coherent oscillations of the metal conduction band electrons in strong resonance with the visible frequencies of light; a phenomenon called surface plasmon resonance (SPR) (Kerker et al. 1983). The SPR frequency is dependent on the size and shape of metal particles. Further, as the diameter size increases, the SPR wavelength maximum redshifts thus providing the capacity for absorption tunability. When nanoparticles form aggregates or assemblies, the SPR maximum shifts to the NIR. NIR-sensitive nanoparticles called gold nanoshells (NSs) are silica-gold core-shell nanoparticles (silica core diameter: 100-200nm; gold shell thickness: 5-20 nm) currently undergoing clinical assessment for tissue-specific photothermal therapy (Lal et al. 2008).

Nanoshells also have tunable plasmonic extinction peaks in the NIR that can be selected through the careful control of the core/shell thickness ratio of the silica/gold layers. The NIR extinction peaks of the nanoshells allow for the optimal heating of subdermal tissue for photothermal therapy upon co-localization with the targeted tissue (Gobin et al. 2007). Due to their outer gold surface, nanoshells are water soluble and their surfaces can be easily modified for cellular targeting and biocompatibility using thiol-functionalized monoclonal antibodies, peptides, antibiotics and biocompatible polymers linkers (Lowery et al. 2006). Because of this, nanoshells can be conjugated with surface

moieties that target resistant bacterial strains thus providing a platform for nanoparticle-mediated photothermal therapy at the site of infection.

Nanoparticle-mediated PTT has been performed with a number of different biological applications. Nanoshells have been co-conjugated with HER2-antibody and PEG biocompatibility polymers to be used to detect and destroy breast carcinoma cells *in vitro* (Loo et al. 2005). Further, PT tumor (subcutaneous injected murine colon carcinoma cells) ablation in immune-competent mice was achieved using gold nanoshells (O'Neal et al. 2004) showing the *in vivo* application of PTT. Even further, the pathogenic bacteria *Pseudomonas aeruginosa*, have been eradicated using targeted gold nanorods for PTT (Norman et al. 2007) showing the bacterial application of PTT. The combination of this background provides a suitable literature based backdrop that exposes the need for a novel treatment of MDR bacterial infections.

Nanotechnology-mediated Magnetic Extraction of Bacteria

Superparamagnetic iron-oxide nanoparticles (SPION) are magnetized only in the presence of an externally applied magnetic field. This is due to the presence of only one magnetic domain in a single particle. Without an applied field, the magnetic moments in a population of SPIONs are not aligned, resulting in no net magnetization and no particle-particle magnetic attraction (Ortega & Giorgio 2012). Core-shell nanoparticles can be formed when the SPIONs are coated with shells of gold possessing atomic-scale thickness to provide a surface for molecular functionalization while retaining nearly all of the superparamagnetic characteristics. Even further, surface functionalization (molecular

conjugation) can provide ligands for a specific target, producing a nanoparticle that can specifically bind to a desired molecular structure. Thereafter, the nanoparticle can transduce an applied magnetic field into a magnetomotive force which will mechanically transport the target structure toward the externally applied magnetic field. These FeOx/Au core/shell nanoparticles can also be self-assembled into larger particles through specific fabrication techniques or crosslinking of bifunctional molecules, (i.e colistin). This clustering increases the group magnetization thereby enhancing the magnetomotive potential of the nanoconstruct.

Innovative approaches have been devised including the development of extracorporeal devices aiming to mechanically cleanse bacteria from body fluids using magnetic particles. Most investigations utilize pathogen and endotoxin targeted magnetic nanotechnology with an external device acting as a filter or spleen mimic. A blood-cleansing extracorporeal device, inspired by the spleen, which continuously removes pathogens and toxins from blood has been previously described in the literature (Kang et al. 2014). Magnetic nanoparticles conjugated with mannose-binding lectin were developed forming a nano-engineered human opsonin. Magnets inside the device were used to pull opsonin-bound pathogens from the blood flowing through a microfluidic device at a >90% efficiency. Further, investigators have shown synthetic conjugates can been utilized for highly-selective, rapid separation of bacteria from whole blood with almost 100% clearance (Lee et al. 2014). These results support the relevance of extracorporeal *adjuvant* therapies as a potentially relevant treatment of bacteremia.

The use of extracorpeal devices for the adjuvant treatment of *A. baumannii* has not been described in the literature. Furthermore, no-robust motif for nanoparticulate targeting, to the *A. baumannii* surface has been described for these purposes. To initiate the development of such a treatment, robust nanoparticulate platforms possessing a combination of composite characteristics must be developed.

Design and Use of Novel Multilayered Magnetoplasmonic NPs in Biomedical Applications

My dissertation is organized into several manuscripts, one of which is already published at the time of this writing. These manuscripts outline the design of novel multilayered, magnetoplasmonic nanoparticles for the binding and depletion of *A. baumannii*. This dissertation identifies nanotechnology design problems, as well as a clinically-relevant application, and thereafter provides the nanoengineering solutions to implement a novel therapeutic approach. This was accomplished based on the following steps: (1) Design of novel, multilayered, magnetoplasmonic, core/shell nanomaterials which surpass previous constraints, (2) Optimization of nanoparticulate design and fabrication protocols to enhance the nanoparticulate composite characteristics, (3) Implementation of the multilayered, magnetoplasmonic nanomaterials to pioneer novel therapeutic strategies for *Acinetobacter baumannii* treatment *in vitro*.

CHAPTER II

THE MULTISTRATA NANOPARTICLE: A FeOx/Au CORE/SHELL ENVELOPED IN A SILICA-GOLD SHELL

The utilization of biomedical diagnostics and therapeutic advances including magnetic resonance imaging (MRI), computed (CT), photoacoustic (PAT) and photothermal optical coherence tomography (PT-OCT), photothermal therapy (PTT) have been shown to effectively detect and decrease pathological effects in a number of aggressive diseases such as head and neck cancer, colorectal cancer, and microbial diseases. However, the use of these modalities without the addition of contrast agents is limited as far as: (1) the lack of tissue discernment at site of disease due to challenges in imaging contrast; and (2) poor diagnostic and/or therapeutic localization at the site of action due to lack of active targeting. Core-shell nanoparticles have been utilized as targeted contrast agents in order to relieve the limitations of the modalities above. Core-shell nanoparticles are primarily designed in order to provide new properties based on the characteristics of each individual layer in a synergistic fashion. Specifically, metal nanoshells (NS, dielectric/metal nanoparticles) and metal-plated iron-oxide nanoparticles (FeOx/Au nanoparticles) have been implemented in order to both improve X-ray and magnetically based imaging contrast (CT, MRI, PAT, PT-OCT) based on the inherent properties of the materials in the nanostructure (Figure 1). Even further, the surface of these nanoparticles can be chemically modulated to target pathogenic tissue thus improving diagnostic imaging capacity and photonics-based therapeutic treatment to the site of disease. For patients who wish to undergo cross-modality diagnostic imaging and then request photonics-based

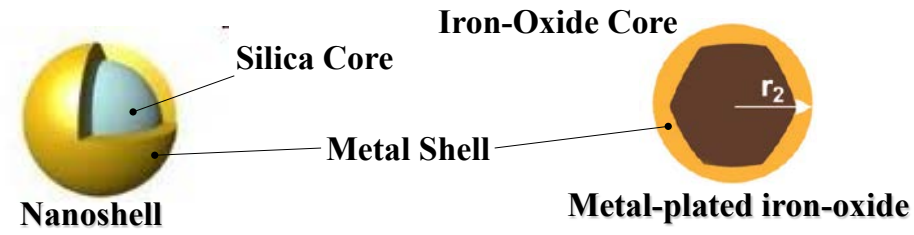

Figure 1. The interior structure of core-shell nanoparticles. The gold nanoshell (Au-NS), which is comprised of a dielectric silica core and gold shell, is shown to the left. The superparamagnetic gold-plated iron-oxide nanoparticle (FeOx/Au core/shell NP), which is comprised of an iron oxide core and a gold shell is shown on the right.

therapeutic treatment, multiple imaging contrast and therapeutic agents must be administered.

To alleviate this problem, I designed a nanomaterial that combines the properties necessary to enhance the imaging and therapeutic capacity of the above modalities while conserving the nanometer size and surface modification capability. The Multistrata nanoparticle is the culmination of tunable, dual-peak, UV-Vis-NIR spectrum extinction characteristics, tri-modal imaging contrast, simple synthesis and facile surface modification capability into a single <60nm diameter, novel, multi-functional, multilayered nanosphere. Seeking to relieve current methodological limitations by coupling diagnostics and therapeutics into one single theranostic tool, herein I will specifically describe particle fabrication and characterization. For further elucidation of the antimicrobial properties and functionality of the designed nanoconstruct, multiple plasmonically active metals will be included in the design of the nanomaterial, comparatively. For the purposes of this dissertation, the results provided in this chapter accomplished an important objective leading to the validation of the core hypothesis. Herein, we develop multilayered nanomaterials that combine at least two nanoscale characteristics into a single, nanoscale entity. Furthermore, results supporting the claims that: (1) a novel multilayered, magneto-metallodielectric, core/shell nanoparticle can be fabricated using a unique synthesis protocol; the (2) multimodal nanoscale characteristics and the (3) theranostic potential of the nanomaterial can be elucidated and will be reinforced herein thus fulfilling *Specific Aim 1* of this dissertation.

Introduction

Emerging materials and methods in biomedical imaging and biophotonics are improving patient outcomes. More specifically, the utilization of biomedical diagnostics and therapeutic advances in methods such as magnetic resonance imaging (MRI), computed tomography (CT) imaging, photoacoustic tomography (PAT), photothermal optical coherence tomography (PT-OCT) and targeted photothermal therapy (PTT) have been shown to effectively detect and decrease pathological effects in head-neck cancer (R. Popovtzer et al. 2008; M. Saksena et al. 2006), colorectal cancer (O. Will et al. 2006; T. Islam & M. Harisinghani 2009), and breast cancer (M. Yezhelyev et al. 2006). Optical (V. Runge 1999), MRI (L. E. Ginsberg et al. 1998), and CT (G. Antoch 2002) based imaging contrast of pathologic tissues, therapeutic localization at the site of action at the cellular level (N. Portney & M. Ozkan 2006), and the inability to unite diagnosis and treatment into a single entity (L. Johnson et al. 2010) continue to limit the practical power and application of these current emerging technologies. In order to relieve these limitations and couple diagnostics and therapeutics into a single theranostic material, we have prepared an enhancement technology via the synthesis of a novel, multi-functional, multilayered nanomaterial. Our approach provides tunable dual-peak (Vis-NIR) extinction characteristics, tri-modal (optical, MRI and CT) imaging contrast with easy synthesis and surface modification as a <60nm diameter nanosphere. This work describes our current progress regarding the preparation and initial characterization of the Multistrata Nanoparticle (MSNP).

Multilayered, core/shell nanoparticles have been previously described (Schärtl 2010; Hirsch et al. 2006; R. Hao et al. 2010; M Melancon & C Li 2009). Classified as inorganic or hybrid (organic-inorganic), core/shell nanoparticles are designed to provide

new properties based on the characteristics of each individual layer in a synergistic fashion. Rational design principles can be employed to create nanomaterials with functional applications such as tissue specific recognition, image contrast and therapeutic delivery can be simultaneously enhanced with a single nanoscale platform. For example, FeOx/Au, or iron-oxide/gold core/shell nanoparticles, have been synthesized to utilize both the magnetic relaxivity of the FeOx and surface plasmon resonance properties of the spherical gold shell (J. Aaron et al. 2006; B. Brinson C. Levin, et. al 2008; L. Wang et al. 2008). These nanoparticles have been implemented for simultaneous MR image contrast with cancer phototherapy (D. Kirui & C. Batt 2010). SiO_2/Au nanoshells, or silica/gold core/shell nanoparticles, have been clinically assessed for tissue-specific photothermal therapy (Hirsch et al. 2006) optimized for *in vivo* use by design of the surface plasmonic properties of the nanomaterial. Unlike FeOx/Au nanoparticles, which have plasmonic extinction peaks in the visible spectrum, extinction peaks in the near-infrared (NIR, 700-1200 nm) can be achieved by control of the core/shell thickness ratio of the silica/gold layers. Extinction peaks in the NIR allow for the optimal heating of subdermal tissue for photothermal therapy (Hirsch et al. 2003) and efficient optical imaging. Harnessing the surface plasmon resonance properties of core/shell materials, the nanosphere-in-a-nanoshell (i.e. the "gold nanomatryushka") was synthesized and demonstrated to provide specific extinction maxima in the UV-Vis-NIR spectrum that are associated with the nanoscale structure (Bardhan et al. 2010). A multilayered, metallodielectric nanostructure, the nanomatryushka consists of a gold nanosphere surrounded by concentric silica/gold shells. Governed by surface plasmon hybridization theory (Halas 2004), concentric metal layers separated by a dielectric spacer layer causes plasmon interactions which generate

multi-peak extinction UV-Vis-NIR spectra. The location of the multi-extinction peaks are controlled by the metal shell and dielectric layer geometric ratio allowing for specific "tunability" of the optical characteristics of the nanostructure.

The Au Multistrata nanoparticle (Au-MSNP) is inspired by the material characteristics of its predecessors, the FeOx/Au nanoparticle and Au-manomatryushka. Designed to exhibit MRI contrast, X-ray contrast for CT, photonic contrast for OCT, absorbance in the NIR for PTT, tunability of extinction characteristics during fabrication, theranostic potential, easy surface modulation for cellular targeting and biocompatibility and a nanostructure diameter of <60nm to support vascular extravasation ability, the fabrication of each 'primary' and 'subsidiary' *strata* – or functional layer – must be carefully controlled through fabrication methods. We report here our preliminary findings regarding the multi-step fabrication and initial characterization of the Au-MSNP. Furthermore, we specify methods necessary to fabricate extremely thin shells (as small as 1-2 nm to maintain an overall particle diameter less than 60 nm) and to ensure magnetic material retention throughout the fabrication process. Relaxometry characterization, suggesting MRI contrast capacity, is reported.

Materials and Methods

Fabrication of γ-Fe_2O_3 core Nanoparticles: γ-Fe_2O_3 with 12 ±1 nm diameter were fabricated by a thermal decomposition, aeration and reflux protocol previously described (K. Woo et al. 2004). Briefly, 20 ml of octyl ether (Sigma-Aldrich, St. Louis, MO) and 1.92 ml of oleic acid (Sigma-Aldrich) were stirred under N_2 gas flow and reflux. The sample was heated to 100ºC prior to addition of 0.4 ml $Fe(CO)_5$ (Sigma-Aldrich). The reaction was heated from

150ºC to 280ºC where the reaction solution color changed from boil, to orange, orange/colorless, to very dark orange. Sample was aerated at 80ºC for 14 hours and refluxed while boiling for 2 hours. The γ-Fe_2O_3 cores were centrifuged (15 min, 770 rcf) and washed in ethanol (EtOH, 200 proof, Sigma-Aldrich) twice, and dried under air.

Amination of γ-Fe_2O_3 core Nanoparticles: 150 mg of γ-Fe_2O_3 core (FeOx) were coated with the first strata using a modified (3-aminopropyl)triethoxysilane (APTES, Sigma-Aldrich) functionalization procedure. Core particles were added to 40 ml of tetrahydrofluran (THF, Thermo Fisher Scientific, Waltham, MA) and stirred briskly using a magnetic stir plate and stirring rod. 5 ml of APTES was added to the reaction solution and thereafter spiked with 5 µl of acetic acid (Sigma-Aldrich), 516 µl of MilliQ (18 MΩ) DI H_2O, and stirred for 48 hours. The reaction flask was then placed in an oil bath and heated to 80ºC. EtOH was used to replace evaporated THF throughout the 2 hour boiling period. Reaction solution was concentrated via rotovap to 40 ml of EtOH. Hexane was added to the solution in a 4:1 ratio and centrifuged (10 min, 800 rcf). Recovered FeOx-NH_2 nanoparticles (NPs) were resuspended in EtOH and stored at room temperature where they remained stable throughout the length of this study (>5 months).

Gold Plating of FeOx-NH_2 Nanoparticles: FeOx-NH_2 nanoparticles were plated with a gold layer, the second strata, as adapted from the literature (W. Wu H. Chen, J. Tang and L. Nie 2007). Sonicated FeOx-NH_2 nanoparticles (~1.5%wt) were added in equal volume to DI H_2O-based,1% $HAuCl_4$ (Sigma-Aldrich, dark aged 24-72 hours) under ultrasonic perturbation. 20 mM sodium citrate in DI H_2O was added dropwise under sonication until

the light yellow-brown color of the reaction solution changes to a dark purple. The solution of AuFeOx-NPs was washed via centrifugation (5 min, 800 rfc) and resuspended in EtOH and stored for 18 hours at 4ºC where they remained stable for 5 months.

Silica Coating and Silanization of AuFeOx Nanoparticles: AuFeOx NPs were coated with a silica layer, the third strata. 1 ml of AuFeOx NPs in EtOH from the previous step was added to 5 ml of fresh EtOH. Under ultrasonic perturbation, 35 µl of 0.4% NH_4OH and 25-50µl of 10 mM ethanolic tetraethyl orthosilicate (TEOS, Sigma-Aldrich) were added. Sonication was continued at room temperature for 45 minutes and thereafter stored at 4ºC for 24 hours. SiO_2AuFeOx NPs where coated with *N*-*n*-butyl-aza-dimethoxysilacyclopentane (cyclic silane, Gelest, SIB1932.4), the fourth strata, as adapted from the literature (Bardhan et al. 2010). 400 µl of 1 mM ethanolic cyclic silane was added under ultrasonic perturbation to the ethanolic suspension of SiO_2AuFeOx-NPs. The solution of NH_2-SiO_2AuFeOx NPs was stored at 4ºC for 24 hours where they remained stable until completely utilized (>3 months).

Decoration of NH_2-SiO_2AuFeOx Nanoparticles: Additionally adapted from literature (Hirsch et al. 2005), NH_2-SiO_2AuFeOx NPs were decorated through emersion in Duff (D. Duff et al. 1993) gold colloid (2-4 nm, dark-aged for 3 weeks in 4ºC) in a 1:4, particle to colloid ratio. Briefly, 1 ml of NH_2-SiO_2AuFeOx was mixed with 4 ml of Duff Au colloid. This mixture was left unperturbed at room temperature (20-23ºC) for 24 to 96 hours, centrifuged (10 min, 800 rcf), supernatant removed via magnetic assisted aspiration and resuspended in 1 ml of MilliQ DI H_2O via ultrasonic sonication. More specifically, magnetic assisted aspiration is

conducted via a 1 Tesla neodymium 1" cube magnet (CMS Magnetics, Plano, TX) placed at the bottom of the reaction vial in order to retain magnetic material in its pellet form during aspiration. These decorated particles were immediately used for the next step.

Electroless Gold Plating of Decorated $SiO_2AuFeOx$ Nanoparticles: The final gold layer was fabricated by seed-mediated electroless plating as from literature (Hirsch et al. 2005). Decorated particles were vigorously mixed with a 1%$HAuCl_4$-K_2CO_3 plating solution in a 1:10 ratio. Briefly, 25 mg of K_2CO_3 (Sigma-Aldrich) was added to 100 ml of H_2O where 1% $HAuCl_4$ (dark-aged for 14 days prior) was added and dark-aged for 96 hours. 10 µl of H_2CO (Sigma-Aldrich) was added as a catalyst which began the release of Au ions thus causing a color change from clear to bright pink. Following a 10 min reaction time, particles were centrifuged (10 min, 800 rcf) and the supernatant was removed via magnetic assisted aspiration. Completed Multistrata nanoparticles were re-suspended in 1 ml of EtOH, thus quenching the plating solution, and stored at 4ºC for further characterization. For storage longer than 10 days, MSNPs were re-suspended in 1 ml of 1.8 mM K_2CO_3 at 4ºC.

Silver Multistrata Nanoparticle Fabrication. Silver MSNPs were fabricated similarly to their gold counterpart. Briefly, in fabrication steps where gold (1% $HAuCl_4$) was added to a reaction, silver (0.431% $AgNO_3$) was added as a substitute. To fabricate FeOx/Ag core/shell nanoparticles, 0.431% $AgNO_3$ was added dropwise and mixed 1:1 with aminated γ-Fe_2O_3 cores in the presence of sodium citrate and under vigorous ultrasonic agitation. The Au Duff colloid analog, Ag-THPC nanoparticles, were synthesized. Briefly, THPC-stabilized Ag nanoparticles were synthesized by adding 1.2 ml of 1M NaOH to 180 ml of

MilliQ H2O in a 250 ml beaker. A small stir bar was added and the reaction mixture was allowed to stir at 50% max rate for 5 minutes. 4 ml of 0.95% THPC (Tetrakis (hydroxymethyl) phosphonium chloride) solution was added, and the reaction mixture was allowed to continue stirring for 5 minutes. The entire reaction solution was then added to a fresh reaction vessel, and 69 µl of 0.04% NH_4OH was added, and 6.75 ml of $AgNO_3$ (0.431% soln) was added under 100% vortex level. The color changed from clear to a brown, dark brown "cola" color. To form Ag precursor particles, 400 µl of THPC-Ag nanoparticles were added to 100 µl of FeOx-Ag-SiO_2-NH_2 precursor nanoparticles. Upon mixing, an immediate color change occurred, causing the solution to turn dark amber red. After approximately 45-60 seconds, the color changed to redish purple, supporting the conclusion that FeOx-Au-SiO_2 nanoparticles were decorated with the Ag particles. These particles were immediately measured for their extinction characteristics. After seeding the Ag precursor nanoparticles, the final Ag layer was plated in a similar manner to the final gold layer in the Au-MSNPs. A thickness of <3 nm of silver is preferred to maintain plasmonic interactions.

Particle Characterization: Multistrata nanoparticles were characterized by obtaining transmission electron microscopy (TEM) Phillips CM20 microscope and spectroscopic extinction measurements using a Varian Cary 50 UV-Vis-NIR spectrophotometer. Relaxometry measurements were obtained on a Maran DRX-II 0.5T NMR spectroscopic scanner following sample preparation using 5 ml of 1X PBS as a solvent. Whole sample spectroscopic T2 relaxation measurements were made with a Carr-Purcell-Meiboom-Gill (CPMG) sequence with the following parameters: relaxation time (TR) = 30 seconds, echo time (TE) of first echo = 6ms, spacing of subsequent echoes = 2ms, and 1200 echoes. Zeta

potential measurements were performed on a Malvern Zetasizer (Malvern Instruments, Westborough, MA) following sample preparation using 1 ml of 1.8 mM K_2CO_3 as a solvent. MSNP size and statistical distributions were estimated from TEM images using Amt V600 and ImageJ software.

Results and Discussion

In order to generate a FeOx/Au enveloped in an SiO_2/Au shell, the Multistrata nanoparticle resembles a single core - five layer "onion," each strata possessing a specific function (Figure 2). The core fabrication begins with the generation of γ-Fe_2O_3 superparamagnetic iron-oxide nanoparticles by thermal decomposition of $Fe(CO)_5$ in the presence of oxygen after aeration and reflux as described previously (K. Woo & 2004). Such synthesis provides the oleic acid surface chemistry suitable for subsequent chemical modification. The first subsidiary strata, APTES [(3-aminopropyl)triethoxysilane], displaces the oleic acid in an exchange reaction and acts as a coupling layer between the γ-Fe_2O_3 (FeOx) core and the initial gold layer to be applied. The APTES coating provides -NH_2 groups that have a high affinity for Au^{3+} ions to facilitate the initial gold coating. Conventional aminoxysilane reactions, like those that utilize APTES, involve single solvents such as DI H_2O, ethanol (EtOH), toluene and tetrahydrofuran (THF) and are fully detailed in synthetic chemical literature[23]. One particular modification to the conventional APTES reaction was the necessity to perform multiple solvent exchanges throughout to optimize APTES deposition, -NH_2 availability, and magnetic material recovery. THF was used as the primary solvent due to its ability to maximize APTES localization on the surface of the FeOx cores through

both specific and non-specific bonding(I. Bruce & T. Chen 2005). The reaction solution was spiked with a small amount of MilliQ H_2O to catalyze the reaction and acetic acid to balance

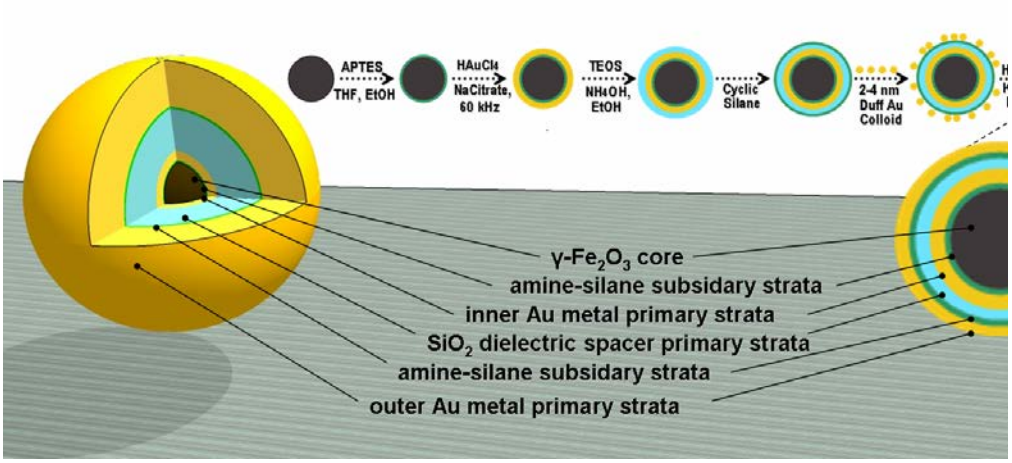

Figure 2. Schematic representation of the gold multistrata nanoparticle (MSNP) structure and the stepwise multistrata fabrication protocol.

the reaction solution at pH ~ 6.5. The THF was exchanged and washed with EtOH to release the non-specific APTES adsorption. When suspended in EtOH, the aminated FeOx cores are highly colloidal and difficult to sediment by centrifugation; therefore, the washed cores were added to hexanes to prepare the material for purification and extraction through centrifugation. Following three purification cycles, the FeOx-NH_2 particles were suspended and stored in EtOH in preparation for the deposition of the first gold layer.

Utilizing the high affinity of $-NH_2$ groups and Au^{3+} ions, a thin gold shell – the first primary strata - can be added to the surface of the FeOx-NH_2 nanoparticles using a specific sonochemical plating, or sonoplation, method. This method of gold deposition employs the physiochemical effects of ultrasound which arise from acoustic cavitation. This effect can be physically described as the implosive collapse of bubbles formed at the surface of the FeOx-NH_2 nanoparticles. Through adiabatic compression, this collapse generates a localized hotspot due to the formation of a shockwave within the gas phase of the collapsing bubble. In their sonochemistry review, Mason and Lorimal described the empirically determined extreme, transient conditions of 5000 K temperatures, pressures of 1800 atm and cooling rates beyond 10^{10} K s^{-1} at these hotspots (T. Mason & J. Lorimal 2002). This extreme local environment formed by the sonoplation reaction produces similar conditions generated through conventional "high-heat, high-stir rate" nanoparticle and nanolayer formation methods implemented throughout nano-literature. Due to the inherent chelating ability between juxtaposed Au^{3+} ions liberated from $HAuCl_4$ and available $-NH_2$ groups, a thin layer of gold may be *quickly* deposited onto the surface of the FeOx-NH_2 through the use of sodium citrate as a reducing agent and the sonoplation

ultrasonic frequency as a reaction catalyst (Wu et al. 2007). A distinct color change from a flocculated (due to immediate repulsive electrostatic interactions prior to Au^{3+} liberation by the sodium citrate) yellow-brown mixture to a black-purple, fully colloidal suspension, following the induction of the reducing agent and catalyst, signals the generation of FeOx/Au core/shell particles, the FeOx/Au nanoparticles. This addition of an outer gold shell was substantiated by the appearance of a surface plasmon resonance extinction maxima ($\lambda_{max} \sim$ 540-570 nm) in the sample absorbance spectra which is not evident in the FeOx nanoparticles (Figure 3). In addition, high-resolution TEM images shown in Figure 3 document the detailed formation of gold "plates" on the iron oxide surface and the development of gold fringe patterns (111 planes, 0.24 nm) consistent with well characterized images in electron microscopy literature.[26]

The dielectric silica layer is deposited by sonoplation. Under ultrasonic agitation, tetraethyl orthosilicate (TEOS) mixed with an alkaline initiator (NH_4OH) deposits as a SiO_2 layer. Thickness of the SiO_2 is controlled by the ratio of particle volume to TEOS volume. This modulation is documented by example in Figure 4b in which volume variation of TEOS between MSNP batches yields differences in the location of the plasmon maxima in the NIR. Extinction maxima shifted from λ_1= 533 nm and λ_2=705 nm to λ_1= 533 nm and λ_2=763 nm when an additional 25 µl of TEOS was provided. An intermediate strata was added to aminate the surface of the silica in preparation for gold deposition. The addition of *N*-*n*-butyl-aza-2,2-dimethoxysilacyclopentane (cyclic silane) was used to avoid the multi-step process required by APTES amination and to reduce the possibility of particle flocculation due to the generation of reaction side products and self-polymerization

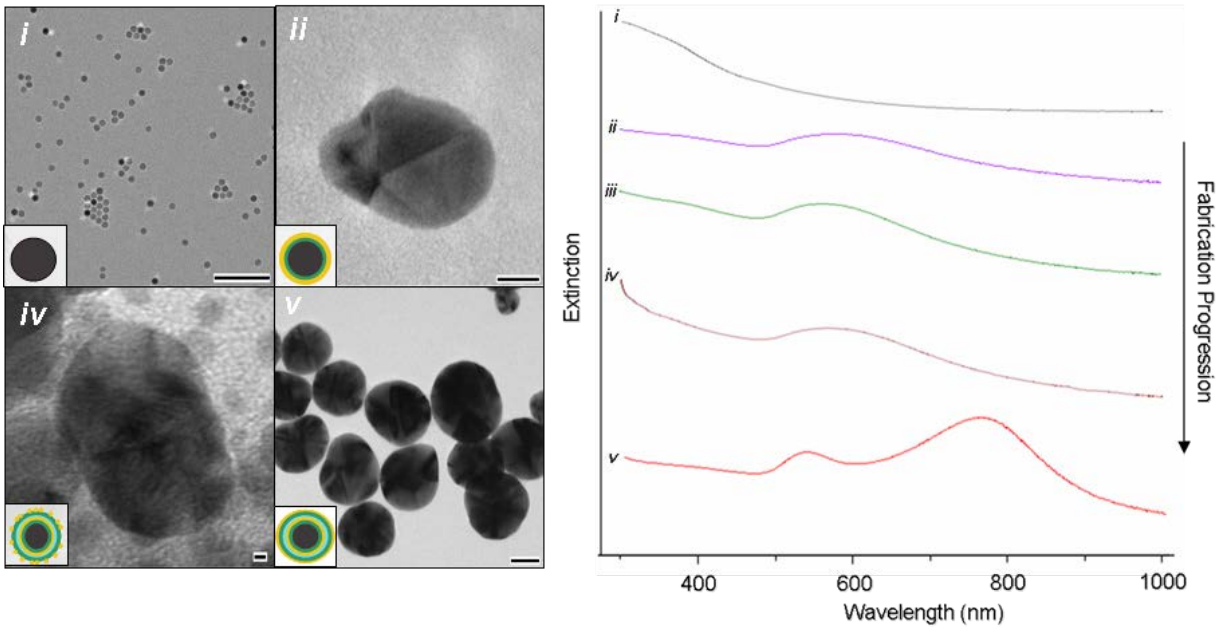

Figure 3. The multistep fabrication of the Multistrata nanoparticle (MSNP) was confirmed by TEM (*i-ii, iv-v*) showing images of resultant primary strata and the concordant UV-Vis-NIR (*i-v*) spectra of the products of each step. More specifically: (*i*) FeOx nanoparticles of radius r_1 = 6 nm; (*ii*) AuFeOx nanoparticles (r_1 = 6, r_2 = 10 ± 2 nm); (*iii*) SiO_2AuFeOx nanoparticles (r_1 = 6, r_2 = 6.45 ± 0.2, r_3 = 7.2 ± 0.3 nm) and those particles decorated by surrounding AuDuff colloid of 2-5 nm radius (*vi*); (*v*) Complete MSNPs, AuSiO_2AuFeOx (r_1 = 6, r_2 = 6.45 ± 0.2, r_3 = 8.3 ± 0.5, r_4 = 21 ± 5 nm). Scale bars for TEMs *i, ii, iv,* and *v* are 100 nm, 5 nm, 1 nm, and 20 nm, respectively. Insets are schematics corresponding to that particular fabrication step from Figure 2.

(Bardhan et al. 2010). Following the silanization of the silica surface, the available -NH_2 sites were decorated with 2-5 nm Duff Au colloids (D. Duff et al. 1993) which act as nucleation or "seed" sites for subsequent gold deposition. We speculate that Au decoration of these particles is consistent with the existence of a peak in the 900 nm wavelength range suggestive of plasmonic interactions between the decorated gold particles, which are aggregating over the surface area of the precursor particle, and the inner Au strata shown in Figure 3. The final strata, a complete outer Au layer, was catalyzed onto the decorated particles through the reduction of Au ions from a 1% $HAuCl_4$ solution in the presence of H_2CO – a formaldehyde electroless plating reaction (B. Brinson et al. 2008). The deposition of this final layer is supported by the change in surface plasmon extinction spectra of the MSNP and the formation of a metallic-gold outer layer (Figure 3*v*). The characteristic double-peak spectra of a multilayered, gold-dielectric-gold material appears following electroless plating (Figure 3*v* and Figure 4b). In order to maintain the stability of the outer Au strata, particles were resuspended in 1.8mM K_2CO_3 which acts as a stabilizing agent. A zeta potential of -75.6 ± 0.902 was measured to confirm the stability of the MSNPs in this solution. This negative charge is also consistent with the existence of -CO_3^{2-} ions stabilizing the Au surface. As for gold nanoparticles, which present the same surface chemistry, these stabilizing ions are easily place-exchanged with a number of conjugates that proximally present amine, sulfhydryl or other functional groups. From a surface modification perspective, MSNP behavior is the same as for other gold surfaces, for which many robust methods are well known to provide a wide range of molecular coatings. These fabrication reactions yield monodisperse batches of MSNPs as shown in Figure 4c. In addition, these reactions are scaleable making the fabrication of bulk quantities possible.

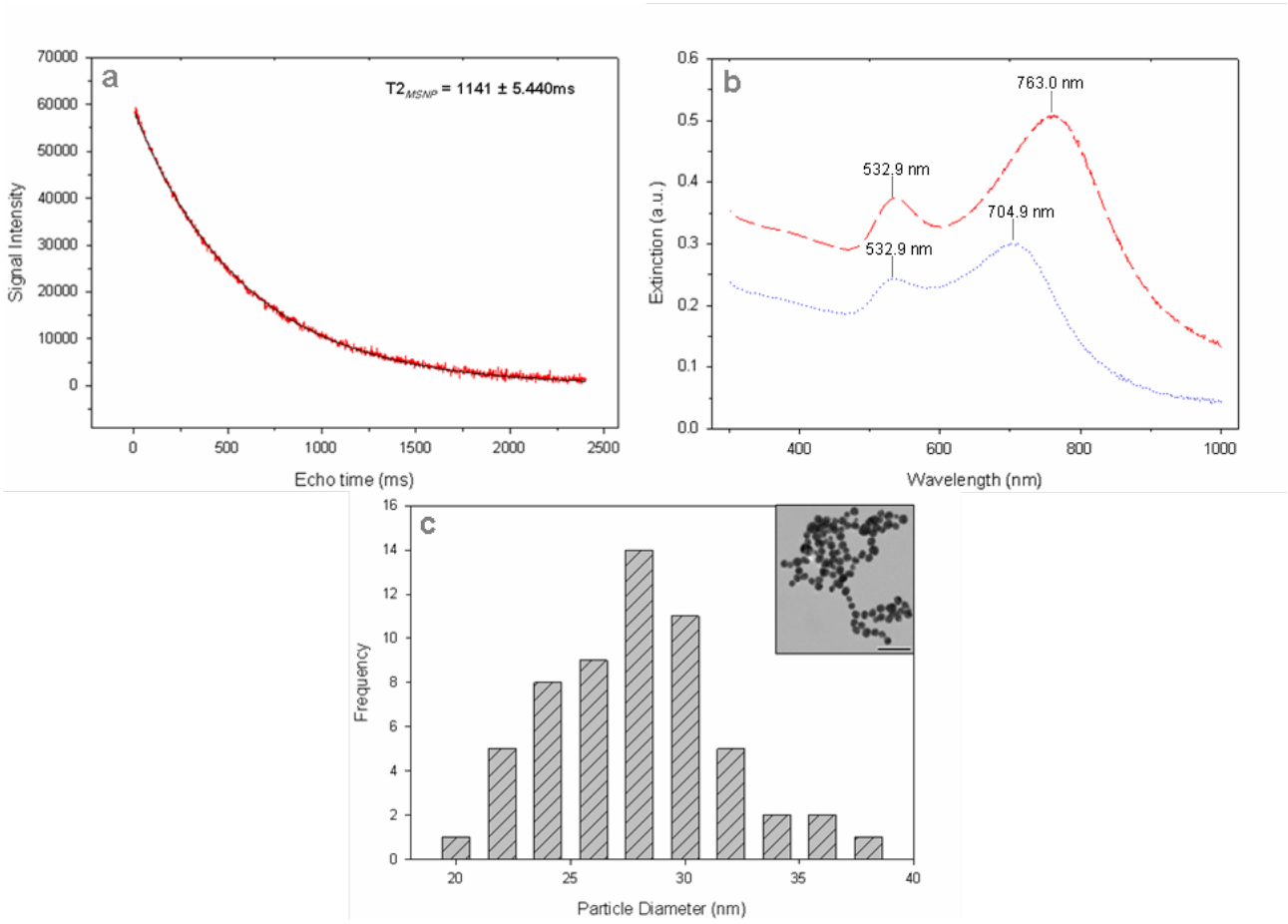

Figure 4. (a) Relaxometric response of multistrata nanoparticles (MSNP) at an absorbance of 0.1098 a.u. T2 relaxation curve fit was conducted with a 95% confidence interval (n=4) of 2.72ms. (b) Differences in the SiO_2 to outer Au layer ratio between MSNP trials *i* (r_1 = 6, r_2 = 6.45 ± 0.2, r_3 = 8.3 ± 0.5, r_4 = 21 ± 5 nm) and *ii* (r_1 = 6, r_2 = 6.45 ± 0.2, r_3 = 7.3 ± 0.6, r_4 = 17 ± 4 nm) caused an extinction shift in the NIR. (c) Diameter histogram providing the resultant dispersion properties of a sample batch of MSNP. Diameters average 26.8 ± 3.7 nm based on analysis of TEM images. Inset is a sample TEM with the scale bar representing 100 nm.

For more than half a decade, gold nanotechnology has been shown to act as X-ray and computed tomography contrast agents, increasing the utility of each technique imaging biological samples (J. Hainfeld et al. 2006). MSNP capacity for MRI contrast can be evaluated through relaxometric measurements. Prior to sample preparation, the extinction peak located in the visible spectrum was measured at 0.1098 a.u. The MSNPs exhibit a T2 relaxation time at 1141 ± 5.4 ms fit via a 95% confidence interval based on four repetitions. This relaxation time can be differentiated from the T2 values of healthy human tissue[30] and are predicted to alter the relaxation times of proximal tissues. These results support the MR contrast capacity of MSNPs.

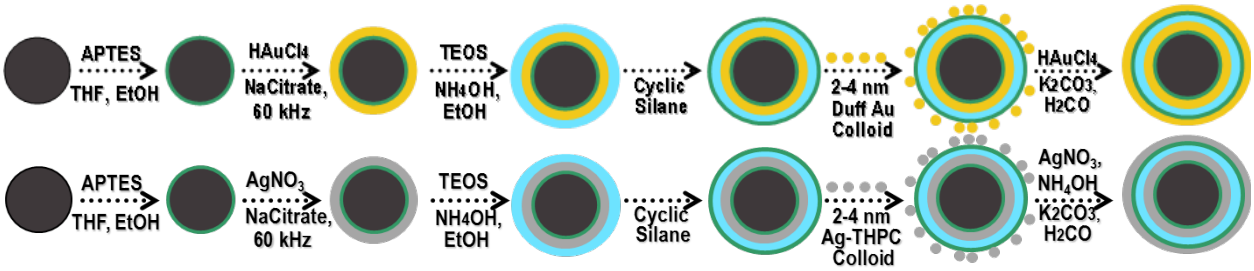

Figure 5. Stepwise Comparison of Gold (top) and Silver Multistrata Fabrication Protocols

To further support the design and functionality of the MSNP, gold was replaced with silver, another plasmonically active metal, during the synthesis process as shown in Figure 5. In this figure, the Au-MSNP and Ag-MSNP synthesis processes are compared in a stepwise fashion. The gold was completely substituted for silver to such an extent that the development of Ag-THPC nanoparticles (Woo 2014) was included as a substitute for the Duff Au colloids. This stark substitution was deliberate to ensure that Ag-MSNP plasmonic

results could only be attributed to the effect of the silver-dielectric-silver concentric shells and not due to the presence of gold in the particle architecture.

Upon comparing the extinction characteristics of the Au-MSNPs and Ag-MSNPs it is clear that there is value in modifying the plasmonically-active metal which comprises the nanoconstruct. As shown in Figure 6, Ag-MSNP extinction peaks deviate from Au-MSNP peaks where the first peak appears at the interface of the long wave UV and visible spectrum. Furthermore, the second peak appears in the visible but can be tuned into the NIR. These results support the hypothesis that a multilayered, metallodielectric nanoparticle which has combined multiple nanoscale characteristics into a single <60 nm nanoconstruct could be developed. Furthermore, Ag-MSNPs could provide double the therapeutic value due to the coupling of the inherent antimicrobial behavior of Ag at the surface of the material with the ability to tune the plasmonic characteristics of nanoconstruct to enable photothermal therapy.

It should be reiterated and appreciated that the fundamental difference between Au and Ag containing MSNPs is their plasmon active metal (Bell & Yu 2011). Varying the plasmonic metals that comprise the nanoconstruct generates different MSNPs for different usage and applications. For example, silver MSNPs generally have secondary peaks in the 500-700 nm "visible" spectrum, thus eliminating their potential for use in NIR photothermal therapy via NIR laser irradiation, In contrast, gold particles are generally NIR sensitive and may be used in photothermal therapeutic procedures. However, as shown above, silver MSNPs can be designed to absorb in the NIR. However, their

absorbance in this spectral range is minimal in comparison to their gold counterparts. Further, silver has documented bactericidal properties which could be leveraged in a number of external medical applications. *In vivo* uses of silver are

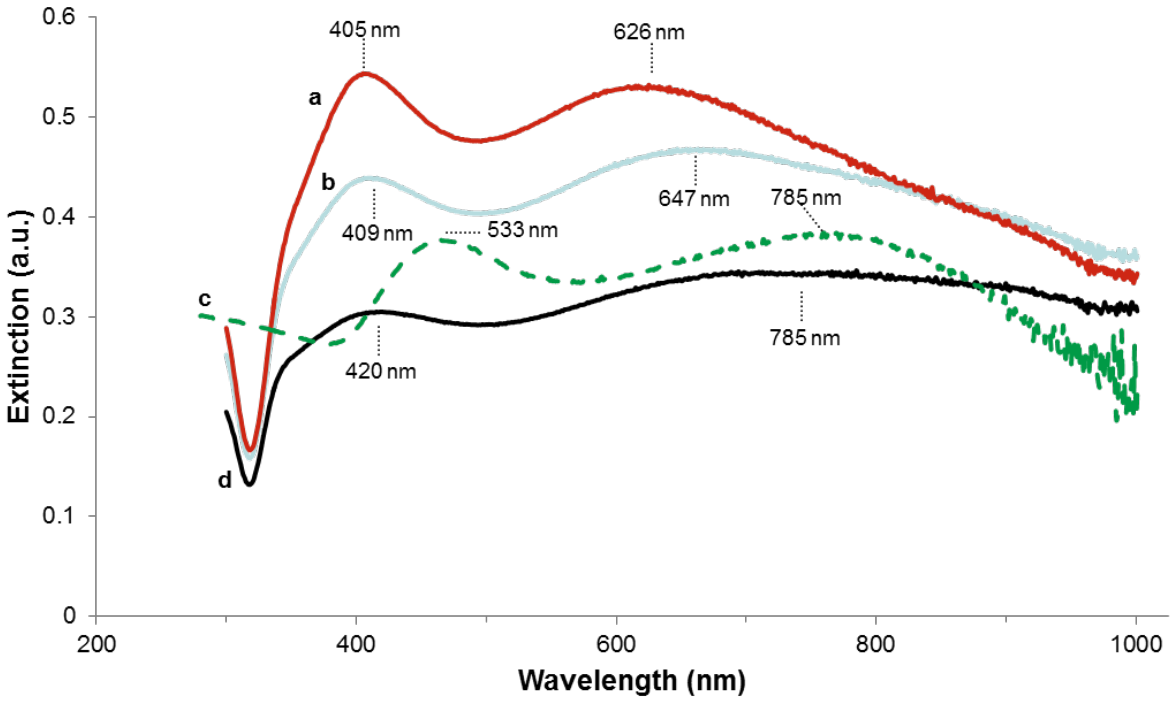

Figure 6. Comparative extinction properties of Au-MSNPs (c; dashed) and Ag-MSNP batches (a, b, d) of varying TEOS reactant volumes (37.5, 25, and 50 µl, respectively) - and thus SiO2 strata radii. It should be noted that the first extinction peak distinguishes the two particle types yet the second peak allows for NIR based multimodal theranostic applications in *both* gold and silver particle types.

not widely studied as there are fears of toxicity in humans and laboratory animals. Both of these particles could be utilized in a number of laboratory-based or clinical (Au-MSNPs) imaging applications. New (cutting-edge) hybrid imaging modalities which depend on the

combined biomagnetophotonic properties of their imaging contrast agents could employ both Au-MSNPs and Ag-MSNPS as potential contrast agents.

Conclusions

In conclusion, we have demonstrated the fabrication of a single core, five layered nanostructure with the potential capacity for both CT and MR imaging contrast. This contrast agent may allow for the simultaneous use of both technologies as well as other hybrid imaging modalities. Furthermore, we have characterized these particles for their metallodielectric properties and have measured dual-peak UV-Vis-NIR extinction spectra. We have also shown evidence of the geometric-dependent 'tunability' of the optical extinction characteristics. This tunability will allow predictable optimization of the nanoparticulate performance based on controllable synthesis conditions. We speculate that this technology can be further applied for laser absorption and consequent thermal characteristics in the NIR. Successful demonstration of significant optical absorption and heat generation is consistent with future applications in theranostic disease treatment.

Summary

A nanoconstruct that combines the properties necessary to enhance the imaging and therapeutic capacity of the above modalities while conserving the nanometer size and surface chemical modification capability was designed, fabricated and characterized. Furthermore, a comparable variant of the nanoconstruct was fabricated and characterized to further substantiate the results and conclusions of the study. The Multistrata nanoparticle is the culmination of tunable, dual-peak, UV-Vis-NIR spectrum extinction characteristics, tri-modal imaging contrast, simple synthesis and facile surface modification capability into a single <60nm diameter, novel, multi-functional, multilayered nanosphere. Through careful design, we have coupled diagnostics and therapeutics into one single

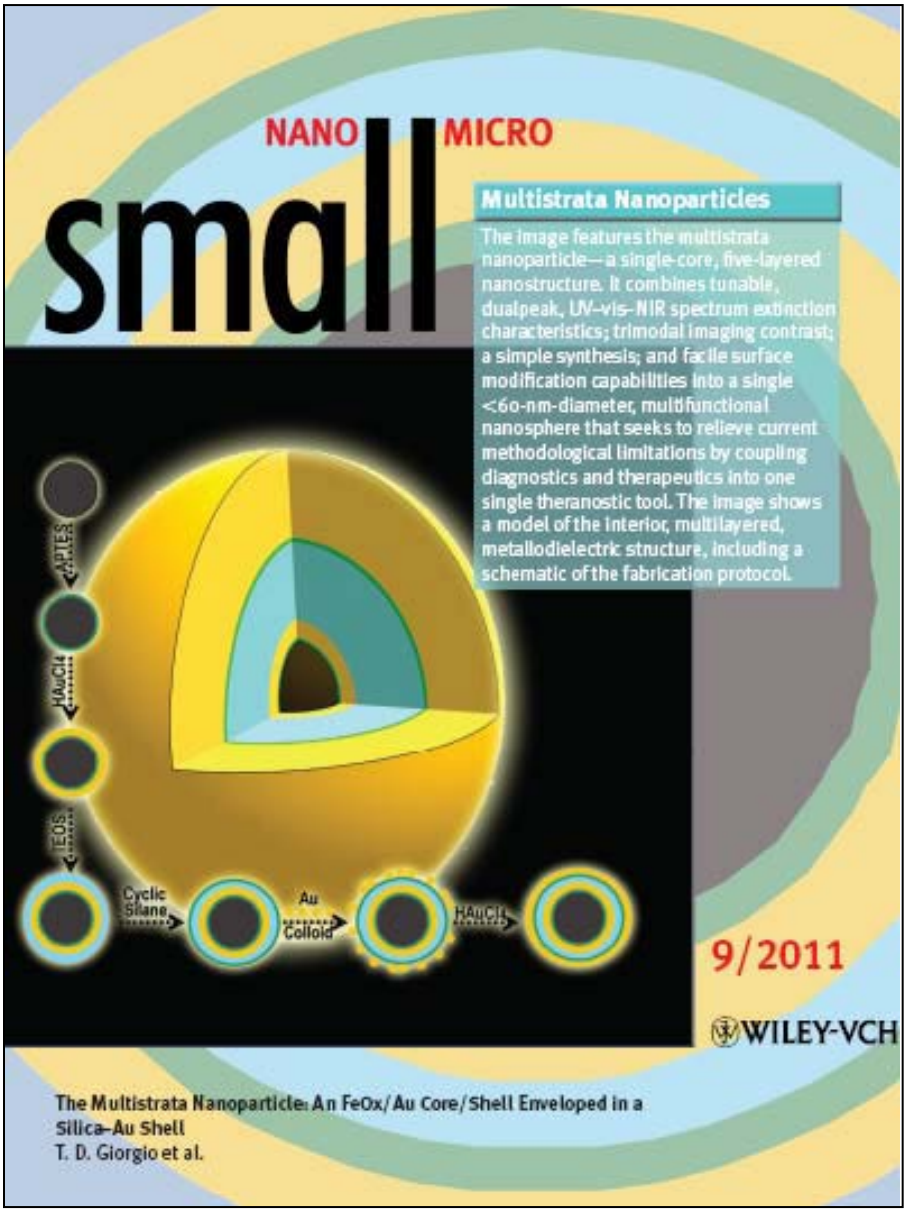

Figure 7. The Multistrata Nanoparticle was featured on the Frontispiece, reserved for highlighting articles that present outstanding results, of the renowned, peer-review journal *Small* (ISI IF 2011: 8.349).

theranostic tool to alleviate current methodological limitations. For the purposes of this dissertation, the results provided in this chapter accomplished an important objective leading to the validation of the core hypothesis. We have developed multilayered nanomaterials that combine at least two nanoscale characteristics into a single, nanoscale entity. Furthermore, results support the claims that: (1) novel multilayered, magneto-metallodielectric, core/shell nanoparticles were fabricated using a unique synthesis protocol, the (2) multimodal nanoscale characteristics and the (3) theranostic potential of the nanomaterial were successfully elucidated and described herein thus fulfilling *Specific Aim 1* of this dissertation. Even further, I am very proud that this work was featured on the Frontispiece of Volume 7, Issue 9 of the premier nanoscale/microscale peer reviewed journal, *Small* (Bell et al. 2011). This spot is reserved for highlighting articles that present outstanding results. In summary, I have provided a sample of this achievement in Figure 7.

CHAPTER III

SONOCHEMICAL SYNTHESIS AND TOMOGRAPHIC CHARACTERIZATION OF SUPERPARAMAGNETIC FeOx/Au CORE/SHELL COMPOSITE NANOPARTICLES

Core/shell nanomaterials have become an increasingly significant sector of the nanotechnology field (Chaudhuri & Paria 2012) and have been applied in a multitude of applications, most notably in the biomedical domain (Chatterjee et al. 2014). Hybrid materials can be designed to exhibit a multiplicity of properties depending on the composite materials present and the orientation at which those materials comprise the nanoparticle. This ability to integrate a multiplicity of properties into a single nanometer length scale embodiment is of significant impact. Inorganic magentoplasmonic core/shell nanomaterials are of considerable interest as they possess both the plasmonic and magnetomotive properties necessary for a multitude of theranostic applications. However, for biological applications, the ability to rapidly synthesize these nanomaterials to achieve the desired nanoparticulate characteristics is paramount. A sonochemical synthesis procedure will be utilized to reduce the overall duration of synthesis while ensuring the decreased magnetic relaxivity and increasing the magnetomotivity of the nanoparticles. The effects of this change in synthesis protocol on the plasmonic, magnetic and morphologic characteristics of the nanoparticles will be elucidated. Furthermore, for the first time, scanning transmission electron tomography will be utilized to further elucidate the morphology of the resultant magnetoplasmonic iron-oxide/gold core/shell nanomaterials. For the purposes of this dissertation, the results provided in this chapter will accomplish an important objective leading to the validation of a portion of the core

hypothesis. Herein, we develop multilayered nanomaterials that combine at least two nanoscale characteristics into a single, nanoscale entity. Furthermore, results from this chapter will fulfill the goals in *Specific Aim 2* of this dissertation. I will show that multilayered, magnetoplasmonic core/shell nanoparticles can be fabricated by adapting the synthesis protocol used in Chapter II. Furthermore, I will show that the magnetic properties of the magnetoplasmonic nanomaterials will be enhanced to provide magnetomotive functionality. I will also describe a revised fabrication strategy which will decrease the overall synthetic period. This will enable rapid fabrication and use of fresh nanomaterials for future biological applications.

Introduction

Core/shell nanomaterials have become an increasingly significant sector of the nanotechnology field (Ghosh Chaudhuri & Paria 2012) and have been applied in a multitude of applications, especially in the biomedical domain (Chatterjee et al. 2014). Core/shell nanoparticles are primarily composed of two or more separate phases which possess differing structure or chemical composition (Runowski 2014). Such hybrid materials can be designed to exhibit a multiplicity of properties depending on the composite materials present and the orientation at which those materials comprise the nanoparticle. This ability to integrate a multiplicity of properties into a single nanometer length scale embodiment is of significant impact and has remained state of the art for over a decade (Wolfgang Schärtl 2010).

Classes of core/shell nanomaterials include: concentric-spherical (Shakhov et al. 2014), hexagonal (Yuan et al. 2014), multi-core/single shell (H. Wang et al. 2011), nanomatryushka (Bardhan et al. 2010) or movable core within a hollow shell core/shell nanoparticles (Shevchenko et al. 2008). Although the most notable of the group are concentric-spherical and hexagonal core/shell materials, these classes of nanoparticles possess varying morphologies which are dependent on: (1) the materials which comprise the particle, (2) their orientation within the structure and (3) the synthesis procedures utilized to develop the materials. As a result, in order to achieve the desired multifunctional properties, core/shell nanoparticles which are comprised of the same material with the same structural orientation may be forced to deviate in their

morphological appearance. Such deviations in morphology must be studied to further understand the inherent nature of the nanomaterial.

Methods to enhance the study of the morphological appearance of materials at the nanometer scale have vastly improved over the past decade. The enhancement of conventional transmission electron microscopy to include aberration-corrected, electron beam rastering is of great significance as it provides a technical basis for the implementation of analysis techniques such as energy dispersive X-ray (EDX) spectroscopy (EDS)(Herzing et al. 2008) and high angle annular dark field (HAADF) imaging (Jesson & Pennycook 1995). The combination of HAADF-STEM imaging allows for the formation of micrographs where contrast is directly correlated the atomic number of the elements in the specimen. Because of this, following a shift-corrected tilt series, 3D tomograms can be efficiently generated as HAADF-STEM image intensities vary with the mass-thickness of low atomic number, microscale samples. Electron tomography allows for in depth, 3D morphological analysis of submicron nanomaterials (Midgley et al. 2006) not previously achievable.

Inorganic magnetoplasmonic core/shell nanomaterials are of considerable interest as they possess the properties necessary for a multitude of theranostic applications. The presence of a plasmonically-active, metallic surface provides the nanoparticle the ability to act as a colorimetric probe. Based upon the nanoparticle size, structural morphology and colloidal behavior, a solution of metallically coated core-shell nanomaterials will change color by absorbing electromagnetic radiation at particular wavelengths. This phenomenon

can be attributed to the resonant absorption of the radiation by the metallic surface plasmons – oscillating, surface valence electrons (Barnes et al. 2003). Even further, this magnetic response is tunable where modification of nanoparticulate size, shape or composite materials can yield a desired plasmonic characteristic (Link et al. 1999). These characteristics are not only ideal for diagnostic strategies which utilize visible, colorimetric detection (Zeng et al. 2014) or photonic image contrast (Brongersma 2003); but are also suitable for photonic-based therapies once the appropriate tuning of the plasmonic properties has been achieved. Coupling the plasmonic characteristics with the capacity for magnetic manipulation (magnetomotive ability), as governed by the superparamagnetic nanoparticle at the core of the nanomaterial, unleashes a host of possible applications.

As core/shell nanotechnology as a field matures, the ability to rapidly synthesize these nanomaterials to achieve the desired nanoparticulate characteristics is paramount. In this study, we sought to adapt the protocol used to synthesize the inner core/shell of the multistrata metallodiaelectic nanoparticle (Bell et al. 2011) to rapidly synthesize magnetoplasmonic iron-oxide/gold core/shell nanomaterials (Liang et al. 2009; Zhou et al. 2012; Li et al. 2014). Surface modification of nanoparticles can be rapidly achieved by exploiting the liquid-based, acoustic cavitation phenomenon which occur during sonochemical modification reactions. More specifically, acoustic cavitation occurs when bubble formation, growth and collapse occur in liquid which is under ultrasonic perturbation. This phenomenon occurs throughout the reaction volume but most notably at liquid-nanostructure interfaces. The collapse of the bubbles is nearly an adiabatic process where there is a significant accumulation of energy inside the bubble. Upon

implosion, this energy is rapidly released resulting in hotspots which possess high temperatures and pressures at the liquid-nanoscale interface. Extreme, transient conditions of 5000 K temperatures, pressures exceeding 1800 atm and cooling rates beyond 10^{10} K s^{-1} were empirically determined (T. Mason 2002) at these microscale hotspots. This local microenvironment results in the chemical excitation of matter inside or proximal to the hotspot thus catalyzing chemical reactions between reagent ligands and the nanoscale surface. Successful sonochemical synthesis, or sonoplation, of gold ions to aminated FeOx nanoparticles has been previously described (W. Wu et al. 2007). Furthermore, a rapid sonochemical protocol for the amination of the oleic acid capped FeOx nanoparticles has been described (Sodipo & Aziz 2014). However, incorporating both sonochemical synthesis processes with a <3hr core/shell synthesis period for the development of a core/shell magnetophotonic nanomaterial has not been described.

This sonochemical synthesis procedure was utilized to reduce the overall duration of synthesis while ensuring decreased magnetic relaxivity thus increasing the magnetomotivity of the nanoparticles. The effects of this change in synthesis protocol on the plasmonic, magnetic and morphologic characteristics of the nanoparticles were elucidated. Furthermore, for the first time, scanning transmission electron tomography was utilized to further elucidate the morphology of the resultant magnetoplasmonic iron-oxide/gold core/shell nanomaterials.

Methods and Materials

Fabrication of γ-Fe_2O_3 Superparamagnetic Nanoparticles: γ-Fe_2O_3 (FeOx) with ~10 nm diameter were fabricated via a thermal decomposition, aeration and reflux protocol pioneered by Woo et al.(K. Woo et al. 2004) Octyl ether (Sigma-Aldrich, St. Louis, 200 mL) and oleic acid (Sigma-Aldrich, 28.5 mL) were mixed in a 500 mL round-bottom flask under reflux and Ar gas flow. The volume was heated to 100°C prior to the injection of $Fe(CO)_5$ (Sigma-Aldrich, 2.0 mL). The vessel was quickly heated from 150°C to 295°C using a heating mantle and glass wool to ensure insulation. During this heating process, the solution color changed from yellow to orange, orange/colorless, to very dark orange then black. The reaction was aerated at 80(±10)°C for 14 h and refluxed while boiling for an additional 2 h. The γ-Fe_2O_3 nanoparticles were harvested using ethanol (EtOH, 200 proof, Sigma-Aldrich) and purified via three iterations of centrifuge (20 min, 800 relative centrifugal force (rcf)), supernatant extraction and EtOH resuspension. γ-Fe_2O_3 nanoparticle cores were dried under air for 48 h.

Conventional Amination of γ-Fe_2O_3 Core Nanoparticles: 150 mg of γ-Fe_2O_3 cores (FeOx) were coated using a conventional (3-Aminopropyl)triethoxysilane (APTES; Sigma-Aldrich) functionalization procedure(Bell et al. 2011). FeOx particles were added to tetrahydrofluran (THF; Thermo Fisher Scientific, Waltham, MA, 40 mL) and briskly stirred using a magnetic stir plate and stirring rod. APTES (5 mL) was added to the reaction solution and thereafter spiked with acetic acid (Sigma-Aldrich, 5 µL), dH_2O (516 µ L), and stirred for 48 h. The reaction flask was then placed into a heating mantle, wrapped in steel wool, and heated to 80 ° C. EtOH was used to incrementally replace evaporated THF

throughout the 2 h boiling period. This incremental replacement was tuned until the reaction solution was concentrated to 40 mL of EtOH. Hexane was added to the solution in a 4:1 ratio and centrifuged (10 min, 800 rcf). Recovered FeOx–NH_2 nanoparticles were resuspended in EtOH and stored at room temperature where they remained stable for at least three months.

Sonochemical Amination of γ-Fe_2O_3 Core Nanoparticles: Aminated γ-Fe_2O_3 ~11 nm diameter were fabricated via a place exchange reaction in an ultrasonic agitation reaction environment. γ-Fe_2O_3 nanoparticles (10 mg) were dissolved into a 1% wt APTES (Sigma-Aldrich) solution in anhydrous toluene (Sigma-Aldrich). This volume was reacted under ultrasonic agitation (90 min, 20°C) and vortexed intermittently at 15 minute intervals to ensure even mixing. Using a 1T neodymium 1" cube magnet, the aminated γ-Fe_2O_3 were magnetically separated from the toluene based solvent and washed with anhydrous ethanol (EtOH, 200 proof, Sigma-Aldrich). Aminated γ-Fe_2O_3 nanoparticles (10 mg/ml, 1ml) were stored at 4°C.

Gold Sonoplation of Conventionally Aminated γ-Fe_2O_3 Nanoparticles: FeOx–NH_2 NPs were plated with a gold layer using protocols adapted from Wu et al (Wu et al. 2007). Sonicated FeOx–NH_2 nanoparticles (≈ 1.5% wt.) were added in equal volume to aqueous, 1% $HAuCl_4$ (Sigma-Aldrich, dark aged 72 h) in an ultrasonic perturbation reaction environment. Sodium citrate (20 mM) in dH_2O was added dropwise under sonication until the light yellow–brown color of the reaction solution changes to a dark purple. The solution of FeOx/Au core/shell nanoparticles (referred to hereafter as FeOx/Au) was washed via

centrifugation (800 rcf, 5 min) and resuspended in EtOH and stored for 18 h at 4°C where they remained stable for at least 5 months.

Gold Sonoplation of Sonochemically Aminated γ-Fe_2O_3 Core Nanoparticles: Au, (γ-Fe_2O_3) composite nanoclusters (FeOx-Au) were fabricated via an electroless plating reaction in an ultrasonic agitation reaction environment. Adapted from a protocol described in the literature (Bell et al. 2011), an aqueous 1% $HAuCl_4$ solution was mixed with an ethanolic solution of aminated γ-Fe_2O_3 nanoparticles (1 mg/ml) in ratios prescribed in Table 1. Under an ultrasonic agitation environment, 12 mL of aqueous sodium citrate (20 mM, Sigma-Aldrich) was added in 800 µL incremental injections every 30 seconds. The resultant FeOx/Au nanoclusters were centrifuged (800 rcf, 10 min). The supernatant was removed while the pellet was preserved via a 1T neodymium magnet. The pellet was resuspended into 10 ml of dH_2O and the resultant FeOx-Au nanomaterials (200 µg/mL) were stored at 4°C.

Nanocluster Magnetomotive Characterization: Unconjugated FeOx/Au nanoclusters were tested for their magnetomotivity in dH_2O. Briefly, a 6 point standard curve was produced through serial dilution from a stock concentration of 200 µg/mL FeOx/Au nanoclusters was produced. A 2 mL microcentrifuge tube of FeOx/Au nanoculsters (200 µg/mL) was fastened to a 1T neodymium 1" cube magnet. Every 5 min for 20 min then every 10 min thereafter, 200 uL of the solution was removed from the side of the tube distal to the magnet. Each separated solution was diluted into 800 µL of DI water and measured on the

Varian Cary 50 at a 595 nm wavelength. A 6 point curve was generated quantifying the percent capture with respect to time.

Nanoparticle Characterization: Synthesized nanoparticles were characterized utilizing multiple modalities. Relaxometric measurements were performed on a Maran DRX-II 0.5T NMR spectroscopic scanner following the preparation of samples in Nanopure dH_2O at a diluted nanoparticulate concentration (40 μg/mL; 1 mL). Spectroscopic extinction measurements were performed in dH_2O using a Varian Cary 50 UV-vis-NIR spectrophotometer (Agilent Technologies, Santa Clara, CA). Spectroscopic T2 relaxation measurements were performed in a Carr-Purcell-Meiboom-Gill (CPMG) sequence with the following parameters: relaxations time (TR) = 30 s, echo time (TE) of first echo = 6 ms, spacing of subsequent echos = 2 ms, and 1200 echos. Size and zeta potential measurements were performed on a Malvern Zetasizer (Malvern Instruments, Westborough, MA) following nanoparticulate dilution (40 μg/mL; 1 mL) in dH_2O. The diameter of individual nanoparticles was measured from TEM images using ImageJ software. For standard morphological analysis, standard TEM micrographs with EDX (energy dispersive x-ray spectroscopy) elemental analysis were obtained on a FEI Tecnai Osiris S/TEM Microscope (FEI, Hillsboro, OR).

Tomographic Imaging and Reconstruction: The surface structure of FeOx-Au nanoclusters were examined in more detail by determining the 3D morphology of the individual nanoparticles. STEM micrographs were collected on a FEI Tecnai Osiris S/TEM Microscope. A group of nanoparticles possessing varying 2D morphologies was imaged.

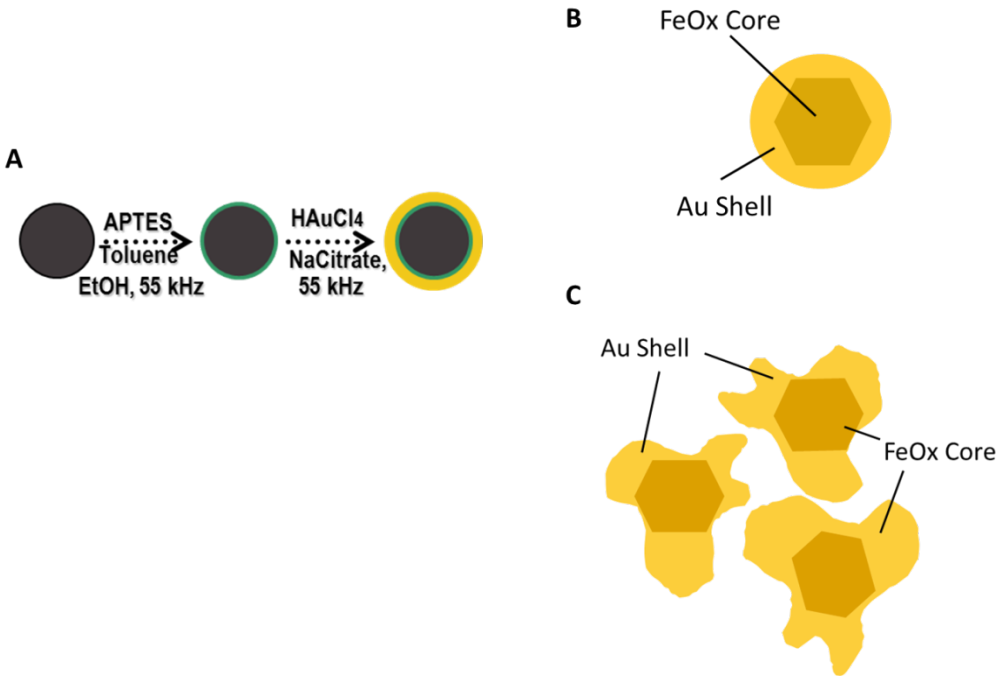

Figure 8. (a) General functionalization protocol of sonochemically synthesized nanomaterials; (b) schematic morphology of conventionally synthesized FeOx/Au core/shell nanoparticles; (c) schematic morphology of sonochemically synthesized FeOx-Au core/shell composite nanoclusters.

Micrographs were collected at 13.5 kx magnification and auto-focused at 24kx/56 kx magnifications across a ±60° tilt series where single bright field and dark field images were collected at every degree. Micrograph tilt series were reconstructed using Inspect 3D (FEI, Hillsboro, OR) software using an iterative approach (*n*=30) to interpolate and approximate the data outside of the ±60° tilt. The 3D data was imported into AMIRA 3D (FEI, Hillsboro, OR) and the data was reconstructed into a volume and rendered in 3D. A ±60° dark field, tilt series and 3D volume rendering of the morphology of the nanoclusters was produced.

Results and Discussion

FeOx/Au core/shell nanoparticles were successfully synthesized. The characterization of the resultant nanoparticles is shown in Figure 9. The micrographs shown in Figure 9A depict the morphology of the FeOx/Au nanoparticles. More specifically, bright field TEM micrographs of FeOx-NH_2 (9.47±1.56 nm dia.) and FeOx/Au nanoparticles (13.5±4.13 nm dia.) are shown in Figure 9Aa and Figure 9Ab, respectively. The morphology of both nanoparticle types is comparable to TEM micrographs depicted previously in literature (Bell et al. 2011) where the micrograph of FeOx/Au nanoparticles depict the formation of gold 'plates' on the iron oxide surface. The HAADF-STEM micrograph shown in Figure 9Ac shows the spherical nature of the FeOx/Au nanoparticle synthesized using this method. The formation of this gold coating is substantiated in Figure 9B where an extinction peak in the visible spectral range (Figure 9Bb) is evidential of the surface plasmon resonance of the gold coated material. This peak is only apparent post-synthesis and differs from the extinction profile of non-plated FeOx-NH_2 particles which lack an absorbance peak in the visible spectral range. Measurement of the relaxivity (Figure 9C) of these nanomaterials

confirmed that FeOx-NH_2 nanomaterials possessed the potential to be mechanically manipulated by a magnetic field. FeOx/Au core/shell nanomaterials did not possess this

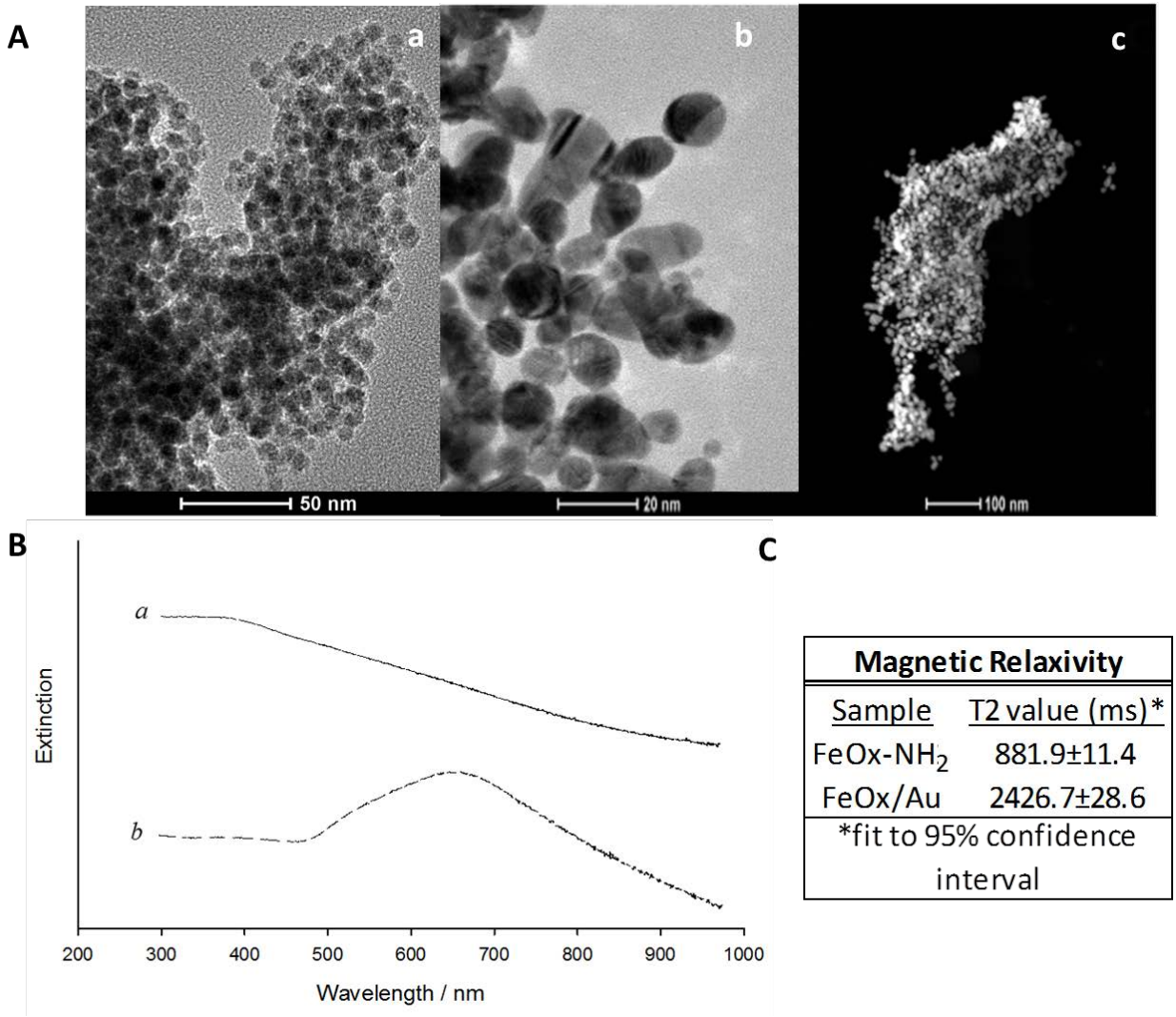

Magnetic Relaxivity	
Sample	T2 value (ms)*
FeOx-NH_2	881.9±11.4
FeOx/Au	2426.7±28.6
*fit to 95% confidence interval	

Figure 9. Characterization of FeOx/Au core/shell nanoparticles. (A) Electron micrographs of (a) conventionally aminated iron oxide nanoparticles (FeOx-NH_2); TEM micrograph (b), dark field STEM micrograph (c) of FeOx/Au core/shell nanoparticles; (B) plasmonic extinction of (a) conventionally aminated FeOx-NH_2 and (b) FeOx/Au; and the (C) the magnetic relaxivity of each.

magnetomotive ability. This was observed when a volume of the nanoparticles was exposed to a 1T magnetic field and no significant bulk movement of the material was observed for ~20 min. These observations were substantiated by the long T2 relaxivity values (T2=2426.7±28.6) which support a lack of magnetomotive ability.

For applications which require plasmonic materials to possess magnetomotive ability, the FeOx/Au core/shell nanoparticles, as synthesized, do not possess these characteristics. From a design perspective, it was concluded that extremely thin shells were necessary to enhance the magnetomotive ability of the core/shell materials. This is due to the inverse relationship between the magnetic properties and shell thickness (i.e. the distance from the magnetic core to the aqueous solution). Any magnetomotive particle must possess a significant saturation magnetization, M_{sat}, which is the maximum magnetization a particle can experience. This characteristic is described in Eq. 1 and defines a single core/shell magnetic nanoparticle, where the magnetic properties of the particle arise from the core which is coated in a thin outer shell of magnetically inert material,

$$M_{sat} = mM_{so}\left(\frac{r-d}{d}\right)^3 \quad (1)$$

where M_{so} is the saturation magnetization of the bulk material in units of A/m/g, r is the particle radius, d is shell thickness and m is the mass of the individual particle. Any significant increase in the shell thickness, d, has significant detrimental effect on the

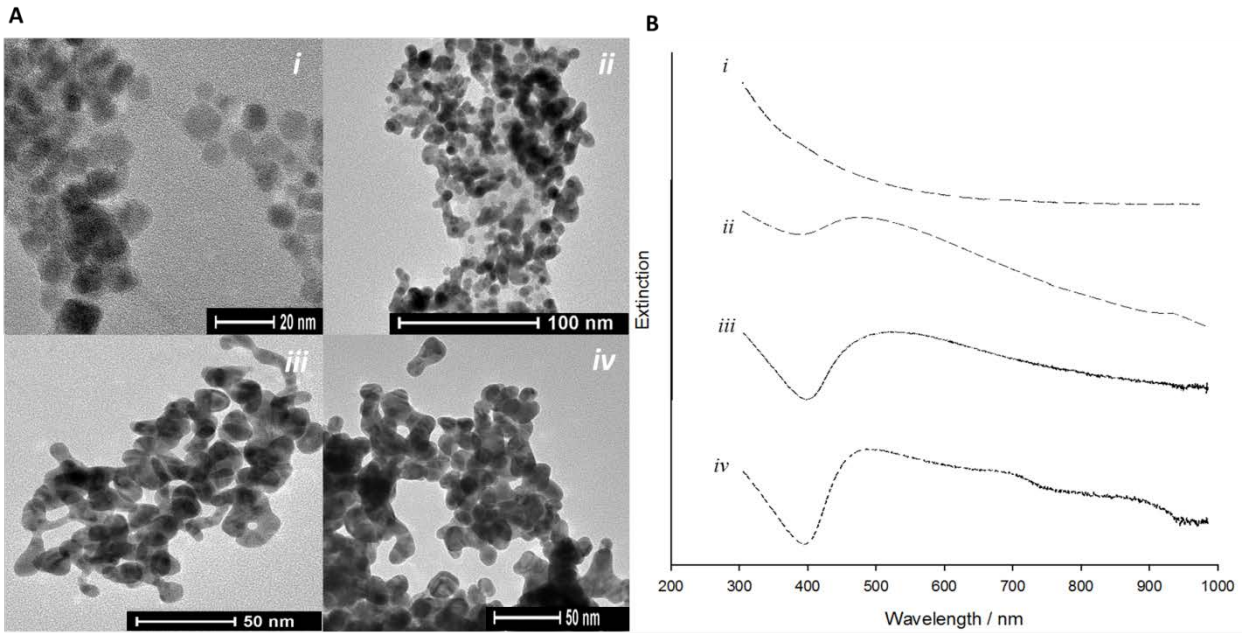

Figure 10. TEM micrographs and the corresponding plasmonic extinction of FeOx-NH_2 nanoparticles and FeOx-Au core/shell composite nanoclusters. (*i*) FeOx-NH_2 nanoparticles and FeOx-Au nanoclusters synthesized at $HAuCl_4$:FeOx-NH_2 reagent ratios of (*ii*) 1:13.3 (*iii*) 1:2 (*iv*) 3:4.

saturation magnetization of the particle. In order to successfully synthesize extremely thin outer gold and intermediary silane shells, the amount of 1% $HAuCl_4$ was decreased and a sonochemical silanization protocol was implemented until the magnetomotive properties were observed.

FeOx-Au composite nanoclusters were successfully synthesized by using a rapid, sonochemical method as described at a high level in Figure 8. FeOx-Au nanoparticulates were synthesized using decreased gold chloride reagent volumes as shown in Table 1. These nanoparticles were characterized in Figure 10. The resultant polymorphous morphology of the FeOx-Au differs from the aesthetically-uniform, spherical FeOx/Au counterpart. While some spherical particles are observed, the appearance of oblong, jagged and elliptical particles is apparent. It was deduced that the decrease in reagent gold chloride was the cause of the significant changes in the morphology of the nanoparticles. As shown in the micrographs in Figure 10A, this hypothesis is substantiated by the reappearance of the particles possessing a spherical morphology with increasing $HAuCl_4$:FeOx reagent ratios from particle populations *ii* (13.01±1.56 nm dia), *iii* (13.23±2.86 nm dia), and *iv* (14.17±4.35 nm dia). Although this increase in spherical morphology was evident, the polymorphous particles continued to be observed. Even further, it is apparent that all FeOx-Au nanoparticulates tend to cluster. This observation of stabilized flocking is supported by hydrodynamic radii measurements on the order of ~O(100 nm) (Table 1). This is important as previous mathematical modeling of superparamagnetic core/shell nanoparticle clustering has shown that the magnetization of

clustered nanoparticles is higher than an equal quantity of dispersed nanoparticles (Ortega & Giorgio 2012).

The use of a sonochemical synthesis process did not have a morphological effect on the FeOx-NH_2 nanoparticles (11.26±1.83 nm dia) as shown in the micrograph in Figure 10A*ii*. Future work includes imaging of the intermediary silane corona in order to determine if a single monolayer or a polymerized layer was formed. Formation of a polymerized layer could have a significant effect on the morphology of the FeOx-Au and could be contributing to the polymorphous morphology of the FeOx-Au. Although not of importance in this study, if spherical, non-clustering nanoparticles are required for a particular application, modification of the sonochemical amination protocol could be performed to ensure the formation of silane monolayers to improve the probability of synthesizing spherically-shelled nanoparticles.

Sample	Reagent Presciptions			Peak λ (nm)	NP Dia. (nm)	Nanocluster Hydrodyn. radii (nm)	Zeta Pot. (mV)	Relaxivity (ms)
	1% HAuCl4 (ml)	1 mg/ml FeOx-NH2 (ml)	Ratio					
(i) FeOx-NH_2	-	2	-	-	11.3±1.8	-	+32.0±3.0	152.6±3.2
(ii) FeOx-Au	0.15	2	1:13.3	564	13.0±1.6	296.8±6.9	-34.7±0.7	121.7±1.0
(iii) FeOx-Au	1	2	1:2	591	13.2±2.9	156.5±6.0	-31.1±0.4	188.9±1.1
(iv) FeOx-Au	1.5	2	3:4	560	14.2±4.4	310.8±3.5	-29.1±0.9	164.9±1.7

Table 1. Summary of Nanoparticle Characterization Results

The plasmonic properties of FeOx-Au (Figure 10B) were observed as expected where, in all three core/shell preparations, extinction peaks in the visible electromagnetic spectrum were observed. Like the FeOx/Au nanoparticles, observation of visible spectrum extinction peaks suggests that the grafting of the gold shell onto the iron oxide core was successful. The observation of a small 700 nm extinction peak in the *iv* nanoparticle batch suggests nanoparticulate aggregation or the presence of elliptical or rod-like morphologies in the sample. In all FeOx-Au batches, small extinction peaks in the infrared spectrum from 900-1000nm appear which suggests nanoparticle-mediated light scattering at these wavelengths due to incomplete shell formation and colloidal flocking (i.e. formation of nanoparticulate clusters). The presence of these infrared extinction characteristics further supports the assertion that the FeOx-Au composites were clustering.

To ensure the sonochemical fabrication protocol successfully fabricated core/shell nanoparticles, a single spherical nanoparticle from the FeOx-Au (*iv*) preparation was isolated and imaged as shown in the micrograph in Figure 11A. To determine the elemental composition of the specimen, TEM-EDS was utilized and the resultant spectrum is shown in Figure 5B. The elemental appearance of copper is expected as the TEM sample grids are composed of the element. The detection of x-rays characteristic of gold, silicon, and iron elements which have radiated from a single nanoparticle suggests the encapsulation of an iron-oxide core by an intermediary silane and outer gold shell.

Magnetomotive capacity is inversely related to the $HAuCl_4$:FeOx-NH_2 reagent ratios. The magnetomotivity of the FeOx-Au nanoclusters is depicted physically in Figure 11C

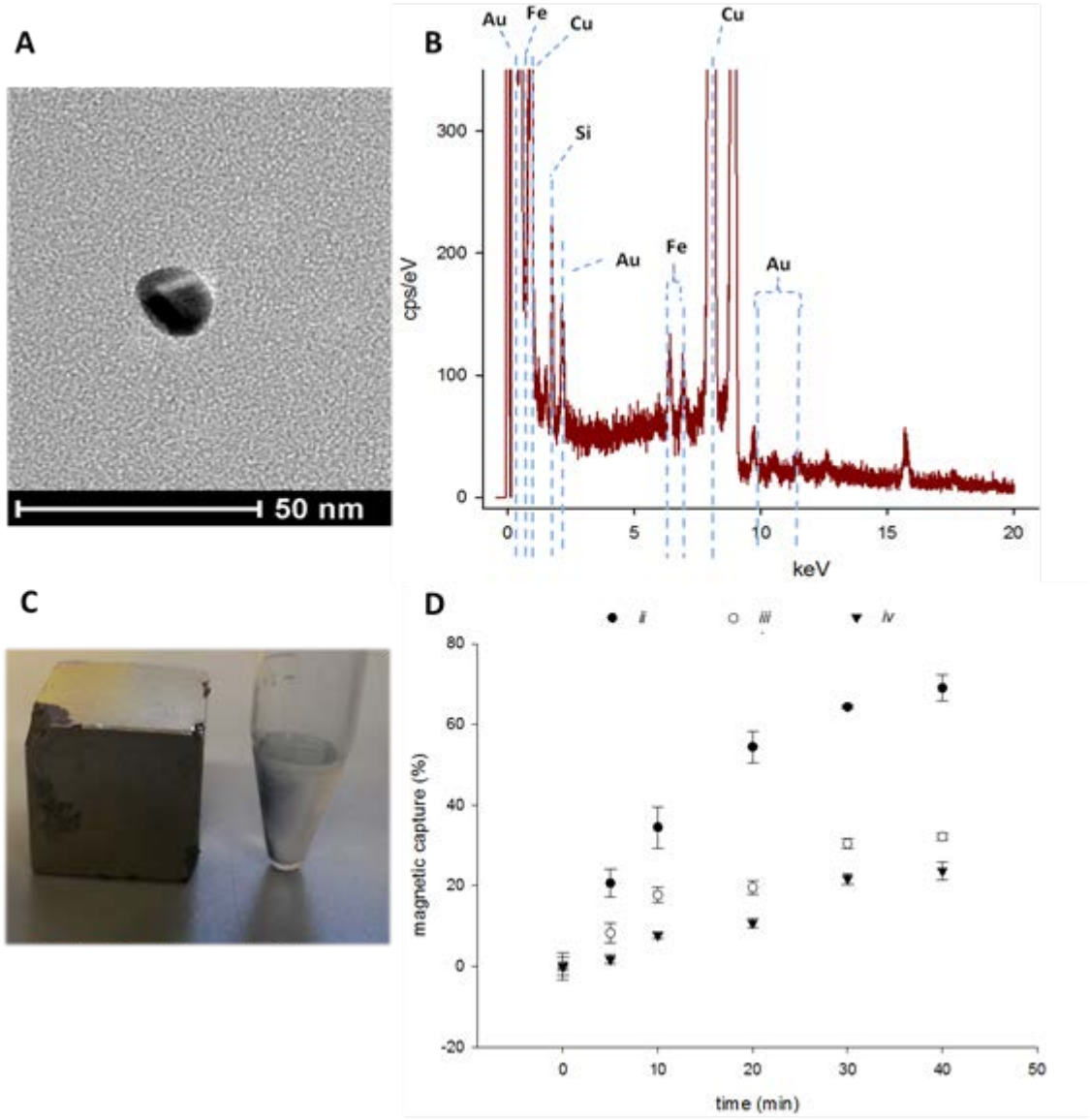

Figure 11. (A) TEM micrograph of a single FeOx-Au composite nanoparticle synthesized at a reagent ratio a 3:4 HAuCl4:FeOx-NH2; (B) the corresponding EDX spectrum of the electron micrograph; (C) an image of the magnetotive nature of the FeOx-Au nanoclusters in a 1T magnetic field provided by a neodymium magnet; (D) the magnetomotive characterization of the different FeOx-Au compositie nanoclusters at varying $HAuCl_4$:FeOx-NH_2 reagent ratios (*ii,* ●) 1:13.3, (*iii,* ○) 1:2, (*iv,* ▼) 3:4.

and quantitatively in Figure 11D. Figure 11D shows that the magnetomotivity is greatest when the FeOx-Au nanoclusters are synthesized at lower $HAuCl_4$:FeOx-NH_2 reagent ratios. We speculate that there is a threshold at which reagent ratios are too low to effectively create core-shell materials; however, we assert that the magnetomotive capacity will continue to increase as the lack of full shell coverage will increase the saturation magnetization of the nanomaterials. The FeOx-Au nanoclusters were effectively separated from solution with repeatability using a 1T magnet as shown in Figure 11C. The ability to visualize the separation with the naked eye due to the plasmonic extinction properties of the nanomaterial suggests that the FeOx-Au nanoclusters are viable nanoprobes for applications which require visible, nanoscale tagging and extraction.

To assess the nanoparticulate morphology in a three dimensional space, 3D tomographs of FeOx-Au composite nanoclusters from the *ii* nanoparticle batch were generated and are shown in Figure 12A-B. A selected micrograph from the HAADF-STEM ±60° tilt series used to generate the tomographic volume is shown in Figure 12C. 3D tomographic animations and videos of both the unaligned and aligned tilt series were compiled. As previously shown in the micrographs in Figure 10, the nanoparticles shown here are polymorphous and vary in shape which includes spherical, oblong, elliptical and jagged forms. Tomographic analysis confirms these morphological characteristics are not artifacts of a 2D transmission electron slice but are evident in a three dimensional volume. The green and blue colors depict variations in elemental density throughout the cluster of nanoparticles as detected by the high angle annular dark field detector in the STEM (Figure 12E). Gold atoms appear

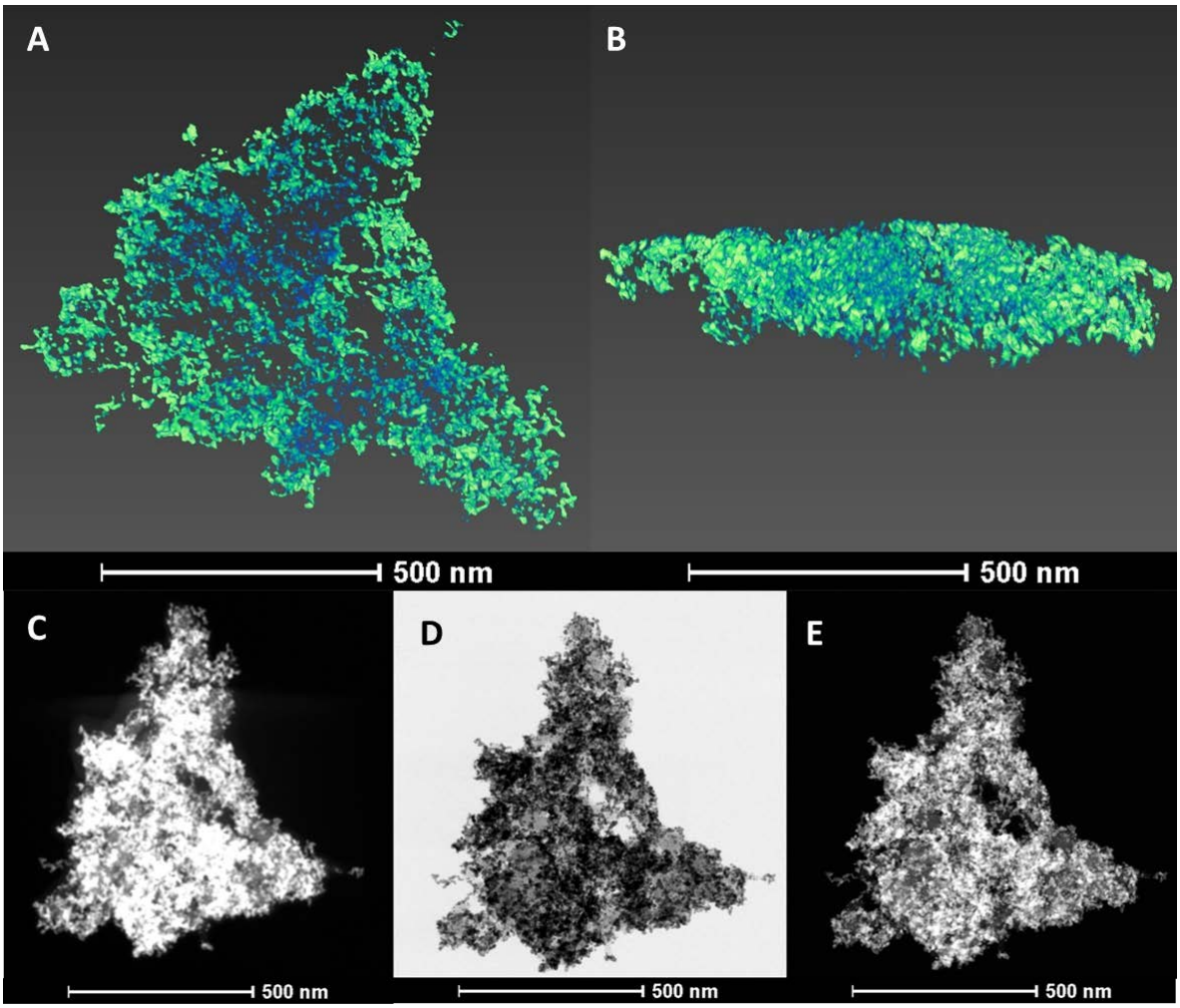

Figure 12. Morphological analysis of FeOx-Au composite nanoclusters. Tomographic 3D reconstruction and rendering of FeOx-Au nanoclusters from a top view (A) and side view (B); (C) screen capture of the realigned tilt series reconstructed from single STEM images; (D) selected bright field and (E) dark field, high angle annular dark field (HAADF) STEM micrographs which comprise the reconstructed tilt series.

brighter than iron atoms because of their ability to incoherently scatter electrons at a high angle due to their higher atomic number. It cannot be assumed that these elemental areas of contrast are iron, silicon or gold until a tilt-series is performed at higher magnification providing greater resolution. Future directions include utilizing a STEM-EDS mapping technique during each tilt of the ±60° tilt series which would better elucidate and enumerate the position and quantity of each element in the 3D tomograph, respectively.

Conclusion

We have successfully demonstrated that superparamagnetic FeOx-Au composite nanoparticles, which manifest as magnetic nanoclusters, can be synthesized to effectively exhibit both plasmonic and magnetomotive characteristics. The nanomaterials were successfully fabricated where both the intermediary silane and outer gold shells were grafted via a sonochemical synthesis process. Although the morphological aesthetics, in comparison to FeOx/Au core/shell nanoparticles, were sacrificed for enhanced functionality with respect to the magnetomotivity of the material, the nanomaterial maintained its general magnetoplasmonic properties. For the first time, 3D tomographic analysis was utilized in order to better understand the morphological characteristics of a magnetoplasmonic composite material. The successful development and characterization of these materials provides another robust nanotechnology-based platform for applications, including biomedical theranostics, which can be enhanced by plasmonic nanoprobes that possess the ability to be mechanically manipulated via an external, contact-free command.

Summary

Inorganic magentoplasmonic core/shell nanomaterials are of considerable interest as they possess both the plasmonic and magnetomotive properties necessary for a multitude of theranostic applications. A sonochemical synthesis procedure was utilized to reduce the overall duration of synthesis while ensuring the increased magnetomotivity of the nanoparticles. The effects of this change in synthesis protocol on the plasmonic, magnetic and morphologic characteristics of the nanoparticles were elucidated. Furthermore, for the first time, scanning transmission electron tomography was utilized to further elucidate the morphology of magnetoplasmonic iron-oxide/gold core/shell nanoconstructs. For the purposes of this dissertation, the results provided in this chapter accomplished one of the objectives. We (2) successfully modified the synthesis strategy to enhance the properties of the composite material while decreasing the synthesis duration such that freshly synthesized materials can be rapidly utilized in a biological application. We developed multilayered nanomaterials that combine at least two nanoscale characteristics into a single, nanoscale entity. Furthermore, we enhanced the magnetic properites of the magnetoplasmonic nanomaterial enabling magnetomotive functionality. We showed that multilayered, magnetoplasmonic core/shell nanoparticles were fabricated by adapting the synthesis protocol used in Chapter II. This revised fabrication strategy was also shown to decrease the overall fabrication period thus enabling rapid fabrication and use of fresh nanomaterials for biological applications. These results validate my core hypothesis and objective..

CHAPTER IV

NANOTECHNOLOGY-MEDIATED MAGNETIC SEPARATION OF *ACINETOBACTER BAUMANNII* USING LIPOPOLYSACCHARIDE TARGETED POLYMYXIN-E COATED γ-Fe_2O_3/Au CORE/SHELL COMPOSITE NANOCLUSTERS

Acinetobacter baumannii is a gram-negative bacterium of increasing interest due to its significant virulence and enhanced persistence in combat and healthcare environments (Peleg et al. 2008). Incidence in both community-acquired and nosocomial infection are on the rise in both foreign and domestic US healthcare facilities (Dijkshoorn et al. 2007). Treatment options are limited due to the rapid acquisition of multi-drug resistance to the few antibiotics readily available (Fournier et al. 2006). Currently, the most effective pharmaceutically-based treatment is the antibiotic colistin (polymyxin E) (Li et al. 2005). With decreased cytocompatibility the common problem with administration of toxic therapeutics, we propose the development of a nanotechnology-mediated treatment strategy. Such a therapy will function as an adjuvant to conventional antibiotic regimens in order to effectively curtail bacteremia.

In Chapters II and III, I have described how we have developed novel multilayered, magnetoplasmonic nanoconstructs with the ability to be biofunctionalized for use in biological applications. These nanomaterials will be biofunctionalized to bind to the surface of *Acinetobacter baumannii*. This binding event will enable magnetic extraction of the bacteria due to the magnetomotive characteristics of the nanomaterial. For the purposes of this dissertation, this chapter will confirm the central hypothesis of my dissertation that inorganic, multilayered, magnetoplasmonic core/shell nanomaterials can

be specifically designed and synthesized for biological applications which require both diagnostic detection and therapeutic elimination of a disease causing agent. I will provide results that support my hypothesis that these nanomaterials can be fabricated in such a way that biomedical functionalization of the material can proceed without detriment to the function of the biological component. These results will achieve our final objective where the activity of the conjugated biological component will be conserved while binding and extracting a disease causing agent *in vitro*.

In Chapter IV, the goals described in *Aim 3*, will be achieved. The magnetoplasmonic core/shell nanoparticles fabricated in *Aim 2* will be biofunctionalized with an antibiotic which targets and binds gram negative bacteria. These biofunctionalized nanostructures will then be characterized and utilized to magnetically extract *Acinetobacter baumannii* from saline solution *in vitro*.

Introduction

Acinetobacter baumannii has emerged as a bacterial species of great interest due to its significant virulence and enhanced persistence in combat and healthcare environments (Peleg et al. 2008; Camp & Tatum 2010). A gram-negative bacterium initially found in the Middle East, *A. baumannii* possess an enhanced ability to thrive in dry environments (Wendt et al. 1997) and persist following conventional surface cleaning (Manian et al. 2013) and wound treatments (Maragakis & Perl 2008). Over the last decade, the recent increase in incidence stems from US military combat in Iraq and Afghanistan (Aronson et al. 2006). Incidence in both community-acquired and nosocomial infection are on the rise

in both foreign and domestic US healthcare facilities (Dijkshoorn et al. 2007); which can be attributed to the return of infected cargo and veterans.

Acinetobacter species can cause a multitude of ailments including pneumonia, bacteremia, meningitis, urinary tract infections, peritonitis, and skin and soft tissues infections (Bergogne-Bérézin & Towner 1996). These primary ailments contribute to the incidence of *Acinetobacter* species bloodstream infections (BSIs) which account for over 3% of all nosocomial acquired BSIs (Hidron et al. 2008). The mortality rate associated with *A. baumannii* infection is high where *A. baumannii* bacteremia is associated with a 52% mortality rate and pneumonia associated mortality ranges from 23% to 73% (Rodriguez-Guardado et al. 2013).

Treatment options are increasingly limited due to the rapid acquisition of multi-drug resistance to the few antibiotics readily available (Fournier et al. 2006). Currently, the most effective pharmaceutically-based treatment is the antibiotic colistin (colistimethate [colsitin sulfomethate] or polymixin E) (Li et al. 2005). Colistin is a cationic polypeptide and potent broad-spectrum antibiotic. Previously not prescribed due to reported nephrotoxicity and neurotoxicity, colistin has been revisited as a treatment due to its potency against gram-negative bacilli. Polymyxins interact electrostatically with the outer membrane of Gram negative bacterium by competitively displacing divalent cations – most notably calcium and magnesium – from the negatively charged phosphate groups of membrane lipids. This interaction disrupts the outer membrane and lipopolysaccharide is released (Peterson et al. 1985). It has been shown that masking the five primary amine

groups on the lariat of the colistin molecule weakens the antibacterial activity. Therefore, it is presumed that positively charged amine groups in the lariat of the antibiotic play an important role in the interaction with the bacterial lipopolysaccharides as well as the bactericidal effects of the molecule at physiological pH (Li et al. 2005). Although colistin may be effective at high dosage, conservative administration is necessary due to the nephrotoxicity, neurotoxicity, and broncho-restrictive effects that occur at aggressive dosage (Justo & Bosso 2015). A non-aggressive administration regimen, however, can lead to unchecked virulence thus leading to mortality.

With decreased cytocompatibility the common problem upon administration of toxic therapeutics, many have investigated a number of therapies which function as adjuvants to conventional antibiotic regimens in order to effectively curtail bacteremia. Taking a pharmaceutically-centered approach, combinatorial delivery of colistin with sulbactam, rifampin and tigecycline proved suboptimal as it has been shown to lead to the development of resistance (Vila & Pachón 2008). Non-pharmaceutically centered innovative approaches have been devised including the development of extracorporeal devices aiming to mechanically cleanse bacteria from body fluids. Most investigations utilize pathogen and endotoxin targeted magnetic nanotechnology with an external device acting as a filter or spleen mimic. A blood-cleansing extracorporeal device, inspired by the spleen, to continuously remove pathogens and toxins from blood has been described in the literature (Kang et al. 2014). Magnetic nanoparticles conjugated with mannose-binding lectin were developed forming a nano-engineered human opsonin. Magnets inside the device were used to pull opsonin-bound pathogens from the blood flowing through a

microfluidic device at a >90% efficiency. Other investigators have shown synthetic ligands, more specifically zinc-coordinated bis(dipicolylamine), can been utilized for highly selective and rapid separation of bacteria from whole blood with almost 100% clearance (Lee et al. 2014). These results support the relevance of extracorpeal *adjuvant* therapy as a potentially relevant treatment of bacteremia.

The use of extracorpeal devices for the adjuvant treatment of *A. baumannii* has not been described in literature. Furthermore, no-robust motif for nanoparticulate targeting, with respect to binding affinity, to the *A. baumannii* surface has been described for these purposes. To initiate the development of such a treatment, robust nanoparticulate platforms must be developed and their capture ability in physiological phantoms must be quantified. Here, for the first time, gold iron-oxide composite nanoclusters were biologically modified and utilized for both their optical and magnetomotive properties. Due to its mechanism of action, here we also describe the use of colistin as a targeting motif to bind the magnetic gold-iron oxide nanoclusters to the surface of *A. baumannii* without highly significant impact to bacterial survival. As a whole, we describe the separation efficiency of *A. baumannii* using this antibiotic-enabled nanoparticulate platform in a single-pass, macroscale system.

Materials and Methods

All materials were obtained from Sigma-Aldrich (St. Louis, MO) and used as received unless otherwise noted. Deionized water (dH_2O) was obtained through a dedicated, dual bed laboratory installation. FeOx/Au nanocluster synthesis protocol is briefly summarized in Figure 13.

Fabrication of oleic acid capped γ-Fe2O3 Superparamagnetic Nanoparticles: γ-Fe_2O_3 with ~10 nm diameter were fabricated by a thermal decomposition, aeration and reflux protocol pioneered by Woo et al. (K. Woo et al. 2004). Briefly, octyl ether (Sigma-Aldrich, St. Louis, 200 mL) and oleic acid (Sigma-Aldrich, 28.5 mL) were mixed in a 500 mL round-bottom flask under reflux and Ar gas flow. The mixture was heated to 100°C prior to the injection of $Fe(CO)_5$ (Sigma-Aldrich, 2.0 mL). The reaction vessel was quickly heated from 150°C to 295°C using a heating mantle and glass wool to ensure insulation in the midst of the high convection inside the fume hood. During this heating process, the reaction solution color changed from yellow to orange, orange/colorless, to very dark orange then black. The reaction was aerated at ~80(±10)°C for 14 h and refluxed while boiling for an additional 2 h. The γ-Fe_2O_3 nanoparticles were harvested using ethanol (EtOH, 200 proof, Sigma-Aldrich) and purified via three iterations of centrifuge (20 min, 800 relative centrifugal force (rcf)), supernatant removal and EtOH wash. γ-Fe_2O_3 nanoparticle cores were dried under air for 48 h.

Sonicatory Amination of γ-Fe_2O_3 Core Nanoparticles: Aminated γ-Fe_2O_3 ~11 nm diameter were fabricated via a place exchange reaction in an ultrasonic agitation reaction

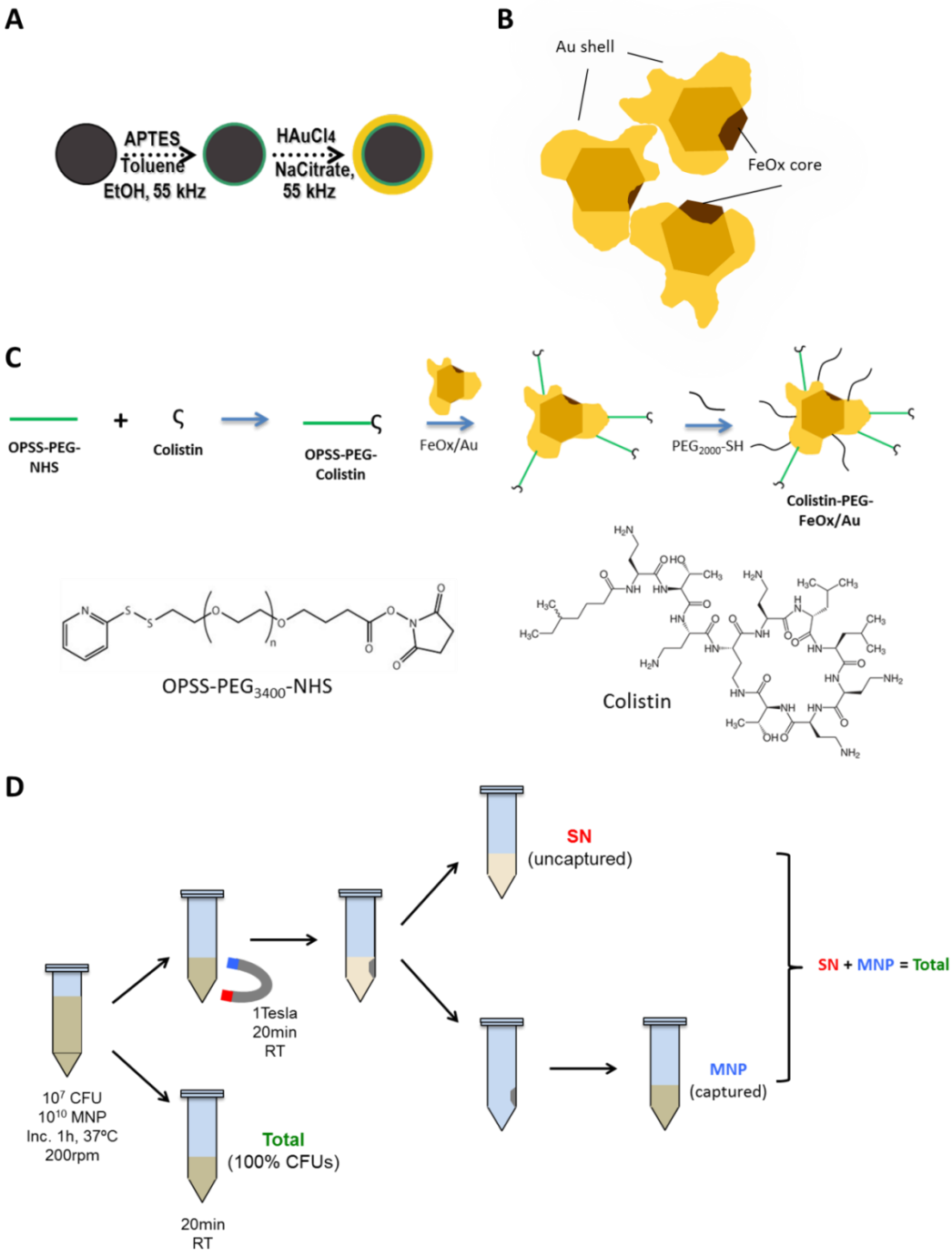

Figure 13. Schematic summary of the A) nanocluster synthesis protocol; B) morphology of the non-spherical FeOx/Au nanoclusters; C) the colistination and pegylation conjugation strategy; D) the nanoparticulate-mediated, magnetic capture of *A. baumannii* experimental procedure.

environment. Oleic acid capped γ-Fe_2O_3 nanoparticles (10 mg) were dissolved into a 1% wt (3-Aminopropyl)triethoxysilane (APTES, Sigma-Aldrich) solution in anhydrous toluene. This volume was reacted under ultrasonic agitation (90 min, 20°C) and vortexed intermittently at 15 minute intervals to ensure homogenous mixing. Using a 1T neodymium 1" cube magnet, the aminated γ-Fe_2O_3 were magnetically separated from the toluene based solvent and washed with anhydrous ethanol (EtOH, 200 proof, Sigma-Aldrich). Aminated γ-Fe_2O_3 nanoparticles (10 mg/ml, 1ml) were stored at 4°C.

Gold Sonoplation of Aminated γ-Fe_2O_3 Core Nanoparticles: Au-(γ-Fe_2O_3) composite nanoclusters (FeOx/Au) were fabricated via an electroless plating reaction in an ultrasonic agitation reaction environment. Adapted from a protocol described previously .(Bell et al. 2011), an aqueous 1% $HAuCl_4$ (150 µl, Sigma-Aldrich) solution was mixed with an ethanolic solution of aminated γ-Fe_2O_3 nanoparticles (1 mg/ml, 2 ml). Under an ultrasonic agitation environment, 12 mL of aqueous sodium citrate (20 mM, Sigma-Aldrich) was added in 800 µL increments every 30 seconds. The resultant FeOx/Au nanoclusters were centrifuged (800 rcf, 10 min). The supernatant was extracted while the pellet was preserved via a 1T neodymium magnet. The pellet was resuspended into 10 ml of dH_2O and the resultant FeOx/Au nanoclusters (200 µg/mL) were stored at 4°C.

Conjugation of colistin antibiotic to heterobifunctional PEG linker: Colistin (polymyxin-E; Sigma-Aldrich) was conjugated to ortho-pyridine disulfide, N-hydroxysuccinimide heterobifunctional polyethylene glycol polymer linker (OPSS-PEG_{3400}-NHS; Creative PEG Works) using a protocol adapted from Nanobiotechnology Protocols (L. Hirsch JL. West

2005). In a 100 mM $NaHCO_3$ solution, OPSS-PEG_{3400}-NHS (0.044 mg/ml, 9 mL) was mixed with colistin (0.2 mg/ml; 900 µL) and allowed to react for 2 h at 20°C. OPSS-PEG_{3400}-colistin conjugates were stored at 4°C for further use for no more than 24 h. Fresh OPSS-PEG_{3400}-colistin conjugates were prepared for conjugations separated by 24 h or more.

Functionalization of FeOx/Au nanoclusters with OPSS-PEG_{3400}-colistin conjugates and PEG_{2000}-SH: FeOx/Au nanoclusters were functionalized with OPSS-PEG_{3400}-colistin conjugates and thiolated PEG (PEG_{2000}-SH; Laysan Bio, Inc.) using protocols adapted from Nanobiotechnology Protocols (L. Hirsch & JL. West 2005). To prepare Col-PEG-FeOx/Au nanoclusters, FeOx/Au nanoclusters (200 µg/mL; 4 ml) were mixed with OPSS-PEG_{3400}-colistin (100 µL; 18.8 µg/ml) for 1 h then mixed with PEG_{2000}-SH (100 µL; 15.6 mg/mL) for an additional hour. Simultaneously, PEG-FeOx/Au nanoclusters were prepared by mixing FeOx/Au nanoclusters (200 µg/mL; 4 ml) with PEG_{2000}-SH (100 µL; 15.6 mg/mL) for 1 h then mixed with dH_2O for an additional hour. To purify, both preparations were centrifuged at 800 rcf for 10 min. The supernatant was removed using magnetic separation to preserve the pellet and saved for unconjugated colistin enumeration. The pellet was then resuspended in a 70% aqueous EtOH sterilization solution to restrict bacteria contamination and promote sterility. Preparations were stored at 4°C until utilized for bacterial separation experiments and characterization no more than 24 hours thereafter.

Nanocluster Characterization: Both conjugated and unconjugated FeOx/Au nanoclusters were characterized similarly. For morphological analysis, standard TEM micrographs with

EDX (energy dispersive x-ray spectroscopy) elemental analysis were obtained on an FEI Tecnai Osiris S/TEM Microscope (FEI, Hillsboro, OR). Spectroscopic extinction measurements were performed in dH_2O using a Varian Cary 50 UV-vis-NIR spectrophotometer (Agilent Technologies, Santa Clara, CA). Relaxometric measurements were obtained on a Maran DRX-II 0.5T NMR spectroscopic scanner following sample preparation in Nanopure dH_2O at a diluted nanocluster concentration (40 μg/mL; 1 mL). Spectroscopic T2 relaxation measurements were performed in a Carr-Purcell-Meiboom-Gill (CPMG) sequence with the following parameters: relaxations time (TR) = 30 s, echo time (TE) of first echo = 6 ms, spacing of subsequent echos = 2 ms, and 1200 echos. Size and zeta potential measurements were performed on a Malvern Zetasizer (Malvern Instruments, Westborough, MA) following nanoparticulate dilution (40 μg/mL; 1 mL) in dH_2O. The size of the individual nanoparticles which comprise the nanoclusters were estimated from TEM images using ImageJ software.

Confirmation of ligand conjugation: A Colistin ELISA Test Kit (Bioo Scientific, Austin, TX) was used to detect and quantify free, unconjugated colistin in the supernatant of the reaction volume. The kit was used as prescribed by the manufacturer with no deviation from the provided protocol.

^1H NMR spectroscopy was used to confirm colistin conjugation to the FeOx/Au nanoclusters. ^1H NMR spectrums were obtained in deuterium oxide (D2O) and measured using a Bruker 600 MHz spectrometer (Bruker, 600 MHz, Billerica, MA). Freshly conjugated Col-PEG-FeOx/Au nanoclusters (2 mL, 2 mg/mL) were lyophilized for 24 h. The

sample was resuspended in 200 µL of D2O to prepare for the iodine-catalyzed nanocluster decomposition reaction (iodination).

Briefly, four to seven iodine crystals were added directly to suspension of nanoclusters. The iodinated sample was vortexed (10s, 100%) intermittently for 10 s, every 20 min, for 1 h. Following a nucleophilic substitution (place exchange reaction) between the iodine molecules and the sulfur groups of the colistin-bound conjugate, the nanoclusters spontaneously settled via precipitation out of solution. This event caused the colistin-bound conjugates and free iodine to be the only remaining reagents in the solution. The sample was stored at 20°C for 12 h to allow the iodine crystals to settle to the bottom of the suspension. Only colistin-bound conjugates remained in the D2O suspension which was measured using ^{1}H NMR within 24 h.

Confirmation of nanocluster binding to A. baumannii: STEM-EDS (energy dispersive X-ray spectrometry) micrographs of bacteria-nanocluster aggregates were also obtained from an FEI Tecnai Osiris S/TEM Microscope using the following fixation protocol. Briefly, following an 1 h incubation with *A. baumannii* in 1X PBS, FeOx/Au nanoclusters bound to bacteria were centrifuged at 12,400 RPM for 5 min. The supernatant was discarded and pellet was resuspended in sterile dH_2O to wash the nanocluster-bound bacteria. The washed sample was centrifuged at 12,400 RPM for 5 min and resuspended in 2% formaldehyde for 30 min at 20°C. Approximately 2 µL of the nanocluster-bound bacteria was dropcast onto carbon film-supported cooper grids (Ted Pella, Inc., Redding, CA) and blotted to dry. Samples were allowed to air dry at 20°C for 2 h prior to imaging. X-rays

emitted from the specimen during EM imaging procedures were collected and analyzed for their elemental composition in ESPRIT imaging software.

Cell culture: HepG2 cells (human liver carcinoma cancer cell line) used in this study were cultured in Dulbecco's modified Eagle's medium (DMEM, Gibco Cell Culture, Carlsbad, CA) supplemented with 10% fetal bovine serum (FBS, Gibco) at 37°C in a humidified atmosphere containing 5% CO_2. HUVEC cells (human umbilical vein endothelial cell line) used in this study were cultured in vascular basal cell medium (ATCC PCS-100-300, Manassas, VA) supplemented with endothelial cell growth kit-VEGF (ATCC PCS-100-41) at 37°C in a humidified atmosphere containing 5% CO_2.

In vitro cytotoxicity studies: The cytotoxicity induced by Col-PEG-FeOx/Au nanoclusters, PEG-FeOx/Au nanoclusters, and free colistin on mammalian cell cultures was determined using the alamarBlue (Invitrogen Co., Carlsbad, CA) assay. HepG2 and HUVEC cells were seeded in clear, flat 96-well plates at a density of 10,000 cells/well in 200 µL of medium and incubated for 24 h at 37°C. Next, cells were treated with free colistin at concentrations of 900, 90, 70, 15, 1 and 0 µM. Similarly, culture medium was removed and exchanged with medium containing fresh Col-PEG-FeOx/Au and PEG-FeOx/Au at concentrations of 2, 1, 0.5, 0.25, and 0 mM, respectively. After incubation for 24 h at 37°C, cells were washed thrice with phosphate buffer solution (PBS), pH 7.4 and treated with 200 µL of alamarBlue containing media. Cells were then incubated for an additional 4 h at 37°C. Fluorescence was quantified using a plate-reader (Tecan, Infinite M1000 Pro, Switzerland), with an excitation wavelength of 540 nm and emission wavelength of 590 nm.

In vitro hemocompatibility studies: Human whole blood was collected from anonymous, consenting human donors in accordance with an approved Institutional Review Board (IRB) protocol (IRB 111251). Red blood cells (RBCs) were isolated according to well-established protocols (Evans et al. 2013). Four different concentrations (1, 5, 40, and 200 ug/mL) of Col-PEG-FeOx/Au and PEG-FeOx/Au nanoclusters were prepared in PBS, pH 7.4, respectively. Free colistin (900, 0.9, 0.4, 0.2, and 0 μM) was also prepared in PBS, pH 7.4. Col-PEG-FeOx/Au, PEG-FeOx/Au, and free colistin were incubated with RBCs for 1h at 37°C, each respectively, at the concentrations outlined above. Following incubation, the samples were centrifuged and the supernatant was spectrophotometrically analyzed for hemoglobin release using a plate-reader (Tecan, Infinite M1000 Pro) at 451 nm in order to determine percent hemolysis relative to the positive control (Triton X-100 detergent). The negative control used was PBS, pH 7.4. Percent of hemoglobin release was calculated according to Equation 1.

$$Hemoglobin\ release\ \% = \frac{(Sample_{451\ nm} - Negative\ control_{451\ nm})}{(Positive\ control_{451\ nm} - Negative\ control_{451\ nm})} \times 100\% \qquad (1)$$

Bacterial cell culture: 50 mL of LB broth (RPI, Mt. Prospect, IL) were inoculated with a single colony of *A. baumannii* (ATCC 17978) using standard sterile techniques. The culture was incubated overnight (18 h) at 37 ºC and agitated at 200 rpm in an orbital shaker. Before using the bacteria for experiments, the culture was diluted 1/100 in fresh LB broth and re-incubated in the same conditions for 2 hours.

Bacterial susceptibility tests: For survival analysis, FeOx/Au nanoclusters and *A. baumannii* were mixed and incubated in LB. FeOx/Au nanoparticle concentration (both Col-PEG-FeOx/Au and PEG-FeOx/Au) was varied from 0 to 10^{11} nanoparticles/mL, while the concentration of *A. baumannii* was adjusted to be 10^6 CFU/mL in all samples. After a 1-hour incubation at 37 ºC and agitation at 200 rpm in an orbital shaker, cultures were diluted, plated on LB agar plates, and incubated for 18 h at 37 ºC. The percentage of surviving cells compared to untreated controls was determined by CFU counting. *A. baumannii* susceptibility to colistin was also analyzed using concentrations from 0 to 2 μg/mL, and following the same protocol.

Bacterial magnetic capture: To determine the magnetic capture efficiency, FeOx/Au nanoclusters (both Col-PEG-FeOx/Au and PEG-FeOx/Au) at 10^{10} nanoclusters and *A. baumannii* at 10^7 CFU in 1 ml PBS were mixed and incubated for 1 h at 37°C and agitated at 200 rpm in an orbital shaker. Magnetic capture process is summarized in Figure 13. After incubation, each sample was divided into two tubes (500 μl each). One of them was kept at RT, as a control of the total concentration of bacteria after incubation (-MF tubes). A permanent magnet (1 Tesla) was placed on the side of the other tube for 20 min at RT. After magnetic separation, supernatants were collected (+MF SN tubes), and nanoclusters were resuspended in 500 μl PBS (+MF NP tubes). 50 μl alamarBlue were added to each tube. All samples were then incubated for 30 min at 37°C, centrifuged, and supernatants were analyzed using a plate reader (Tecan, Infinite F500). Fluorescence was quantified with an excitation wavelength of 535 nm and emission wavelength of 590 nm, and CFU/mL in each sample was determined using a standard curve that correlated the number of

CFU/mL with the fluorescence intensity obtained from the alamarBlue assay. The standard curve was generated and processed in parallel with all the samples. The percentage of magnetic capture was determined by comparison of the CFU/ml in the -MF tubes and the +MF NP tubes.

Statistical Analysis: All experiments were performed in triplicate unless otherwise noted. The results were expressed as the arithmetic mean ± standard deviation (SD). A two-sided, unpaired t-test was used to determine statistical significance, with significance levels ranging from $p < 0.05$ to $p < 0.001$.

Results and Discussion

Colistinated FeOx/Au nanoclusters, utilized as a nanotechnology-enabled platform, were used to successfully capture and magnetically extract *A. baumannii* from saline solution. As shown in Figure 14, colistinated nanoclusters separated 28.8±7.15% of *A. baumannii* in the sample, whereas the PEGylated control nanoclusters separated only 9.65±3.74% of the bacteria. The difference in percent capture was highly significant ($p<0.001$) and suggests that the presence of colistin on the surface of the nanomaterials enhanced both selectivity and binding. This enhanced selectivity and binding is significantly influenced by nanoparticulate surface charge which is mediated by the presence of surface conjugates. This conjugate-mediated selectivity is supported by the 2-fold positive difference in zeta potential between colistinated and PEGylated nanoclusters as shown in Table 3.

Bacteria capture was further elucidated with increased granularity in Figure 15. Performance of capture was performed at a "per tube" level of quantification to confirm that results were influenced by separation and neither by cell death nor some other unforeseen variable. It was expected that significant differences between the number of separated bacteria, per particulate population, should correlate to significant differences between bacteria remaining in the supernatant. Notably, there were highly significant differences between the captured and uncaptured bacteria populations internal and between the PEGylated and colistinated nanoclusters treatments (***$p<0.001$, $n=6$). Further, significant differences between supernatant CFU counts as well further validate this strategy, as expected. Furthermore, summation of separated and remaining bacteria should equal the total number of bacteria in the original sample.

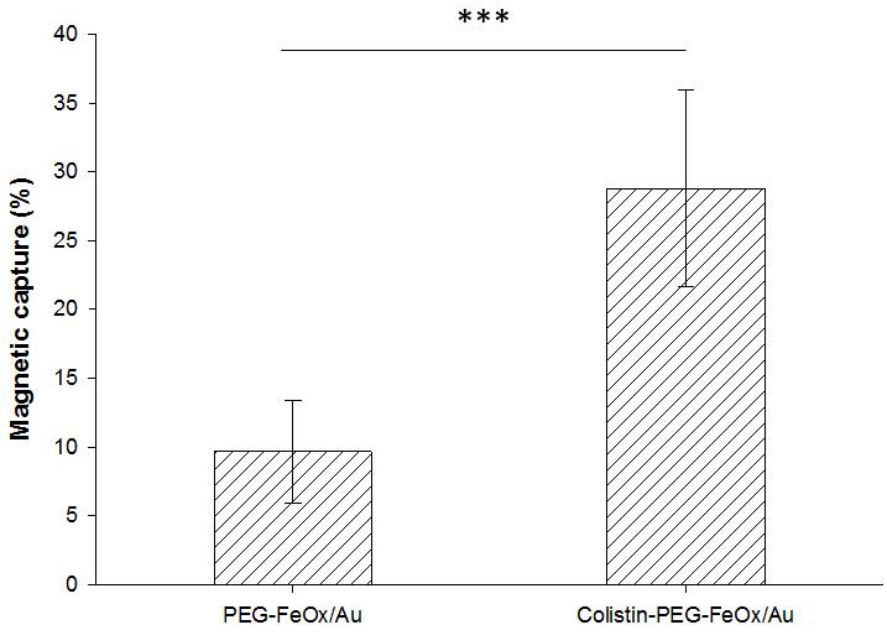

Figure 14. Quantification of macroscale *Acinetobacter baumannii* separation by FeOx/Au nanoclusters. Results depict a highly significant difference in the magnetic capture percentage between colistinated (M=28.8, SD=7.15) and PEGylated (M=9.65, SD=3.74) nanoclusters; (***$p<0.001$; $t(5)=0.000499$; $n=6$).

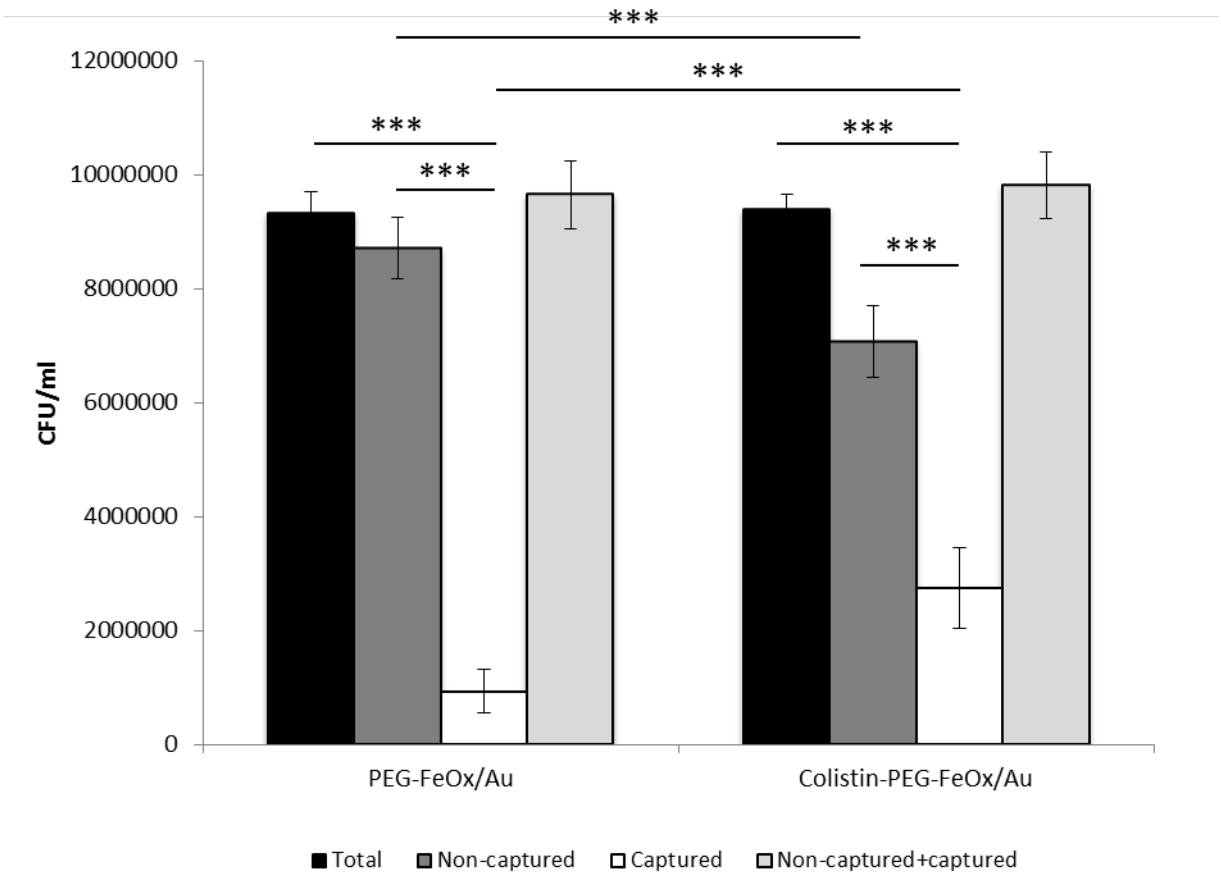

Figure 15. Comparative quantitative analysis of macroscale *Acinetobacter baumannii* separation by FeOx/Au nanoclusters, pure tube. Notably, there were highly significant differences between the captured and uncaptured bacteria populations internal and between the captured and uncaptured bacteria populations internal and between the PEGylated and colistinated nanoclusters treatments (***$p<0.001$, $n=6$). The combination of the CFU/ml between the captured and uncaptured tubes yielded values near 100% (104.6% and 103.4% for PEG-FeOx/Au and Colistin-PEG-FeOx/Au, respectively) for both nanocluster treatments; thus indicating the conservation of bacterium throughout the entire separation procedure. This result is of key importance as it demonstrates that the differences between the captured and uncaptured samples is attributed to nanoparticulate-mediated magnetic separation and not an unaccounted for loss of bacteria in the samples (e.g. cell death).

To account for this, our separation protocol included a 'total' sample as a control which proxies the 'original sample'. The sum of non-captured and captured CFU counts is not significantly different from the "total" (control) CFUs. Quantitatively, the combination of the CFU/mL between the captured and uncaptured tubes yielded values near 100% (104.6% and 103.4% for PEG-FeOx/Au and Colistin-PEG-FeOx/Au, respectively) for both nanocluster treatments; thus indicating the conservation of bacteria throughout the entire separation procedure. This result is of key importance as it demonstrates that the differences between the captured and uncaptured samples is attributed to nanoparticulate-mediated magnetic separation and not an unaccounted for loss of bacteria in the samples (e.g. cell death). The slight increase in the combined CFU/mL in comparison to the control is consistent with cell growth during the time of the experiment that is not of impact due to the highly statistical insignificance ($p<0.001$).

As shown in both Figure 14 and Figure 15, PEGylated nanoclusters non-specifically capture *A. baumannii*. Although statistically insignificant in comparison to separations mediated by colistinated nanomaterials, any exposed portion of the Au shell or FeOx core due to incomplete pegylation could contribute to non-specific binding. In future work, simply increasing the PEG lengths of the thiolated PEG spacers would ensure the formation of mushroom conformations on the surface of the nanomaterials enhancing surface passivation thus resisting non-specific binding. Less likely, the force generated by the bulk fluid motion of the magnetic nanomaterials acting as a ferrofluid could have contributed to the non-specific mechanical separation of the bacteria. This phenomenon is comparable to magnetophoretic, ferrofluid guided systems where bulk movement of a ferromagnetic fluid

in a magnetic field could trap nonmagnetic particulates (Asmatulu et al. 2010). Future work also includes modulating the nanoparticle to bacteria ratio to determine if the nanoparticle concentration has a significant impact on the nonspecific ferrofluid separation potential.

The clustering effect of the nanomaterials is apparent upon binding to the surface of gram-negative *A. baumannii* as shown in the STEM-EDS micrograph map in Figure 16A. The presence of the bacterium is supported by the detection of phosphorous within the cell. The location of the nanoclusters is substantiated by the co-localized detection of iron and gold. We suggest that the binding of the nanoclusters is mediated by colistin as shown with proposed biochemical detail in Figure 16B. The electrostatic interaction of the colistin with the phosphate groups occurs due to the presence of positively-charged primary amine groups. These positively-charged groups, especially those in the lariat of the molecule, displace divalent cations (Mg^{2+} and Ca^{2+}) which under normal conditions stabilize the membrane lipids(Clifton et al. 2015), which compose the cell envelope of the bacterium. It can be presumed that multiple colistin-lipid electrostatic interactions generate enough force to resist detachment during magnetic separation. Furthermore, multiple nanoparticulate binding events further multiplies this binding force.

The lipophilic portion of the colistin molecule penetrates the lipid layer of the bacterium; however, only at high colistin concentrations will enough of these interactions destabilize the lipid bilayer of the bacterium to the point of cell lysis. Even further, at high enough nanoparticle concentrations, the nanoparticles begin to impinge on the cellular

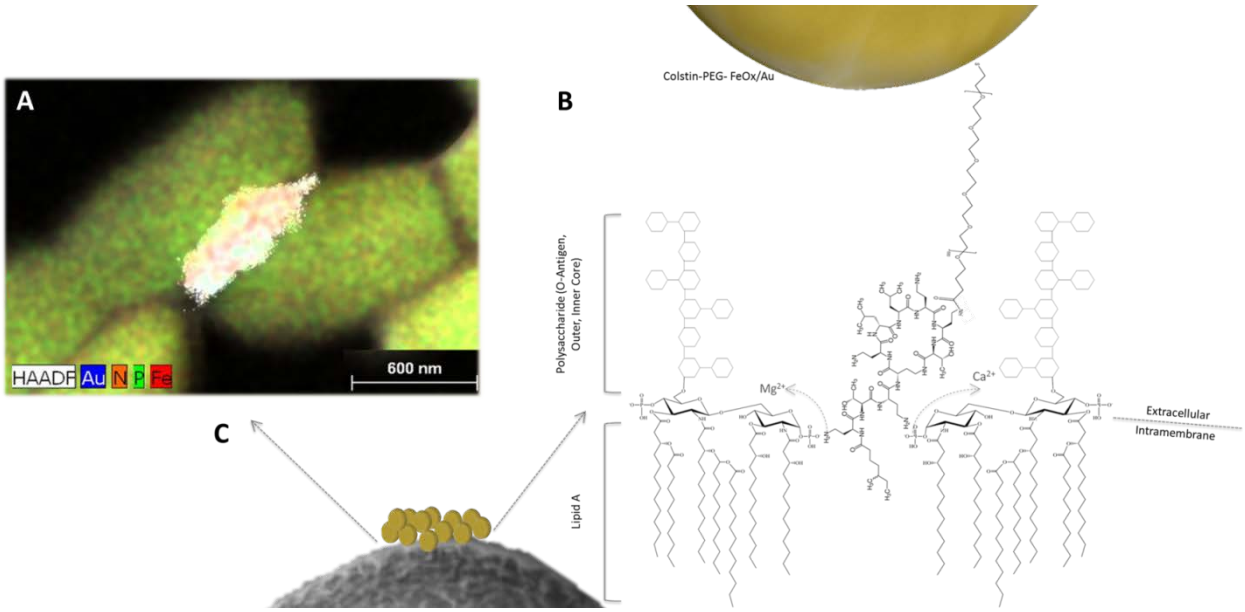

Figure 16. Colistinated nanoclusters bind to the surface of *A. baumannii*. A) STEM-EDS micrograph map of colistinated FeOx/Au binding *A. baumannii*; B) Biochemical schematic of colistin-PEG conjugate interaction with bacterial lipopolysaccharide; C) schematic of FeOx/Au nanoclusters binding to *A. baumannii* bacterium (STEM micrograph).

function of the bacterium by disrupting the cell membrane in a dose-dependent manner (Seil & Webster 2012). Due to this, the highest nanoparticle to bacterium ratio that could be tolerated by the bacteria had to be determined. The dose-dependent bacterial toxicity of both PEGylated and colistinated nanoclusters with *A. baumannii in vitro* is described quantitatively in Figure 17. PEGylated nanomaterials were nontoxic until becoming significantly toxic ($p<0.05$) when nanoparticle to bacteria ratios exceeded 10000:1. Colistinated particles were nontoxic in comparison to untreated populations until becoming significantly toxic ($p<0.05$) in ratios which exceeded 10000:1. More importantly, this data supports the chosen 1000:1 nanoparticle to bacterium ratio for the capture experiments. From a therapeutic standpoint, cell lysis is to be avoided as bacterium release cytotoxic agents into the bloodstream or into the local, internal environment during death. In future devices, blood return to the patient should remain free of bacteria as well as free of the remains of lysed cells.

At 1000:1 nanoparticle to bacterium ratios (NP:b), the greatest capture percentage achieved was 38.5% with a minimum of 21.7%. Magnetic separations at these magnitudes are acceptable for adjuvant therapies. However, we believe magnetic separations exceeding 90% are achievable. Modification of the NP:b ratios may increase magnetic separation. Augmentation of these ratios may require the simultaneous adjustment of colistin surface density. Increasing the number of nanoparticles present in the sample further increases the total concentration of colistin potentially impinging bacterial survivability. Future directions include optimizing the balance between these ratios and colistin surface coverage to maximize magnetic separation. Further, variation of separation

duration and an introduction of the sample into mesofluidic fluid flow may enhance bacterial separation percentages.

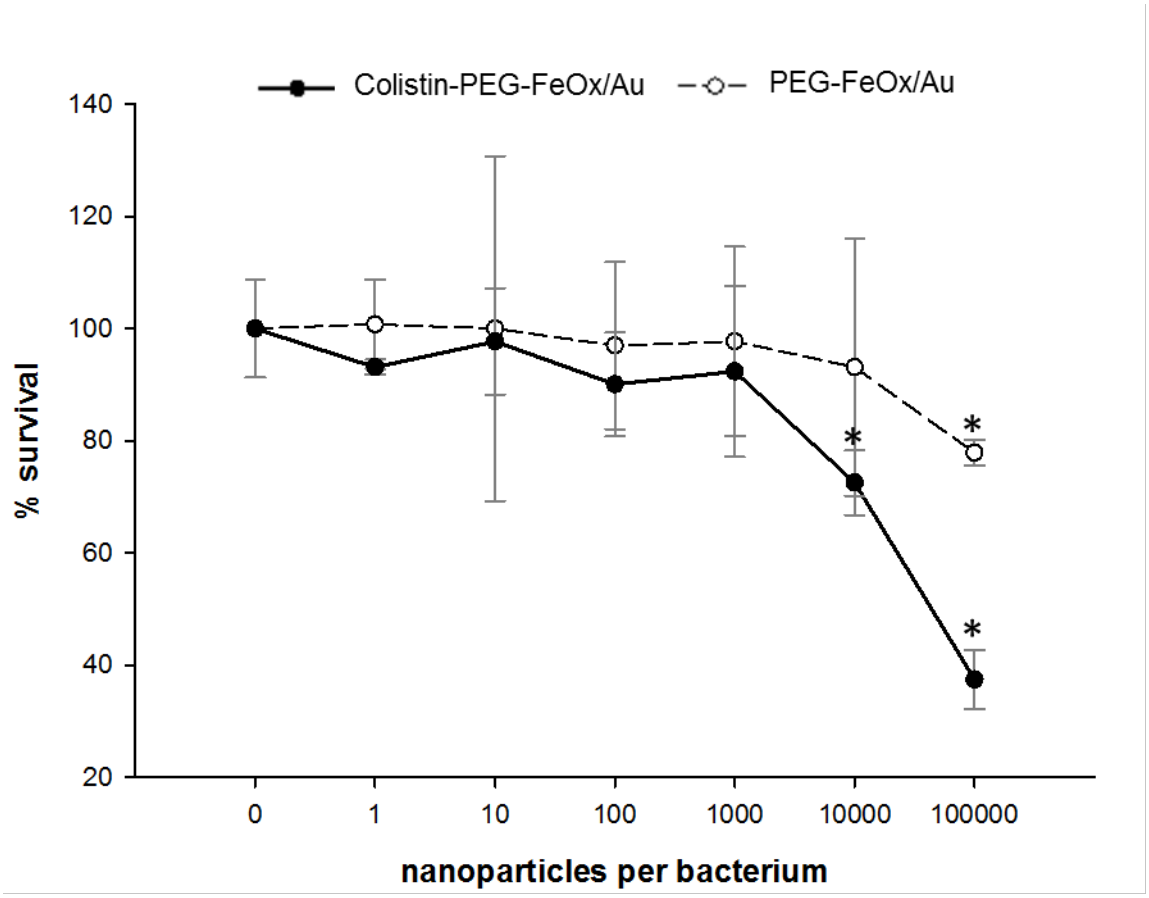

Figure 17. Bacterial toxicity of PEGylated and colistinated nanoclusters with *A. baumannii in vitro*. PEGylated nanomaterials were nontoxic until becoming significantly toxic ($p<0.05$) when cell:NP ratios exceeded 1:10000. In comparison to untreated populations, colistinated particles were nontoxic until becoming statistically toxic ($p<0.05$) in ratios which exceeded 1:10000.

Both colistinated and PEGylated nanoclusters are biocompatible with HUVEC and HepG2 cell lines *in vitro* with nanoparticulate concentrations as high as 900 mM ($p<0.5$, $n=3$). These results are shown in Figure 18. Free colistin alone was tolerated up to 0.9 μM. As expected, free colistin concentrations exceeding 900 μM resulted in cytotoxicity ($p<0.5$, $n=3$). The colistin reagent used to derive the free colistin cytotoxicity results was also used in colistination reactions. From this, we can conclude that the colistin preparation was active and supports the results depicting a lack of nanoparticulate cytotoxic effects. Furthermore, the lack of cytotoxic effects with both HUVEC and HepG2 cell lines reflects compatibility with both vasculature and liver tissue. Similarly, both colistinated and PEGylated nanoclusters were biocompatible with red blood cells *in vitro* and did not cause hemolysis. Colistinated and PEGylated nanoclusters lysed, at maximum, 1.2%±0.2 of red blood cells at nanoparticulate concentrations ranging from 1 μg/mL to 200 μg/mL (Table 2). Free colistin lysed no more than 0.8% ±1.5 at concentrations up to 900 m*M* (Table 2).

Table 2a. Red Blood Cell Hemolysis

Sample	**Hemolysis (%)**
1 μg/mL Col-PEG-FeOxNPs	1.1 ± 0.2
1 μg/mL PEG-FeOxNPs	-1.4 ± 0.2
5 μg/mL Col-PEG-FeOxNPs	-0.6 ± 0.5
5 μg/mL PEG-FeOxNPs	0.02 ± 0.6
40 μg/mL Col-PEG-FeOxNPs	0.7 ± 0.2
40 μg/mL PEG- FeOxNPs	0.3 ± 0.4
200 μg/mL Col-PEG-FeOxNPs	0.5 ± 0.3
200 μg/mL PEG- FeOxNPs	-0.1 ± 0.05
Positive control (20% triton-X)	100 ± 3.4
Negative control (PBS, pH 7.4)	0.0 ± 0.4

Table 2b. Red Blood Cell Hemolysis

Sample	**Hemolysis (%)**
0.2 m*M* Free Colistin	-0.7 ± 0.6
0.4 m*M* Free Colistin	-0.8 ±1.1
0.9 m*M* Free Colistin	0.8 ± 1.5
900 m*M* Free Colistin	-0.4 ± 0.8
Positive control (20% triton-X)	100 ±1.9
Negative control (PBS, pH 7.4)	0.0 ± 0.4

Table 2. Conjugated nanoparticles do not cause hemolysis.

These cytocompatibility results are of great importance with regard to future development of a robust therapeutic. Failure to retain the magnetic nanomaterials and allowing them to re-enter the patient is a major failure mode of an extracorporeal device. Upon entry into the patient, the nanomaterials would have immediate interaction with the vascular tissue and would accumulate in the liver because of their size and charge (Longmire et al. 2008). Due to their cytocompatibility with these tissues, catastrophic failure of an extracorporeal device would be better tolerated by a patient in comparison to devices which utilize nanomaterials which are cytotoxic. The hemolysis results demonstrate that colisitnated nanomaterials have the potential to cohabit with patient blood for 1 hr with no adverse risk of hemolysis. Alleviation of strict $\sim O$(min) flow durations aid in the development of efficient extracorporeal devices which maximize the removal of bacteria and enhance patient outcomes.

Following synthesis, the nanomaterials were fully characterized for their elemental composition and their optical, magnetic and morphological properties. Following sonicatory amination of γ-Fe_2O_3 nanoparticles, there were no significant changes in the morphology of the nanomaterials (Figure 19A) where the materials remained monomorphous. However, after gold sonoplation, the morphology of the nanoparticles became polymorphous. While there appear to be many spherical particles, the formation of jagged, oblong and elliptical particles is apparent following sonoplation (Figure 19A*ii*). Furthermore, these polymorphous particles tended to cluster together forming on the order of $\sim O$(100 nm) clusters of core/shell nanomaterials.

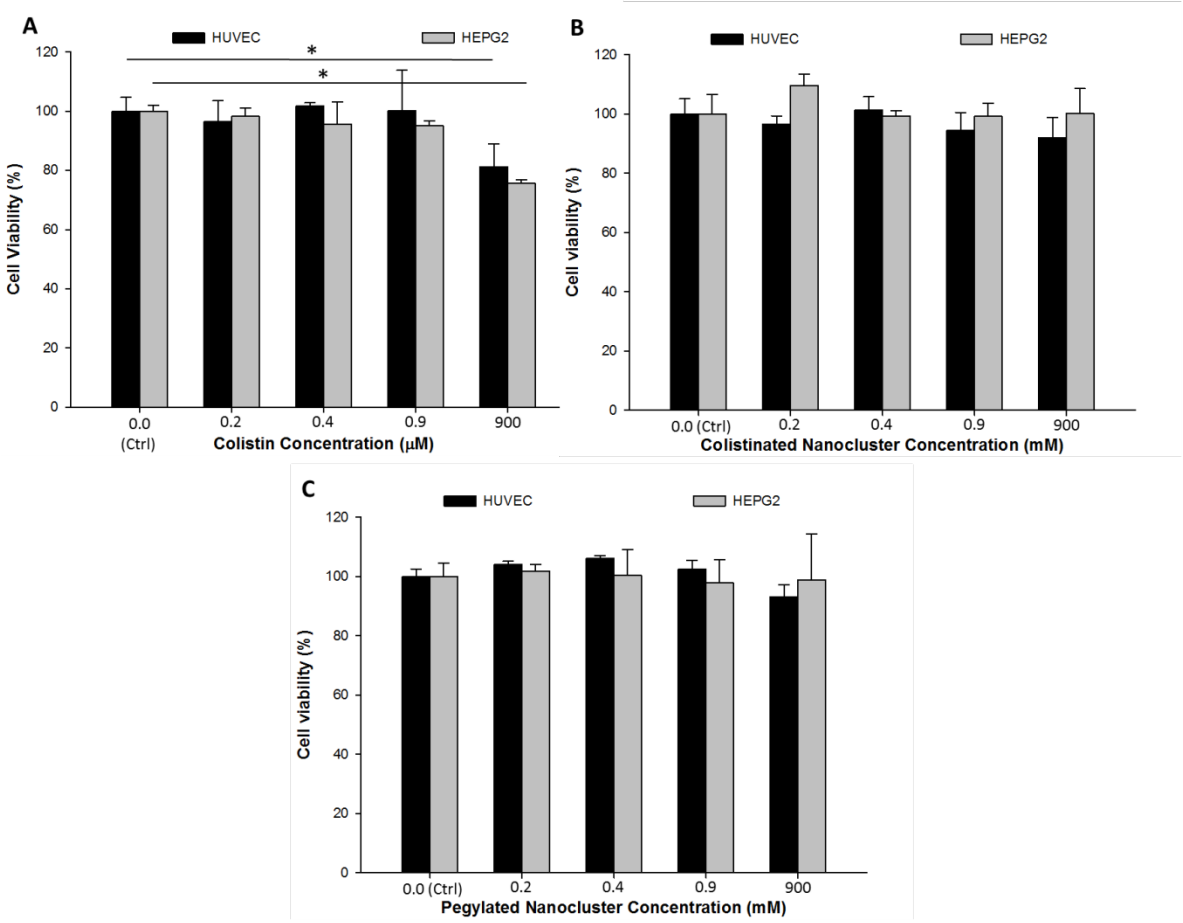

Figure 18. Cytocompatibility results showing toxicity of free colistin, pegylated, and colistinated nanoclusters in HUVEC and HepG2 cells *in vitro*. Both pegylated and colistinated particulate populations caused no significant toxicity in both HUVEC and HepG2 cells *in vitro*. Both pegylated and colistinated particulate populations caused no significant toxicity in both HUVEC and HepG2 cells ($p<0.05$, $n=3$).

The formation of these particle morphologies is likely due to insufficient amounts of gold chloride in the reaction volume. Although troublesome for therapeutic or diagnostic strategies that require spherical gold-clad particles, our strategy requires nanomaterials which are magnetomotive. Core/shell nanomaterials with significant shell thicknesses have diminished magnetic properties as shown in Equation 2. This equation describes the saturation magnetization, the maximum magnetization a particle can experience, M_{sat} of a single core/shell magnetic nanoparticle where the magnetic properties of the particle stem from the core which is coated with a thin outer shell of magnetically inert material.

$$M_{sat} = mM_{so}\left(\frac{r-d}{d}\right)^3 \qquad (2)$$

where M_{so} is the saturation magnetization of the bulk material in units of A/m/g, m is the mass of the individual particle, r is the particle radius, and d is shell thickness. Any significant increase in the shell thickness, d, has significant detrimental effect on the saturation magnetization of the particle. From this equation, we concluded that minimizing the shell thickness in order to maximize the magnetic properties, and thus the probability of magnetomotion in the presence of a magnetic field, of the nanomaterials was paramount. Following statistical analysis of nanoparticle diameters, ~1.75nm gold shell thicknesses were observed. It has been previously described that as magnetic nanomaterials cluster together and form nanocluster units, the magnetization force of the nanocluster increases (Ortega & Giorgio 2012). Here, this phenomenon increased the magnetization saturation of the nanoclusters thus increasing their magnetomotive potential. This increase in magnetization is supported by the decrease in the magnetic relaxivity of the FeOx/Au

nanoclusters shown in Table 3. This decrease in relaxivity suggests a higher nanocluster magnetomotive potential; thus increasing the probability that the nanomaterials will be able to effectively separate bacteria upon introduction into a magnetic field.

The optical properties of the nanomaterials change significantly upon the sonochemical deposition , sonoplation, of gold to the surface of the γ-Fe_2O_3 nanoparticles. Appearance of a surface plasmon resonance peak in the visible range of the spectrum is a clear indicator of the formation of gold clad nanomaterials. Following conjugation with PEG and colistin, the absorbance peak blue-shifts by ten nanometers signaling a change in the surface plasmon resonance. This shift in the surface plasmon resonance is expected as it signals that a chemical conjugation or ligand binding event has occurred on the gold surface of the nanomaterial (Ghosh et al. 2004). The presence FeOx/Au core/shell nanoparticles following synthesis was substantiated via HRTEM-EDS of an isolated nanoparticle. The micrograph in Figure 19C shows an isolated nanoparticle with 2.4Å fringe patterns – fringe spacing indicative of a gold clad material. This single nanoparticle was characterized for its elemental composition via the EDS functionality of the S/TEM-EDS microscope. Following 8 minutes of x-ray collection, the EDS spectrum (Figure 19D) contained gold, as expected, but also both iron and silicon. The detection of elemental iron and silicon substantiates the existence of both an iron core and the intermediary aminosilane layers which comprise the core/shell nanoparticle.

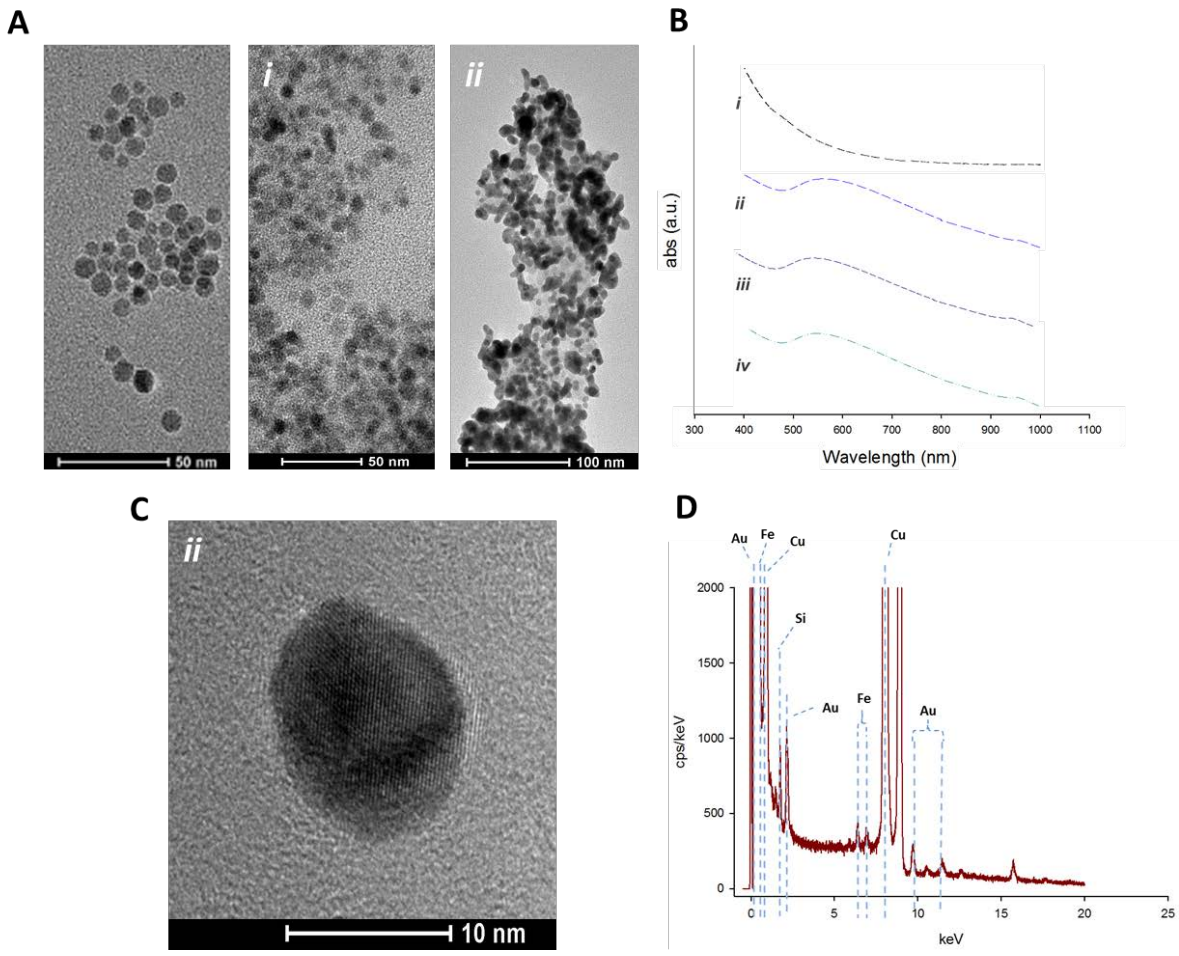

Figure 19. FeOx/Au nanoparticulate characterization confirming nanomaterial synthesis. A) TEM micrographs of FeOx nanoparticles, (*i*) aminated FeOx nanoparticles, and (*ii*) gold-clad iron oxide (FeOx/Au) nanoparticles; B) UV-vis-NIR spectra of (*i*) FeOx-NH_2, (*ii*) FeOx/Au, (*iii*) colistin-PEG-FeOx/Au, (*iv*) PEG-FeOx/Au; C) HRTEM micrograph of single FeOx/Au core-shell nanoparticles depicting Au lattice fringe patterns; D) EDS spectra of single FeOx/Au core-shell nanoparticles shown in (C) depicting the expected elemental presence of both Fe, Si and Au.

The dual, magnetoplasmonic nature of these nanomaterials enables their usefulness in theranostic applications. Extracorpeal devices, while designed foremost to be therapeutic devices, can also be utilized to specifically detect the species of bacteria leading to rapid diagnosis. In the future, such a theranostic approach could be implemented in a multiplexed fashion on patients who present with septic-like symptoms but remain undiagnosed due to diagnostic limitations. Such a device could act as a "broad-spectrum" therapeutic designed to extract a multitude of species while each species specific nanomaterial could be a unique probe that identifies the extracted bacteria for early diagnostic purposes.

The conjugation of colistin to the surface of the FeOx/Au nanoclusters was confirmed. Following conjugation, the 2-fold, statistically significant ($p<0.05$) positive shift

Sample	Peak λ (nm)	NP Dia. (nm)	Nanocluster Hydrodyn. radii (nm)	Zeta Pot. (mV)	Relaxivity (ms)
(*i*) FeOx-NH2	-	11.3±1.8	-	+32.0±3.0	152.6±3.2
(*ii*) FeOx/Au	564	13.0±1.6	296.8±7.0	-34.7±0.7	121.7±1.0
(*iii*) FeOx/Au-Colistin	553	13.0±1.6	244.1±2.1	-10.5±0.3	148.0±1.8
(*iv*) FeOx/Au-PEG	552	13.0±1.6	275.6±5.1	-31.2±0.4	132.7±2.0

Table 3. **Conjugated and Unconjugated Nanoparticle Characterization.**

in zeta potential between colistinated and pegylated nanoclusters is an indicator of conjugation as the colistin molecule has a higher positive charge than PEG (Table 3). There was also a significant positive shift in zeta potential of both conjugated particle populations when compared to the unconjugated particles, further confirming conjugation. The iodine-catalyzed decomposition of the colstinated nanomaterials ensured that all bound colistin would be liberated into solution from the gold surface. Thereafter, the iodinated gold flocculated, losing its colloidal properties and settled in the tube. The inset of Figure 20A depicts this observation, where colloidal, colistinated FeOx/Au nanoclusters (left) are compared to iodinated gold with the colistin conjugates liberated into solution. ^{1}H NMR spectra of free colistin shows strong methyl-methyl peaks around 0.8-0.9 ppm whereas primary amine groups are detected around 8 ppm. We expected to see a ppm shift in the spectra due to diamagnetic shielding. The additional electrons surrounding the colistin, which are contributed by the bound polymer, shield the molecule which causes a 0.5-1ppm shift in the resultant spectrum. As shown in the ppm in Figure 8A, ^{1}H NMR spectra of the supernatant of this reaction depicts the presence of colistin substantiated by the appearance of methyl-methyl peaks (0.5 -1 ppm). Most importantly, the appearance of primary amines primary amines (8-8.5ppm) as shown in Figure 20B substantiates the presence of liberated colistin.

To ensure no free colistin was contributing to the 1H NMR results, a free colistin ELISA kit was performed on the first-wash supernatants of both colistination and pegylation conjugation reactions. Per the ELISA kit, there was no free colistin in the sample as the returned concentration (0.0015 ng/ml) was below the standard curve

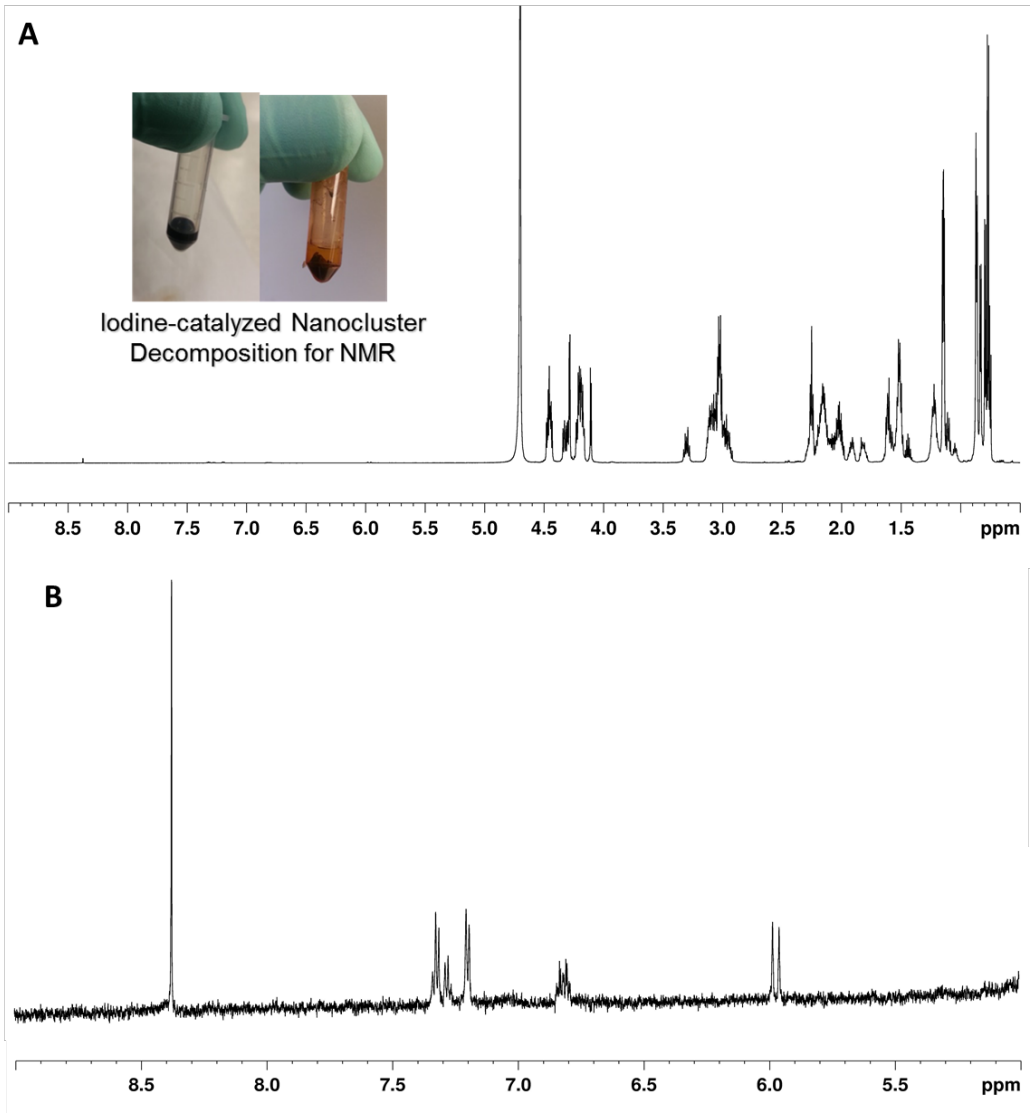

Figure 20. The conjugation of colistin to FeOx/Au nanoclusters was confirmed. A) ^{1}H NMR spectra of colistin-PEG conjugates liberated from the nanoparticulate surface following iodine-catalyzed nanocluster decomposition confirming the presence of colistin of the surface of the nanomaterials [inset: concentrated FeOx/Au nanoclusters before (left) and after decomposition]; B) ^{1}H NMR spectra (5-9 ppm) of colistin-PEG conjugates depicting the presence of primary amine groups.

recommendations (0.1 ng/ml) suggested by the manufacturer. As expected, there was no colistin detected in PEGylated supernatants as the returned concentration was below the concentration detected in the blank sample. Even further, ^{1}H NMR detection of colistin at concentrations less than 10 μg/mL was extremely difficult and would not have yielded detectable signal at the levels detected by the ELISA kit.

Conclusion

We have successfully demonstrated that superparamagnetic FeOx/Au core/shell nanoparticles, which form magnetic nanoclusters, can be used to magnetically capture and separate *Acinetobacter baumannii* using colistin as the microbial targeting ligand. The nanomaterials were successfully synthesized and characterized for their magnetoplasmonic properties and potential for use in theranostic applications. Successful conjugation was confirmed and nanocluster binding to the bacterial surface was observed. This result, for the first time, demonstrates a robust, pharmaceutical-based motif for high affinity nanoparticulate targeting to the *A. baumannii* surface. The antibiotic-activated nanomaterials demonstrated cytocompatibility with human cells, bacterial tolerance below 1:10000 bacteria to nanoparticle concentrations, and bacterial toxicity at higher levels. With maximal separation efficiencies exceeding 38%, this nanotechnology-mediated platform is well suited for adjuvant therapies which assist in the treatment of sepsis.

These results reveal an opportunity for the development of an adjuvant treatment option for patients suffering from *Acinetonacter baumannii* bacteremia and other gram-negative bacteria. Possible adjuvant treatments include the development of extracorporeal

devices to mechanically remove bacteria while intravenous injections of the antibiotic work concurrently to stifle the systemic infection. Our development and characterization of a robust nanoparticulate platform for targeting and capture of *Acinteobacter baumannii* in physiological phantoms paves the way for the translational development of such an adjuvant treatment. Furthermore, due to the dual, magnetophotonic nature of the nanotechnology platform, a theranostic approach could be developed in a multiplexed fashion for patients who present with septic-like symptoms but remain undiagnosed due to diagnostic limitations. In the future, development of "broad-spectrum" theranostics as well as other adjuvant therapies based on this antibiotic-mediated nanotechnology platform will significantly improve the clinical outcomes of septic patients.

Summary

This Chapter confirmed the central hypothesis of my dissertation: inorganic, multilayered, magnetoplasmonic core/shell nanomaterials were specifically designed and synthesized for biological applications which required both detection and therapeutic elimination of a disease causing agent. More specifically, this work successfully demonstrated that superparamagnetic FeOx/Au core/shell nanoparticles, which form magnetic nanoclusters, can be used to magnetically capture and separate *Acinetobacter baumannii* using polymyxin E as the microbial targeting ligand. The nanomaterials were synthesized and assessed for their magnetoplasmonic properties and potential for use in theranostic applications. Importantly, for the first time, a robust, pharmaceutical-based motif for high affinity nanoparticulate targeting to the *A. baumannii* surface was demonstrated.

Furthermore, the goals described in *Aim 3*, were achieved in Chapter IV. The magnetoplasmonic core/shell nanoparticles fabricated in *Aim 2* were biofunctionalized with antibiotic, polymyxin E, which targets and binds gram negative bacteria. These biofunctionalized nanostructures were characterized and utilized to magnetically extract *Acinetobacter baumannii* from saline solution *in vitro*. These results support my hypothesis that these nanomaterials can be fabricated in such a way that biomedical functionalization of the material can proceed without detriment to the function of the biological component. These results achieve our final objective where the activity of the conjugated biological component was conserved while binding and extracting a disease causing agent, *A. baumannii*, *in vitro*.

CHAPTER V

SYNOPSIS AND CONCLUSIONS

In my dissertation work, I worked towards the development of novel, multilayered, magnetoplasmonic nanoconstructs to enable nanotechnology-mediated, theranostic biomedical applications. In order to develop these materials, I overcame a number of limitations which introduced unfavorable size constraints and limited resultant nanoparticle characteristics. My trial biomedical application, the nanotechnology-mediated removal of *A.baumannii, in vitro,* introduced further challenges. Nevertheless, I were able to develop the core/shell nanoconstructs necessary to bind and extract *A. baumannii* in a saline solution. While these nanoconstructs and the results of my *in vitro* strategy do not provide a comprehensive, clinical theranostic solution, my work has enabled us to advance in other ways.

As outlined in the chapters of this dissertation, we began by developing novel multilayered, metallodielectric multistrata nanoparticles which possess theranostic characteristics in a less than 60 nm diameter nanoparticulate embodiment (Chapter II). Thereafter, we modified the synthesis strategy to enhance the magnetic properties of the composite material (thus enabling magnetomotion) while decreasing the synthesis duration such that freshly synthesized materials can be rapidly utilized in a biological application (Chapter III). Finally, we confirmed the central hypothesis of my dissertation that inorganic, multilayered, magnetoplasmonic core/shell nanomaterials could be

specifically designed and synthesized for biological applications which require both diagnostic detection and therapeutic elimination of a disease causing agent. More specifically, this work successfully demonstrated that superparamagnetic FeOx/Au core/shell nanoparticles, which form magnetic nanoclusters, can be used to magnetically capture, visualize and separate *Acinetobacter baumannii* using polymyxin E as the microbial targeting ligand (Chapter IV). Combined and utilized, this work provides a launch pad for the development of nanotechnology-mediated, theranostic labeling, detection and magnetic removal of pathogens from blood – or other body fluid. Built into a continuous-flow corporeal device or a batch-process, macrovolume filtering device, the impact of this technology would be extensive and positively affect patient outcomes across the world.

Moving forward, research challenges exist for future work seeking to achieve the development of this technology. Next steps include: (1) optimization of the parameters of the *in vitro* experiment to maximize, or achieve a greater than 90%, separation efficiency; (2) iteration of the *in vitro* magnetic separation experiments in whole, non-diluted blood; (3) development of mesofludic or batch/macroscale instrumentation to facilitate the nanotechnology-mediated separation in an automated fashion in a mechanical environment; (4) iteration of all experiments on robust *in vivo* models; and (5) escalation of the technology for clinical translation. Furthermore, as an entrepreneur, I would be remiss if I did not mention the local and global regulatory challenges governing the clinical rollout of such a technology to both domestic and foreign patients – including military veterans.

Nevertheless, core/shell nanotechnology remains a promising platform to enhance current biomedical diagnostics, therapeutics and the combination thereof; as supported by the rapid growth and implementation of such technology in both academia and industry. Further development of core/shell nanotechnology in biomedical applications will continue to require novel approaches to optimize the composite characteristics of nanoconstructs. These efforts will bolster the technological impact of these biomedical applications thus improving the way we deliver medical care to patients across the globe and beyond.

BIBLIOGRAPHY

Ali, M.E. et al., 2012. Gold nanoparticle sensor for the visual detection of pork adulteration in meatball formulation. *Journal of Nanomaterials*, pp.1–7.

Aronson, N.E., Sanders, J.W. & Moran, K.A., 2006. In harm's way: infections in deployed American military forces. *Clinical infectious diseases : an official publication of the Infectious Diseases Society of America*, 43, pp.1045–1051.

Asmatulu, R., Zhang, B. & Nuraje, N., 2010. A Ferrofluid Guided System for the Rapid Separation of the Non-Magnetic Particles in a Microfluidic Device. *JOURNAL OF NANOSCIENCE AND NANOTECHNOLOGY*, 10, pp.6383–6387.

B. Brinson C. Levin, R. Bardhan, N. Mirin and NJ. Halas, J.L., 2008. Nanoshells Made Easy: Improving Au Layer Growth on Nanoparticle Surfaces. *Langmuir*, 24(24), pp.14166–14171.

Bardhan, R. et al., 2010. Nanosphere-in-a-nanoshell: A simple nanomatryushka. *Journal of Physical Chemistry C*, 114, pp.7378–7383.

Barnes, W.L., Dereux, A. & Ebbesen, T.W., 2003. Surface plasmon subwavelength optics. *Nature*, 424, pp.824–30. Available at: http://www.nature.com/nature/journal/v424/n6950/full/nature01937.html.

Bell, C. & Yu, S.S., 2011. Multistrata nanoparticles and methods for making multistrata nanoparticles.

Bell, C.S., Yu, S.S. & Giorgio, T.D., 2011. Multistrata Nanoparticles: The Multistrata Nanoparticle: an FeOx/Au Core/Shell Enveloped in a Silica–Au Shell (Small 9/2011). *Small*, 7(9), p.1157. Available at: http://dx.doi.org/10.1002/smll.201190031.

Bergogne-Bérézin, E. & Towner, K.J., 1996. Acinetobacter spp. as nosocomial pathogens: Microbiological, clinical, and epidemiological features. *Clinical Microbiology Reviews*, 9, pp.148–165.

Bordelon, H. et al., 2013. A magnetic bead-based method for concentrating DNA from human urine for downstream detection. *PloS one*, 8, p.e68369. Available at: http://www.pubmedcentral.nih.gov/articlerender.fcgi?artid=3704639&tool=pmcentrez&rendertype=abstract.

Bose, A. & Wui Wong, T., 2015. *Nanotechnology Applications for Tissue Engineering*, Available at: http://www.sciencedirect.com/science/article/pii/B978032332889000011X.

Brongersma, M.L., 2003. Nanoscale photonics: Nanoshells: gifts in a gold wrapper. *Nature materials*, 2, pp.296–297.

Cai, Y. et al., 2012. Colistin resistance of Acinetobacter baumannii: Clinical reports, mechanisms and antimicrobial strategies. *Journal of Antimicrobial Chemotherapy*, 67, pp.1607–1615.

Camp, C. & Tatum, O.L., 2010. A Review of Acinetobacter baumannii as a Highly Successful Pathogen in Times of War. *Laboratory Medicine*, 41, pp.649–657.

Chatterjee, K. et al., 2014. Core/shell nanoparticles in biomedical applications. *Advances in Colloid and Interface Science*, 209, pp.8–39. Available at: http://dx.doi.org/10.1016/j.cis.2013.12.008.

Chen, Y. et al., 2015. One-Step Detection of Pathogens and Viruses: Combining Magnetic Relaxation Switching and Magnetic Separation. *ACS Nano*, 9(3), pp.3184–3191. Available at: http://dx.doi.org/10.1021/acsnano.5b00240.

Cheng, X., Chen, G. & Rodriguez, W.R., 2009. Micro- and nanotechnology for viral detection. *Analytical and Bioanalytical Chemistry*, 393, pp.487–501.

Chibani-Chennoufi, S. et al., 2004. In vitro and in vivo bacteriolytic activities of Escherichia coli phages: Implications for phage therapy. *Antimicrobial Agents and Chemotherapy*, 48, pp.2558–2569.

Chung, B.G., Kang, L. & Khademhosseini, A., 2007. Micro- and nanoscale technologies for tissue engineering and drug discovery applications. *Expert Opinion on Drug Discovery*, 2, pp.1653–1668.

Clifton, L.A. et al., 2015. The Effect of Divalent Cation Removal on the Structure of Gram-negative Bacterial Outer Membrane Models. *Langmuir*, 31, pp.404–412. Available at: http://pubs.acs.org/doi/abs/10.1021/la504407v.

D. Duff P. Edwards, A.B., 1993. A new hydrosol of gold clusters, 1: formation and particle size variation. *Langmuir*, 9(2301-2309).

D. Kirui C. Batt, D.R., 2010. Gold hybrid nanoparticles for targeted phototherapy and cancer imaging . *Nanotechnology*, 21(10).

Dijkshoorn, L., Nemec, A. & Seifert, H., 2007. An increasing threat in hospitals: multidrug-resistant Acinetobacter baumannii. *Nature reviews. Microbiology*, 5, pp.939–951.

Driskell, J.D. & Tripp, R. a., 2009. Emerging Technologies in Nanotechnology-Based Pathogen Detection. *Clinical Microbiology Newsletter*, 31, pp.137–144. Available at: http://dx.doi.org/10.1016/j.clinmicnews.2009.08.003.

Dufour, D. et al., 1998. *Surgery for Victims of War*, International Committee of the Red Cross.

Editorial, 2009. "Plenty of room" revisited. *Nature nanotechnology*, 4, p.781.

Ernest, H. & Shetty, R., 2005. Impact of Nanotechnology on Biomedical Sciences: Review of Current Concepts on Convergence of Nanotechnology With Biologye. *AzoNano-Online Journal of Nanotechnology*, 1, pp.1–14.

Evans, B.C. et al., 2013. Ex vivo red blood cell hemolysis assay for the evaluation of pH-responsive endosomolytic agents for cytosolic delivery of biomacromolecular drugs. *Journal of visualized experiments : JoVE*, p.e50166. Available at: http://www.pubmedcentral.nih.gov/articlerender.fcgi?artid=3626231&tool=pmcentrez&rendertype=abstract.

Falk, L.A. (1st L., 1945. Will penicillin be used indiscriminately? *Journal of the American Medical Association*, 127(11), p.672. Available at: http://dx.doi.org/10.1001/jama.1945.02860110052020.

Farokhzad, O.C. & Langer, R., 2009. Impact of nanotechnology on drug delivery. *ACS Nano*, 3, pp.16–20.

Feynman, R.P., 1960. There's plenty of room at the bottom: An invitation to enter a new field of physics. *Engineering and Science*, 23, pp.22–35.

Finland, M., Jones Jr, W. & Barnes, M., 1959. Occurrence of serious bacterial infections since introduction of antibacterial agents. *Journal of the American Medical Association*, 170(18), pp.2188–2197. Available at: http://dx.doi.org/10.1001/jama.1959.63010180008012.

Fishbain, J. & Peleg, A.Y., 2010. Treatment of Acinetobacter infections. *Clinical infectious diseases : an official publication of the Infectious Diseases Society of America*, 51, pp.79–84. Available at: http://www.ncbi.nlm.nih.gov/pubmed/20504234.

Fournier, P.-E. et al., 2006. Comparative genomics of multidrug resistance in Acinetobacter baumannii. *PLoS genetics*, 2, p.e7.

G. Antoch T. Egelhof, J. Stattaus, W. Jentzen, J. Debatin and A. Bockisch, L.F., 2002. Focal Tracer Uptake: A Potential Artifact in Contrast-Enhanced Dual-Modality PET/CT Scans . *The Journal of Nuclear Medicine*, 43(10), p.1339.

Getchell-White, S.I., Donowitz, L.G. & Groschel, D.H., 1989. The inanimate environment of an intensive care unit as a potential source of nosocomial bacteria: evidence for long survival of Acinetobacter calcoaceticus. *Infect Control Hosp Epidemiol*, 10, pp.402–407.

Ghosh Chaudhuri, R. & Paria, S., 2012. Core/shell nanoparticles: Classes, properties, synthesis mechanisms, characterization, and applications. *Chemical Reviews*, 112, pp.2373–2433.

Ghosh, S.K. et al., 2004. Solvent and ligand effects on the localized surface plasmon resonance (LSPR) of gold colloids. *Journal of Physical Chemistry B*, 108, pp.13963–13971.

Gil-Tomás, J. et al., 2007. Lethal photosensitisation of Staphylococcus aureus using a toluidine blue O–tiopronin–gold nanoparticle conjugate. *Journal of Materials Chemistry*, 17, p.3739. Available at: http://discovery.ucl.ac.uk/168236/\nhttp://xlink.rsc.org/?DOI=b706615e.

Gobin, A.M. et al., 2007. Near-Infrared Resonant Nanoshells for Combined Optical Imaging and Photothermal Cancer Therapy. *Nano Letters*, 7(7), pp.1929–1934. Available at: http://dx.doi.org/10.1021/nl070610y.

Górski, A. et al., 2009. Bacteriophage therapy for the treatment of infections. *Current opinion in investigational drugs (London, England : 2000)*, 10, pp.766–74. Available at: http://www.ncbi.nlm.nih.gov/pubmed/19649921.

Gu, H. et al., 2003. Presenting vancomycin on nanoparticles to enhance antimicrobial activities. *Nano Letters*, 3, pp.1261–1263.

Halas, C.R.N.J., 2004. Plasmonic Properties of Concentric Nanoshells. *Nano Lett.*, 4(7), pp.1323–1327.

Heggers, J.P. et al., 1969. Microbial flora of orthopaedic war wounds. *Military Medicine*, 171, pp.602–603.

Herzing, A. a et al., 2008. Energy dispersive X-ray spectroscopy of bimetallic nanoparticles in an aberration corrected scanning transmission electron microscope. *Faraday discussions*, 138, pp.337–351; discussion 421–434.

Hidron, A. et al., 2008. update: antimicrobial-resistant pathogens associated with healthcare-associated infections: annual summary of data reported to the National Healthcare. *Infect Control Hosp …*, 29, pp.996–1011. Available at: http://www.jstor.org/stable/10.1086/591861\nhttp://www.jstor.org.ezp-prod1.hul.harvard.edu/stable/pdfplus/10.1086/591861.pdf?acceptTC=true\nhttp://scholar.google.com/scholar?hl=en&btnG=Search&q=intitle:NHSN+Annual+Update:+Antimicrobial?Resistant+Pathogens.

Hirsch, L. et al., 2006. Metal Nanoshells. *Annals of Biomedical Engineering*, 34(1), pp.15–22. Available at: http://dx.doi.org/10.1007/s10439-005-9001-8.

Hirsch, L., Halas, N. & West, J., 2005. Whole-Blood Immunoassay Facilitated by Gold Nanoshell–Conjugate Antibodies. In S. J. Rosenthal & D. Wright, eds. *NanoBiotechnology Protocols*. Springer, pp. 101–112.

Hirsch, L.R. et al., 2003. Nanoshell-mediated near-infrared thermal therapy of tumors under magnetic resonance guidance. *Proceedings of the National Academy of Sciences*, 100(23), pp.13549–13554. Available at: http://www.pnas.org/content/100/23/13549.abstract.

Hood, M.I. et al., 2010. Acinetobacter baumannii Increases Tolerance to Antibiotics in Response to Monovalent Cations. *Antimicrobial Agents and Chemotherapy*, 54(3), pp.1029–1041. Available at: http://aac.asm.org/content/54/3/1029.abstract.

Huang, X. et al., 2008. Plasmonic photothermal therapy (PPTT) using gold nanoparticles. *Lasers in Medical Science*, 23(3), pp.217–228. Available at: http://dx.doi.org/10.1007/s10103-007-0470-x.

Huh, A.J. & Kwon, Y.J., 2011. "Nanoantibiotics": A new paradigm for treating infectious diseases using nanomaterials in the antibiotics resistant era. *Journal of Controlled Release*, 156, pp.128–145. Available at: http://dx.doi.org/10.1016/j.jconrel.2011.07.002.

I. Bruce, T. Sen, 2005. Surface Modification of Magnetic Nanoparticles with Alkoxysilanes and Their Application in Magnetic Bioseparations. *Langmuir*, 21(15), pp.7029–7035.

Ingle, A. et al., 2008. Mycosynthesis of Silver Nanoparticles Using the Fungus Fusarium acuminatum and its Activity Against Some Human Pathogenic Bacteria. *Current Nanoscience*, 4, pp.141–144.

J. Aaron T. Larson, S. Kumar, T. Milner, K. Sokolov, J.O., 2006. Increased optical contrast in imaging of epidermal growth factor receptor using magnetically actuated hybird gold/iron oxide nanoparticles. *Optics Express*, 14(26), pp.12930–12943.

J. Hainfeld T. Focella, H. Smilowitz, D.S., 2006. Gold nanoparticles: a new X-ray contrast agent. *The British Journal of Radiology*, 79, p.The British Journal of Radiology.

Jacobs, A.C. et al., 2010. Inactivation of Phospholipase D Diminishes Acinetobacter baumannii Pathogenesis. *Infection and Immunity*, 78(5), pp.1952–1962. Available at: http://iai.asm.org/content/78/5/1952.abstract.

Jawad, a. et al., 1998. Survival of Acinetobacter baumannii on dry surfaces: Comparison of outbreak and sporadic isolates. *Journal of Clinical Microbiology*, 36, pp.1938–1941.

Jesson, D.E. & Pennycook, S.J., 1995. Incoherent Imaging of Crystals Using Thermally Scattered Electrons. *Proceedings of the Royal Society A: Mathematical, Physical and Engineering Sciences*, 449, pp.273–293.

Johnson, C.J. et al., 2008. Proteomics, nanotechnology and molecular diagnostics. *Proteomics*, 8, pp.715–730.

Justo, J.A. & Bosso, J.A., 2015. Adverse reactions associated with systemic polymyxin therapy. *Pharmacotherapy*, 35, pp.28–33. Available at: http://www.ncbi.nlm.nih.gov/pubmed/25266910.

K. Woo S. Choi, H.W. Lee, J.P. Ahn, C.S. Kim, and S.W. Lee, J.H., 2004. Easy Synthesis and Magnetic Properties of Iron Oxide Nanoparticles. *Chem. Mater.*, 16(14), pp.2814–2818.

Kaittanis, C., Santra, S. & Perez, J.M., 2010. Emerging nanotechnology-based strategies for the identification of microbial pathogenesis. *Advanced Drug Delivery Reviews*, 62, pp.408–423. Available at: http://dx.doi.org/10.1016/j.addr.2009.11.013.

Kang, J.H. et al., 2014. An extracorporeal blood-cleansing device for sepsis therapy. *Nature Medicine*, 20, pp.1211–1216. Available at: http://www.nature.com.ezp-prod1.hul.harvard.edu/nm/journal/v20/n10/full/nm.3640.html\nhttp://www.nature.com.ezp-prod1.hul.harvard.edu/nm/journal/v20/n10/pdf/nm.3640.pdf.

Kerker, M., Wang, D.-S. & Giles, C.L., 1983. Electromagnetic scattering by magnetic spheres. *Journal of the Optical Society of America*, 73, p.765. Available at: http://www.osapublishing.org/abstract.cfm?uri=josa-73-6-765.

Kurek, A. et al., 2011. New antibacterial therapeutics and strategies. *Polish Journal of Microbiology*, 60, pp.3–12.

Kurek, A. et al., 2010. Oleanolic acid and ursolic acid affect peptidoglycan metabolism in Listeria monocytogenes. *Antonie van Leeuwenhoek, International Journal of General and Molecular Microbiology*, 97, pp.61–68.

L. E. Ginsberg M.Hashmi, N. Leeds and D. Schomer, G.F., 1998. The Significance of Lack of MR Contrast Enhancement of Supratentorial Brain Tumors in Adults: Histopathological Evaluation of a Series . *Surgical Neurology*, 49(9), pp.436–440.

L. Hirsch JL. West, N.J.H., 2005. Whole-Blood Immunoassay Facilitated by Gold-Nanoshell-Conjugate Antibodies. In D. W. W. SJ. Rosenthal, ed. *NanoBiotechnology Protocols*. Totowa, New Jersey: Humana Press, pp. 101–111.

L. Johnson M. Douek, A.G., 2010. Applications of Nanotechnology in Cancer. *Discovery Medicine*, 9(47), pp.374–379.

L. Wang S. Lim, M. Schadt, D. Mott, J. Luo, X. Wang and CJ. Zhong, H.Y.P., 2008. Core@shell nanomaterials: gold-coated magnetic oxide nanoparticles. *J. Mater. Chem.*, 18, pp.2629–2635.

Lal, S., Clare, S.E. & Halas, N.J., 2008. Nanoshell-Enabled Photothermal Cancer Therapy: Impending Clinical Impact. *Accounts of Chemical Research*, 41(12), pp.1842–1851. Available at: http://dx.doi.org/10.1021/ar800150g.

Lee, J.J. et al., 2014. Synthetic ligand-coated magnetic nanoparticles for microfluidic bacterial separation from blood. *Nano Letters*, 14, pp.1–5.

Levin, A.S. et al., 1999. Intravenous Colistin as Therapy for Nosocomial Infections Caused by Multidrug-Resistant Pseudomonas aeruginosa and Acinetobacter baumannii. *Clinical Infectious Diseases*, 28(5), pp.1008–1011. Available at: http://cid.oxfordjournals.org/content/28/5/1008.abstract.

Levy, S.B., 1998. The challenge of antibiotic resistance. *Scientific American*, 278, pp.46–53.

Li, J. et al., 2005. Evaluation of colistin as an agent against multi-resistant Gram-negative bacteria. *International Journal of Antimicrobial Agents*, 25, pp.11–25.

Li, Y. et al., 2014. Facile preparation of surface-exchangeable core@shell iron oxide@gold nanoparticles for magnetic solid-phase extraction: use of gold shell as the intermediate platform for versatile adsorbents with varying self-assembled monolayers. *Analytica chimica acta*, 811, pp.36–42. Available at: http://www.ncbi.nlm.nih.gov/pubmed/24456592.

Liang, C.H. et al., 2009. Iron oxide/gold core/shell nanoparticles for ultrasensitive detection of carbohydrate-protein interactions. *Analytical Chemistry*, 81, pp.7750–7756.

Lindsay and M.T. Holden, J.A., 2004. Staphylococcus aureus: superbug, super genome? *Trends Microbiol*, 12, pp.378–385.

Link, S., El-Sayed, M. a. & El-Sayed, M., 1999. Spectral Properties and Relaxation Dynamics of Surface Plasmon Electronic Oscillations in Gold and Silver Nanodots and Nanorods. *Journal of Physical Chemistry B*, 103, pp.8410–8426. Available at: http://pubs.acs.org/doi/abs/10.1021/jp9917648.

Lockhart, S.R. et al., 2007. Antimicrobial resistance among Gram-negative bacilli causing infections in intensive care unit patients in the United States between 1993 and 2004. *Journal of clinical microbiology*, 45, pp.3352–9. Available at: http://www.pubmedcentral.nih.gov/articlerender.fcgi?artid=2045364&tool=pmcentrez&rendertype=abstract.

Longmire, M., Choyke, P.L. & Kobayashi, H., 2008. Clearance properties of nano-sized particles and molecules as imaging agents: considerations and caveats. *Nanomedicine (London, England)*, 3, pp.703–717.

Loo, C. et al., 2005. Immunotargeted Nanoshells for Integrated Cancer Imaging and Therapy. *Nano Letters*, 5(4), pp.709–711. Available at: http://dx.doi.org/10.1021/nl050127s.

Lowery AR ES Day, NJ Halas, and JL West, A.M.G., 2006. Immunonanoshells for targeted photothermal ablation of tumor cells. *Int J Nanomedicine*, 1(2), pp.149–154.

Luke, N.R. et al., 2010. Identification and Characterization of a Glycosyltransferase Involved in Acinetobacter baumannii Lipopolysaccharide Core Biosynthesis. *Infection and Immunity*, 78(5), pp.2017–2023. Available at: http://iai.asm.org/content/78/5/2017.abstract.

M Melancon C Li, W.L., 2009. Gold-Based Magneto/Optical Nanostructures: Challenges for In Vivo Applications in Cancer Diagnostics and Therapy. *Mater Res Bull*, 34(6), pp.415–421.

M. Saksena P. Hahn, J.Kim, A. Saokar, B. King and R. Weissleder, M.H., 2006. Comparison of Lymphotropic Nanoparticle-Enhanced MRI Sequences in Patients with Various Primary Cancers. *American Journal of Roentgenology*, 187, pp.582–588.

M. Yezhelyev Y. Xing, A. Al-Hajj, S. Nie, R. O'Regan, X.G., 2006. Emerging use of nanoparticles in diagnosis and treatment of breast cancer. *The Lancet Oncology*, 7, pp.657–667.

Ma, X. et al., 2015. Exploring a new SPION-based MRI contrast agent with excellent water-dispersibility, high specificity to cancer cells and strong MR imaging efficacy. *Colloids and surfaces. B, Biointerfaces*, 126, pp.44–49.

Manian, F. a., Griesnauer, S. & Senkel, D., 2013. Impact of terminal cleaning and disinfection on isolation of Acinetobacter baumannii complex from inanimate surfaces of hospital rooms by quantitative and qualitative methods. *American Journal of Infection Control*, 41, pp.384–385. Available at: http://dx.doi.org/10.1016/j.ajic.2012.04.321.

Maragakis, L.L. & Perl, T.M., 2008. Acinetobacter baumannii: epidemiology, antimicrobial resistance, and treatment options. *Clinical infectious diseases : an official publication of the Infectious Diseases Society of America*, 46, pp.1254–1263.

Matsumoto, T. et al., 1969. Combat surgery in communication zone. I. War wound and bacteriology (preliminary report). *Military Medicine*, 134(9), pp.655–665.

Midgley, P.A. et al., 2006. Nanoscale scanning transmission electron tomography. *Journal of Microscopy*, 223, pp.185–190.

Mumtaz, S. et al., 2011. Burden of meticillin-resistant Staphylococcus aureus colonization and infection in London acute hospitals: retrospective on a voluntary surveillance programme. *The Journal of hospital infection*, 79(4), pp.309–12. Available at:

http://www.sciencedirect.com/science/article/pii/S0195670111003677 [Accessed October 27, 2015].

Murray, C.K., Hospenthal, D.R., et al., 2011. Efficacy of Point-of-Injury Combat Antimicrobials. *The Journal of Trauma*, 71(2), pp.S307–S313 10.1097/TA.0b013e318227af79. Available at: http://journals.lww.com/jtrauma/Fulltext/2011/08002/Efficacy_of_Point_of_Injury_Combat_Antimicrobials.11.aspx.

Murray, C.K., Obremskey, W.T., et al., 2011. Prevention of Infections Associated With Combat-Related Extremity Injuries. *Journal of Trauma and Acute Care Surgery*, 71(2). Available at: http://journals.lww.com/jtrauma/Fulltext/2011/08002/Prevention_of_Infections_Associated_With.4.aspx.

N.Portney, M.O., 2006. Nano-oncology: drug delivery, imaging, and sensing . *Analytical and Bioanalytical Chemistry*, 384(3), pp.620–630.

Nirmala Grace, a. & Pandian, K., 2007. Antibacterial efficacy of aminoglycosidic antibiotics protected gold nanoparticles-A brief study. *Colloids and Surfaces A: Physicochemical and Engineering Aspects*, 297, pp.63–70.

Norman, R.S. et al., 2007. Targeted Photothermal Lysis of the Pathogenic Bacteria, Pseudomonas aeruginosa, with Gold Nanorods. *Nano Letters*, 8(1), pp.302–306. Available at: http://dx.doi.org/10.1021/nl0727056.

O. Will C. Chan, T. Athanasiou, A. Darzi, W. Gedroyc and P. P Tekkis, S.P., 2006. Diagnostic precision of nanoparticle-enhanced MRI for lymph-node metastases: a meta-analysis . *The Lancet Oncology*, 7(1), pp.52–60.

O'Neal, D.P. et al., 2004. Photo-thermal tumor ablation in mice using near infrared-absorbing nanoparticles. *Cancer Letters*, 209(2), pp.171–176. Available at: http://www.sciencedirect.com/science/article/pii/S0304383504001442.

Ortega, R. a. & Giorgio, T.D., 2012. A mathematical model of superparamagnetic iron oxide nanoparticle magnetic behavior to guide the design of novel nanomaterials. *Journal of Nanoparticle Research*, 14, p.1282. Available at: http://link.springer.com/10.1007/s11051-012-1282-x.

Peleg, A.Y., Seifert, H. & Paterson, D.L., 2008. Acinetobacter baumannii: Emergence of a successful pathogen. *Clinical Microbiology Reviews*, 21, pp.538–582.

Perni, S. et al., 2009. The antimicrobial properties of light-activated polymers containing methylene blue and gold nanoparticles. *Biomaterials*, 30, pp.89–93. Available at: http://dx.doi.org/10.1016/j.biomaterials.2008.09.020.

Peterson, A.A., Hancock, R.E. & McGroarty, E.J., 1985. Binding of polycationic antibiotics and polyamines to lipopolysaccharides of Pseudomonas aeruginosa. *Journal of Bacteriology*, 164, pp.1256–1261. Available at: http://jb.asm.org/content/164/3/1256.abstract.

Pham, Q.P., Sharma, U. & Mikos, A.G., 2006. Electrospinning of polymeric nanofibers for tissue engineering applications: a review. *Tissue engineering*, 12, pp.1197–211. Available at: http://www.ncbi.nlm.nih.gov/pubmed/16771634.

Pissuwan, D. et al., 2010. Functionalised gold nanoparticles for controlling pathogenic bacteria. *Trends in Biotechnology*, 28(4), pp.207–213. Available at: http://www.sciencedirect.com/science/article/pii/S0167779909002364.

Pitsillides, C.M. et al., 2003. Selective cell targeting with light-absorbing microparticles and nanoparticles. *Biophysical journal*, 84, pp.4023–4032. Available at: http://dx.doi.org/10.1016/S0006-3495(03)75128-5.

Prabaker, K. & Weinstein, R.A., 2011. Trends in antimicrobial resistance in intensive care units in the United States. *Current opinion in critical care*, 17, pp.472–9. Available at: http://www.ncbi.nlm.nih.gov/pubmed/21900766.

Qureshi, Z. et al., 2014. Colistin-Resistant Acinetobacter baumannii: Beyond Carbapenem Resistance Accepted. *Clinical infectious diseases*, pp.1–33.

R. Hao Z. Xu, Y. Hou, S. Gao, S. Sun, R.X., 2010. Synthesis, functionalization, and biomedical applications of multifunctional magnetic nanoparticles. *Advanced Materials*, 22(25), pp.2729–2742.

R. Popovtzer N. Kotov, A. Popovtzer, J. Balter, T. Carey, R. Kopelman, A.A., 2008. Targeted Gold Nanoparticles enable Molecular CT Imaging of Cancer. *Nano Lett.*, 8(12), pp.4593–4596.

Radisic, M., Iyer, R.K. & Murthy, S.K., 2006. Micro- and nanotechnology in cell separation. *International journal of nanomedicine*, 1, pp.3–14.

Rai, M., Yadav, A. & Gade, A., 2009. Silver nanoparticles as a new generation of antimicrobials. *Biotechnology advances*, 27, pp.76–83. Available at: http://www.ncbi.nlm.nih.gov/pubmed/18854209.

Rasmussen, S. et al., 2015. Early Divergent Strains of Yersinia pestis in Eurasia 5,000 Years Ago. *Cell*, 163(3), pp.571–582. Available at: http://www.sciencedirect.com/science/article/pii/S0092867415013227 [Accessed October 23, 2015].

Roco, M.C., 2003. Nanotechnology: Convergence with modern biology and medicine. *Current Opinion in Biotechnology*, 14, pp.337–346.

Rodriguez-Guardado, A. et al., 2013. Acinetobacter infections: an emerging problem in the neurosurgical intensive care unit. In D. A. Godoy, ed. *Intensive Care in Neurology and Neurosurgery: Pathophysiological Basis for the Management of Acute Cerebral Injury*. SEEd, pp. 1053–1092.

Rozanova, N. & Zhang, J., 2009. Photothermal ablation therapy for cancer based on metal nanostructures. *Science In China Series B Chemistry*, 52, pp.1559–1575.

Runge, V., 1999. Contrast media research. *Invest. Radiol.*, 34, pp.785–790.

Runowski, M., 2014. Nanotechnology – nanomaterials, nanoparticles and multifunctional core/shell type nanostructures. *Chemik*, 68(9), pp.766–775.

Rybak and R.L. Akins, M.J., 2001. Emergence of methicillin-resistant Staphylococcus aureus with intermediate glycopeptide resistance: clinical significance and treatment options. *Drugs*, 61, pp.1–7.

Schärtl, W., 2010. Current directions in core-shell nanoparticle design. *Nanoscale*, 2, pp.829–843.

Schärtl, W., 2010. Current directions in core-shell nanoparticle design. *Nanoscale*, 2, pp.829–843.

Scott, P. et al., 2007. An Outbreak of Multidrug-Resistant Acinetobacter baumannii-calcoaceticus Complex Infection in the US Military Health Care System Associated with Military Operations in Iraq. *Clinical Infectious Diseases*, 44(12), pp.1577–1584. Available at: http://cid.oxfordjournals.org/content/44/12/1577.abstract.

Seil, J.T. & Webster, T.J., 2012. Antimicrobial applications of nanotechnology: Methods and literature. *International Journal of Nanomedicine*, 7, pp.2767–2781.

Shakhov, A.M. et al., 2014. Spherical gold nanoparticles and SiO2/Au core/shell microparticles under intense femtosecond laser excitation: relaxation dynamics of gold nanoparticles and nanostructuring of borosilicate glass using SiO2/Au microparticles. *Quantum Electronics*, 44(9).

Shevchenko, E. V et al., 2008. Gold/Iron Oxide Core/Hollow-Shell Nanoparticles. *Advanced Materials*, 20(22).

Skala, M.C. et al., 2008. Photothermal Optical Coherence Tomography of Epidermal Growth Factor Receptor in Live Cells Using Immunotargeted Gold Nanospheres. *Nano Letters*, 8(10), pp.3461–3467. Available at: http://dx.doi.org/10.1021/nl802351p.

Sodipo, B.K. & Aziz, A.A., 2014. No TitleA sonochemical approach to the direct surface functionalization of superparamagnetic iron oxide nanoparticles with (3-aminopropyl)triethoxysilane. *Beilstein J. Nanotechnol.*, 5, pp.1472–1476.

Soman, C. & Giorgio, T., 2009. Kinetics of molecular recognition mediated nanoparticle self-assembly. *Nano Research*, 2, pp.78–84.

Soman, C.P. & Giorgio, T.D., 2008. Quantum Dot Self-Assembly for Protein Detection with Sub-Picomolar SensitivityTitle. *Langmuir*, 24(8), pp.4399–4404.

Stoecklein, V.M., Osuka, A. & Lederer, J.A., 2012. Trauma equals danger—damage control by the immune system. *Journal of Leukocyte Biology*, 92(3), pp.539–551. Available at: http://www.ncbi.nlm.nih.gov/pmc/articles/PMC3427603/.

T. Islam, M.H., 2009. Overview of nanoparticle use in cancer imaging . *Cancer Biomarkers*, 5(2), pp.61–67.

T. Mason, J.L., 2002. *Applied Sonochemistry*, New York: Wiley.

Tom, R.T. et al., 2004. Ciprofloxacin-protected gold nanoparticles. *Langmuir*, 20, pp.1909–1914.

Tsuchiya, H. et al., 1996. Comparative study on the antibacterial activity of phytochemical flavanones against methicillin-resistant Staphylococcus aureus. *Journal of Ethnopharmacology*, 50, pp.27–34.

Tucker-Schwartz, J.M. et al., 2012. In vivo photothermal optical coherence tomography of gold nanorod contrast agents. *Biomedical Optics Express*, 3, p.2881.

Vila, J. & Pachón, J., 2008. Therapeutic options for Acinetobacter baumannii infections. *Expert opinion on pharmacotherapy*, 9, pp.587–599.

De Villiers, M.M., Aramwit, P. & Kwon, G.S., 2009. *Nanotechnology in Drug Delivery*,

W. Wu H. Chen, J. Tang and L. Nie, Q.H., 2007. Sonochemical synthesis, structure and magnetic properties of air-stable Fe3O4/Au nanoparticles . *Nanotechnology*, 18(14).

Wang, F.H. et al., 2011. Diffusion and clearance of superparamagnetic iron oxide nanoparticles infused into the rat striatum studied by MRI and histochemical techniques. *Nanotechnology*, 22, p.015103.

Wang, H. et al., 2011. Preparation of multi-core/single-shell OA-Fe3O4/PANI bifunctional nanoparticles via miniemulsion polymerization. *Colloids and Surfaces A: Physicochemical and Engineering Aspects*, 384, pp.624–629. Available at: http://dx.doi.org/10.1016/j.colsurfa.2011.05.031.

Wei, F., Lillehoj, P.B. & Ho, C.M., 2010. DNA diagnostics: Nanotechnology-enhanced electrochemical detection of nucleic acids. *Pediatric Research*, 67, pp.458–468.

Wendt, C. et al., 1997. Survival of Acinetobacter baumannii on dry surfaces. *J. Clin. Microbiol.*, 35, pp.1394–1397. Available at: http://jcm.asm.org/cgi/content/abstract/35/6/1394.

Woo, K., 2014. Prompt and synergistic antibacterial activity of silver nanoparticle-decorated silica hybrid particles on air filtration. *Journal of Materials Chemistry B: Materials for biology and medicine*, 2, pp.6714–6722. Available at: http://dx.doi.org/10.1039/C4TB01068J.

Wright, G.D., 2010. Antibiotic resistance in the environment: A link to the clinic? *Current Opinion in Microbiology*, 13, pp.589–594. Available at: http://dx.doi.org/10.1016/j.mib.2010.08.005.

Wu, W. et al., 2007. Sonochemical synthesis, structure and magnetic properties of air-stable Fe 3 O 4 / Au nanoparticles. *Nanotechnology*, 18, p.145609. Available at: http://stacks.iop.org/0957-4484/18/i=14/a=145609.

Yuan, C. et al., 2014. Simultaneous multiple wavelength upconversion in a core-shell nanoparticle for enhanced near infrared light harvesting in a dye-sensitized solar cell. *ACS applied materials & interfaces*, 6, pp.18018–18025. Available at: http://www.ncbi.nlm.nih.gov/pubmed/25238319.

Zeng, J.-B. et al., 2014. A colorimetric agarose gel for formaldehyde measurement based on nanotechnology involving Tollens reaction. *Chemical communications (Cambridge, England)*, pp.10–12. Available at: http://www.ncbi.nlm.nih.gov/pubmed/24846681.

Zharov, V.P. et al., 2006. Photothermal Nanotherapeutics and Nanodiagnostics for Selective Killing of Bacteria Targeted with Gold Nanoparticles. *Biophysical Journal*, 90(2), pp.619–627. Available at: http://www.sciencedirect.com/science/article/pii/S0006349506722408.

Zhou, T., Wu, B. & Xing, D., 2012. Bio-modified Fe3O4 core/Au shell nanoparticles for targeting and multimodal imaging of cancer cells. *Journal of Materials Chemistry*, 22, p.470.